UNIVERSIDADE DO VALE DO RIO DOS SINOS - UNISINOS

Programa de Pós-Graduação em Geologia

Nível Doutorado

JULIA TEDESCO

Proveniência, paleogeografia e sedimentologia dos depósitos do Grupo Itararé no extremo sul da Bacia do Paraná.

São Leopoldo
Julho, 2019

T256p Tedesco, Julia.

Proveniência, paleogeografia e sedimentologia dos depósitos do Grupo Itararé no extremo sul da Bacia do Paraná / Julia Tedesco. – 2019.

124 f. : il. ; 30 cm.

Tese (doutorado) – Universidade do Vale do Rio dos Sinos, Programa de Pós-Graduação em Geologia, 2019.

"Orientadora: Dra. Joice Cagliari Co-orientador: Dr. Farid Chemale Júnior."

Dados Internacionais de Catalogação na Publicação (CIP)
(Bibliotecária: Amanda Schuster – CRB 10/2517)

Julia Tedesco

Tese de Doutorado apresentado como parte das exigências para a obtenção do título de Doutor, pelo programa ao Programa de Pós-Graduação em Geologia da Universidade do Vale do Rio dos Sinos.

Orientadora: Dra. Joice Cagliari

Co-orientador: Dr. Farid Chemale Júnior

São Leopoldo

2019

SUMÁRIO

1. Introdução

O Grupo Itararé registra a sedimentação na Bacia do Paraná durante a Late Paleozoic Ice Age. Seus depósitos apresentam idades principalmente do Pensilvaniano (Carbonífero superior). No extremo sul da Bacia do Paraná, o Grupo Itararé apresenta uma sucessão lateral de fácies complexa, com espessura variável, baixa continuidade lateral e preservação ruim dos afloramentos, dificultando o estudo dos seus depósitos. Desse modo, o Grupo Itararé ainda apresenta ainda várias questões em aberto: idade inicial de deposição, extensão das paleogeleiras, presença ou não de geleiras no período final de deposição, padrão de dispersão sedimentar atuante e como eram e se existiam conexões/influências das bacias do oeste da África com a região.

O objetivo dessa tese é analisar os sistemas de drenagem glacial no sul da Bacia do Paraná durante a Late Paleozoic Ice Age, identificando possíveis áreas fontes e padrões de distribuição dos sedimentos glacio-influenciados. A hipótese era que os paleofluxos de gelo vinham da África ocidental para o sul da Bacia do Paraná, com base em evidências como a configuração paleogeografica, paleocorrentes, pavimentos estriados, e a direção dos paleovales, tanto do Brasil como do oeste da Namíbia.

Para alcançar os objetivos da tese foram feitas descrições das fácies sedimentares do Grupo Itararé e da base da Formação Rio Bonito, elaboração de seções estratigráficas, além da coleta e preparação de 22 amostras de rocha sedimentar. As amostras foram analisadas para geoquímica de rocha total (FRX) e os zircões detríticos coletados foram datados por isótopos de U-Pb.

Como resultado, são apresentados dois manuscritos que compõem os produtos finais da tese: o primeiro, intitulado **“Late Paleozoic Ice Age rhythmites in the southernmost Paraná Basin: a sedimentological and paleoenvironmental analysis”**,

submetido a Journal of Sedimentary Research (Qualis CAPES A2), apresenta a caracterização sedimentológica e paleoambiental das fácies rítmicas, que constituem uma das mais importantes fácies do Grupo Itararé. Esse manuscrito fornece a base do arcobouço sedimentar para o manuscrito 2. O segundo manuscrito, intitulado **"Provenance and paleogeography in Southern Paraná Basin: geochemistry and U-Pb zircon geochronology of the Carboniferous-Permian transition"**, submetido a Sedimentary Geology (Qualis CAPES A2), apresenta um estudo de proveniência do Grupo Itararé e base da Formação Rio Bonito, reconstruindo as áreas fontes e padrões de dispersão sedimentar atuantes no extremo sul da Bacia do Paraná durante esse período.

2. Manuscrito I

LATE PALEOZOIC ICE AGE RHYTHMITES IN THE SOUTHERNMOST PARANÁ BASIN: A SEDIMENTOLOGICAL AND PALEOENVIRONMENTAL ANALYSIS

JULIA TEDESCO[1], JOICE CAGLIARI[1], CAROLINA DANIELSKI AQUINO[2]

[1] *Programa de Pós-Graduação em Geologia, Universidade do Vale do Rio dos Sinos, Av. Unisinos, 950, CEP 93022-000, São Leopoldo-RS, Brazil*

[2] *Departamento de Geologia, Universidade Federal do Paraná, Caixa Postal 19001, 81531-980, Curitiba, PR, Brazil*

ABSTRACT: Fine-grained rhythmite is a recurrent sedimentary facies in glacially-influenced marine and lacustrine sequences throughout geological time. Paleoenvironmental interpretation of these ancient deposits has been a challenged since similar rhythmites may have formed in different depositional contexts. In the Paraná Basin, the Itararé Group contain numerous successions of fine-grained rhythmites, deposited in the Carboniferous during the Late Paleozoic Ice Age (LPIA). Thus, the purpose of this study is: (i) to characterize sedimentological aspects of different rhythmites of the Itararé Group in southern Paraná Basin, and (ii) interpret their depositional environments. The described rhythmites are characterized by the intercalation of fine-grained sandstones and siltstones with clay and clayey siltstones. We have identified two distinct types of rhythmites based on the contact between couplets, couplets thickness, sedimentary structures, and geochemical proxies. Rhythmites type 1 is characterized by intercalation of very fine-grained sandstone/siltstone (60-90%) with claystone (40-10%) and normal grading. Rhythmites type 2 is characterized by couplets of siltstone (50%) and claystone (50%), with a sharp contact within couplets. Rhythmites

type 1 is interpreted as turbidity current deposits and type 2 as distal deposits of hypopycnal flow. Geochemical proxies suggest deposition of the rhythmites under marine conditions, in a period of rising temperatures and humidity, and with intensified chemical weathering. These paleoenvironment characteristics are in agreement with the interglacial period. The preservation of thick rhythmite successions of the Itararé Group in the southern basin was controlled by the constant creation of accommodation space inside paleovalleys.

INTRODUCTION

Rhythmically-laminated sediments (rhythmites) are intercalations or repetitions between two or more lithologies (e.g., Duff et al. 1967; Reineck and Singh 1973; Einsele and Seilacher 1982; Talbot and Allen 1996), in case of fine-grained rhythmites, silt and clay. Rhythmites are deposited by contour currents, tidal currents, turbidity currents, or suspension settling from glacier meltwater plumes (Mackiewicz et al. 1984; Ó Cofaigh and Dowdeswell 2001). Changes in the orbital parameters have been described as one of the factors controlling the long-term deposition of rhythmites (e.g., Einsele and Seilacher 1991), and seasonal climatic changes, the short-term deposition (annual) (De Geer 1912; Zolitschka et al. 2015).

Fine-grained rhythmites are common in glacially-influenced marine and lacustrine sequences throughout geological time. They have been described in the Quaternary (Powell 1981; Syvitski et al. 1985; Cowan and Powell 1990; Eyles 1993; Larsen and Stalsberg 2004), late Paleozoic (LPIA) (Visser 1997; Milana and Lopez 1998), and late Proterozoic (Willians 1998; Crowell 1999) sequences. They are abundant in proglacial environments where high sediment concentrations of silt and clay, and regular changes in discharge facilitate their formation (Cowan and Powell 1990). Rhythmites of glacially-influenced environments can provide a range of paleoenvironmental, paleoclimatic and

palaeoglaciological information (Ó Cofaigh and Dowdeswell 2001; Zolitschka et al. 2015). However, interpret their genesis is a difficult task since different depositional environments may imprint the same sedimentological characteristics (Eyles et al. 1988; Ó Cofaigh and Dowdeswell 2001).

In the Paraná Basin, fine-grained rhythmite is one of the most characteristics facies of the Itararé Group, the unit deposited under glacial influence during the Carboniferous. It has been the subject of several sedimentological studies (Santos et al. 1996; Caetano-Chang and Ferreira 2006; Netto et al. 2009; Franco et al. 2011, 2012; Lima et al. 2015; Brandt et al. 2016), however, a few studies were carried out in the rhythmites of the southern basin (Silveira 2000; Silva and Azambuja Filho 2005a, b). These rhythmites have subtle sedimentological differences, which, along with facies associations, allow the inference of distinct processes. Characterize the different rhythmites is important because of its implications in the paleoenvironment interpretation as the former ice-sheet extension and glacial period duration. Therefore, the aims of this paper are (i) to describe the sedimentological aspects and spatial distribution of the Itararé Group rhythmites in the southernmost Paraná Basin, and (ii) to interpret their depositional environments.

GEOLOGICAL SETTING

The Paraná Basin is an intracratonic basin of the Gondwana paleocontinent, located on the South American platform (Milani et al. 2007). The Itararé Group corresponds to the basal succession of a transgressive-regressive unit, the Gondwana I Supersequence (Milani 1997).

The basement of the Itararé Group in the southern Paraná Basin is composed of igneous, sedimentary, and metamorphic rocks with ages ranging from the Paleoproterozoic to the Ordovician (Chemale Jr. 2000). Basement rocks feature a

paleotopography characterized by valleys, in which the sediments of the Itararé Group were deposited (D'Elboux and Paiva 1980; Piccoli and Bortuluzzi 1981; Lopes 1995; Santos et al. 1996; Tedesco et al. 2016).

Glacial influenced deposits of the Itararé Group have a complex lateral succession of facies, which makes the regional correlation a complex task. In the southern part of the basin (study area, Fig. 1), the low degree of outcrop preservation and the limited lateral continuity increase the difficulty in studying these deposits. In addition, the Itararé Group succession in southern basin is much thinner (thicker succession is ~ 180 m in the Mariana Pimentel paleovalley, Tedesco et al. 2016) than in the rest of the basin, where thickness reaches up 1,400 m (basin depocenter in São Paulo State, Santos et al. 1996).

The Itararé Group shows a regional onlap from north to south (Milani and Ramos 1998), suggesting only the final phases of glaciation (Beurlen et al. 1953; Schneider et al. 1974; Machado 1994; Buso et al. 2018) or the post-glacial stage (Iannuzzi et al. 2010; Fedorchuk et al. 2018) is preserved in the southern basin. In this part of the basin, the Itararé Group is mainly characterized by siltstone, rhythmite, shale, fine-grained sandstone, and diamictite (Schneider et al. 1974). The depositional environment has been attributed to glacially-influenced lacustrine and marine systems in prior studies (Paim et al. 1983; Holz and Dias-Flor 1984; Dias 1993; Silveira 2000).

In the study area (Fig. 1), rhythmites were previously grouped into four classes according to the sandstone/siltstone and claystone ratio of the couplets, and interpreted as varve and turbidite (Silveira 2000). Silveira (2000) and Holz (1995) associated the fining- and thinning-upward nature of the rhythmites succession with gradual increase in distance from the source area, caused by the relative sea level rise or the decrease in flow competence.

Climate cyclicity was previously interpreted to have controlled the deposition of the rhythmites with abrupt contact between couplets (Holz, 1995), and solar cycles were previously interpreted to have influenced the deposition of rhythmites with normal grading (Silva and Azambuja Filho 2005a, b). Besides that, Milankovitch and Bond cycles were also identified in the record, pointing to a millennial time scale for the deposition of the couplets (Franco et al. 2012; Brandt et al. 2016). Preliminary results, obtained from spectral reflectance data, show that the cyclicity recorded in the normal grading rhythmites, in the study area, are likely explained by changes in the orbital parameters (Kochhann et al. 2017).

MATERIALS AND METHODS

In this study, 10 cores (held by CPRM - Geological Survey of Brazil 1982; Aboarrage and Lopes 1986) and two outcrops (Capané and Morro do Papaléo) were analyzed, covering the Mariana Pimentel, the Leão, and the Capané paleovalleys (Fig. 1). Macroscopic facies analysis was focused in the rhythmites, with the description of sedimentary structures, couplets thickness, and lithological boundaries between and within them, in this latter case supported by petrographic analyses of thin sections. From the facies and gamma-ray profiles analysis, a stratigraphic section was constructed, having as datum a maximum flooding surface within the Itararé Group.

A total of 14 samples of sedimentary rocks were collected in the lower, middle, and upper portions of Itararé Group (see Fig. 1 and Tab. S1- supplementary material). Sampling facies correspond to rhythmites, siltstones, sandstones, heteroliths, and conglomerates. The samples were ground in a ring mill apparatus and submitted for fluorescence spectroscopy (XRF) (Bureau Veritas Mineral Laboratories - Canada) in order to obtain whole rock geochemistry of major, minor, trace, and rare earth elements (REE). Geochemical proxies (C-value, CIA, K/Al, Rb/K, V/Sc, and Al/Si ratios) were

used to obtain information about paleoenvironmental conditions: weathering, redox, salinity, temperature, and source area proximity.

RESULTS

Sedimentary Facies

Description.---The Itararé Group succession, in the study area, is characterized, from base to top, by conglomerates, sandstones, rhythmites, and shales (see Table S1 – supplementary materials). Rhythmites have different characteristics of contact type between couplets (rhythmite pair), silt and clay proportion, couplets thickness, and sedimentary structures. Therefore, we have divided the Itararé Group rhythmites into two types: type 1 and type 2 (Fig. 2).

Rhythmite type 1 is characterized by couplets of very fine-grained sandstone or siltstone (light to off-white/gray) and claystone (light to medium gray) (Fig. 2A-H and 4). Fine-grained sandstone or siltstone corresponds to 60-90% of the couplet thickness, however the sandstone/claystone rate decrease upward producing a darker rhythmite (Fig. 2E and H). At the top of the succession, claystone reaches up to 80% of the couplets thickness. Couplets are internally normally graded (rarely sharp, Fig. 2H) with a sharp basal contact (subtle erosional surface) (Fig. 2A-D). At the base of the couplet, subtle plane-parallel lamination occurs in a 0.5 mm- to 3 cm-thick laminae of very fine-grained sandstone locally with carbonate cementation (diagenetic processes). Pebbles and granules are rare, but when present they have a diameter of ~4 cm, and sometimes they deform the underlying laminae (Fig. 2G). Rare bioturbation occurs at the top of the couplet (in the claystone laminae), represented by small horizontal structures (burrows) (Fig. 2F). Throughout this facies, the grain size and the couplets thickness decrease

upward, from 9.5 to 0.2 cm (finning- and thinning-upward, Fig. 2D and Fig. 4). The maximum thickness of this facies is 35 m at the SL-01-RS core.

Rhythmite type 2 is characterized by couplets of siltstone (50%, light to medium gray) and claystone (50%, light to dark gray) (Fig. 3A-F and Fig. 4). Internal contact between siltstone and claystone is sharp, as well as between couplets (Fig. 3A, E and F). This is a structureless facies with rare granules and pebbles (< 2 cm in diameter, Fig. 3B-D) disturbing the lamination. Bioturbation is not common, but when present shows low ichnodiversity and small horizontal burrows (smaller than 5 mm). Thin fine-grained sandstone laminae may occur within couplets (forming triplets) increasing the couplet thicknesses up to 5 cm. Different from the rhythmite type 1, type 2 shows more regular couplets thickness (Fig. 3A and F), ranging between 0.1 and 3 cm. This facies succession is usually thinner than 60 cm in cores, however, in the Capané outcrop, it can reach 4 m.

Interpretation.---*Rhythmite type 1* characteristics suggest deposition from bottom-current flow regime. The variable couplet thicknesses and sharp contact between couplets suggest that each couplet is a single depositional event, where the heavy fraction (silt) is deposits before, and the lighter fraction in suspension decanted after the current dissipation. The basal sharp contact of each couplet is likely the result of the uniform and rapid settling of the coarsest grains. The couplets normal grading is the reflection of the passive nature of the deposition and the waning flow (Shanmugam 1997). Therefore, based on all described evidences, this rhythmite is interpreted as the product of turbidity currents (Bouma 1962), in which silt laminae is Bouma division D and the normal grading to clay is settling of the lofting plume, Bouma division E. Thus, each couplet records the passage of a single turbidity current, with the deposition from current (siltstone) and the residual cloud of fine suspended material (claystone) (Kneller and McCaffrey 2003).

The gradual decrease in grain size (fining-upward) and couplets thickness (tinning-upward) upward of the type 1 rhythmite succession, reflect the decrease in sedimentation rate caused by a gradual distancing from the feeder system, controlled by either the gradual creation of accommodation space or decrease in sediment supply (Phillips et al., 1991; Cowan et al. 1999; Ó Cofaigh and Dowdeswell 2001). These trends suggest that the depositional environment was far away from the sediment source, likely in deep-water settings.

The sharp contact within couplets of the *rhythmite type 2* indicates that the siltstone and claystone laminae were deposited from independent depositional events, alternating over time. Fine-grained sandstone forming triplets indicate episodes of higher hydrodynamic energy. Regular thickness, grain size, and massive dominant structure, suggest the deposition of these facies from hypopycnal flow, related to distal regions from sediment plume spreading (Ó Cofaigh and Dowdeswell 2001). All characteristics are compatible with the central area of a water body or offshore in open marine settings, both under low energy conditions (Ashley 1975; Caetano-Chang and Ferreira 2006). Thus, a low energy hydrodynamic environment, with low rates of sediment supply or a restricted area.

Facies succession and stratigraphy

The Itararé Group succession has a lower portion with finning- and thinning-upward trend, followed by a coarsening-upward package on top. This is seen both in the vertical succession of facies and gamma-ray logs of Figure 5.

The lower succession is characterized, from base to top, by conglomerates and/or fine-grained sandstones overlaid by rhythmites. The thickness of this succession reaches up 80 m but is highly variable, likely reflecting the irregular paleorelief of the basement.

In the Leão-Mariana Pimentel paleovalley the fine-grained sandstone facies predominates over the rhythmites, and in the Capané the opposite occurs. Is worth to mention that rhythmite type 2 is constrained to the Capané paleovalley, while type 1 predominates in the Leão-Mariana Pimentel paleovalley. Considering the rhythmites were deposited by turbidity current and distal hypopycnal flow, and the conglomerate and fine-grained sandstone by more proximal depositional processes (Tab. S1), the lower succession records a transgressive system tract (TST), likely controlled by the sea level rise caused by the deglaciation. The topmost rhythmite has a greater proportion of clay, as seen by the higher values of gamma-ray, marking a maximum flooding surface (MFS) or zone, used here as a datum for core correlation.

The upper succession is mainly characterized by shale and heterolithic facies, with plant debris and vitrinite laminae. In the Leão-Mariana Pimentel paleovalley occurs an alternation of shale and heterolithic facies, while in the Capané, occurs the alternation of shale and rhythmites. The top of the upper succession is marked by coarser-grained facies like as sandstones. The entire succession of facies suggests the decrease in the water depth, more proximal depositional processes, thus we have interpreted as the record of a high-stand system tract (HST).

Geochemical Proxies

Geochemical results for the Itararé Group samples are presented in Table S1 and Figure 6. According to the C-value (Fig. 6A), the aridity prevails throughout the Itararé Group deposition, however, most of the rhythmites were deposited in semiarid and semiarid to semimoist climate. Semiarid to semimoist rhythmites coincide with the top of TST, and the semiarid with the top of the HST (Fig. 6A). CIA and K/Al seems to be robust indicators of chemical weathering intensities. Both present a similar pattern, with chemical weathering increasing upward within each system tract (Fig. 6B and C). Low

CIA values at the base of the TST is explained by the arid conditions, whereas high CIA values point to rising temperatures and humidity during the deposition of rhythmites, in agreement with the C-values curve. Besides that, the increase in CIA and K/Al ratios can be related to factors other than climatic, as a depositional environment becoming closer to the source area (shorter sediment transport distances) and/or an additional change in provenance (e.g., Scheffler 2006; Vögeli et al. 2017).

Rb/K and Al/Si ratios increase upward in each system tract (Fig. 6D and F), indicating salinity and clay-rich increase, respectively. According to Rb/K ratios, the basal system tracts were deposited in a freshwater-brackish conditions, likely controlled by the increase in the melting water inflow in the paleovalley, and the rhythmites under marine conditions. The increase in Rb/K ratios could be connected an increase in chemical weathering, linked to higher clay minerals content (Scheffler et al. 2006). CIA, C-Value and Al/Si values (Fig. 6B) show a similar trend to Rb/K ratios. High Al/Si rates in the rhythmites samples suggest high proportions of clay, and thus a low energy environment. V/Sc ratio shows all samples would be deposited in the oxic zone (Fig. 6E), with the exception of the rhythmites on top of both system tracts which were deposited in suboxic zone, condition likely controlled by the deepening water column.

DISCUSSION

Rhythmite - paleoenvironmental and paleoclimatic considerations

Fine-grained rhythmites deposit in a stable environment with periodic changes in hydrodynamic energy (power of flow or discharge) and sediment supply (e.g. Talbot and Allen 1996). The siltstone is linked to periods of water flow increased, while the claystone to periods under low sediment supply (Ashley 1975; Cowan et al. 1998b). Glacial influence is usually imprinted in the rhythmites periodicity controlled by meltwater

discharges events (Talbot and Allen 1996). Tidal regimes (Mackiewicz et al. 1984; Cowan and Powell 1990; Smith et al. 1990; Dowdeswell 2000) or fluvial input influenced by orbital cyclicity (e.g., Franco et al. 2011, 2012; Brandt et al. 2016) can also imprint periodicity in the rhythmites deposition, besides the annual climatic cycle (summer-winter).

The Itararé Group rhythmites type 1 and 2 are interpreted here as turbidites and distal hypopycnal flow deposits, respectively. Rhythmites type 1 interpretation is in agreement with previous studies, which describe a distal turbidite of a delta system (Lavina and Lopes 1987; Gama Jr. et al. 1992; Santos et al. 1996; Silveira 2000; Vesely and Assine 2004; Vesely et al. 2006; D'Ávila 2009). In this context, sediment input is associated to increasing water flow periods, caused either by a thaw, floods in the feeding rivers and beyond steep slopes, mainly in the Mariana Pimentel palleovalley that presents the valley walls near the depositional site.

The depositional environment of the Itararé Group rhythmites is still an issue in discussion, if whether it is deposited in a marine or lacustrine environment. Previous studies interpreted the Itararé Group rhythmites in the study area as of glacially-lacustrine origin (Corrêa da Silva 1978; Piccoli and Bortoluzzi 1981; Tomazelli and Soliani Jr. 1982; Paim et al. 1983; Dias 1993; Silveira 2000). On the other hand, the occurrence of the algae Tasmanites, Leiosphaeridia sp., and Acritarchs microplankton and ichnology data suggests an environment subject to salinity variations (Dias 1993; Lermen 2006; Smaniotto et al. 2006, Projeto Paraná Sul 2014). Marine sedimentation at the top of the Itararé Group is attributed to the marine transgression at the end of glaciation in southern Paraná Basin (Delaney and Goni 1963; Corrêa da Silva 1978; D'Elboux and Paiva 1980; Silveira 2000).

In this study, we have pieces of evidences of a brackish to a marine environment. First, rhythmite type 1 show normal grading which is usually associated to deposition in saltwater or brackish environment, due the flocculation of clays (Syvitski et al. 1985; Cowan and Powell 1990; Cowan et al. 1998; Ó Cofaigh and Dowdeswell 2001; Caetano-Chang and Ferreira 2006; Meiburg and Kneller 2010; Yawar and Schieber 2017). The occurrence of rare ichnofossils and low ichnodiversity in all types of rhythmites described here suggest an environment with significant stress (Powell 1983; Balistieri 2003; Buatois et al. 2006; Ó Cofaigh and Dowdeswell 2001; Zolitschka et al. 2015), what can indicate salinity variations. However, this information has to be used with caution once core samples analyses could lead to a false impression of absence or low index of bioturbation. Bioturbation is small and restricted to the top of the couplets, thus sometimes they are not visible in vertical profiles. Besides that, its position on the top of the couplet may indicate rapid deposition or high deposition rates (Stow 1984). Finally, the last evidence is the results of the Rb/K proxies indicating that most of the rhythmites (as such as other facies) has ratios compatible with brackish water and a few of them with marine water. `

Although the Itararé Group was deposited in the Carboniferous (Cagliari et al. 2016; Griffis et al. 2018) under the LPIA, evidence of the direct influence of ice on sediment deposition was not found in the described sedimentary facies, suggesting that the glaciers were distant from the depositional site. According to Fedorchuk et al. (2018 in press), there is no clear evidence for glaciation in the Leão-Mariana Pimentel paleovalley. However, several features recording glaciers action are preserved at the base of the Itararé Group in the Capané paleovalley, like as grooved surfaces, erratic blocks, and trail marks of granite clasts in unconsolidated sediments (see Tomazelli and Soliani Jr. 1982, 1997). Besides these ice-related erosional landforms, glacial context is also suggested by faceted

and striated clasts in the conglomerate in both Leão-Mariana Pimentel and Capané paleovalleys.

Conglomerates facies at the TST base, contain faceted and striated clasts but do not present features that would be expected with overriding of the substrate by the ice sheet (e.g. shear stress, sediment deformation). Therefore, the conglomerate facies described here can indicates resedimentation of glacially influenced material. The sparse lonestones present in the rhythmite facies could be transported either by icebergs, small ice rafts, fall from paleovalleys walls or by plant fragments (see Bennett et al. 1996), however, plant debris were not observed in these facies. The small size of the outsized clasts (granules and small pebbles), does not suggest direct ice action but instead indicates these dropstones were carried by floating ice, likely related to seasonal ice (ice rafts) (Gilbert 1990).

Based on CIA and K/Al proxies, rhythmites samples were deposited under intense chemical weathering conditions, which point towards an interglacial period. CIA values of <60 in the basal facies evidence physical weathering dominant at base of TST. The increase the CIA, C-Value and Rb/K values towards the top of the transgressive system tract, is probably linked to milder climate and increased chemical weathering during glacial retreat, as observed for the in a nearby region (Fedorchuk et al. 2019) and in the Karoo and Kalahari Basin (Scheffler 2003, 2006). However, C-values indicate arid conditions along the Itararé Group succession (the same results of Goldberg and Humayun 2010), with semiarid to semimoist climate, restricted to the top of TST and HST. Moreover, the absence of glacial evidence and the presence of plant debris in the HST succession corroborates a milder climate.

Rhythmites of the lower Itararé Group (eastern Paraná Basin) were associated with ice advance cycles deposited during maximum ice advance (Vesely et al. 2018). However,

316 the rhythmites of the study area are likely deposited in the interglacial period, linked to
317 the final deglaciation of the LPIA. Paraná and Karoo basins rhythmites are common in
318 the top of deglacial sequence (Visser 1997; Santos et al. 1996; Vesely and Assine 2006;
319 Vesely et al. 2015; Buso et al. 2017), which corresponds to the transgressive system tract
320 (TST) or maximum flood zone (Elrick and Hinnov 2007). The good preservation of the
321 rhythmites (absence of erosion) suggests deposition in relatively deep waters, but still
322 oxic or suboxic environment according to the V/Sc proxy (Fig. 6D). The couplets regular
323 thickness of rhythmite type 2 corroborates this interpretation, in distal environments fine-
324 grained sediments are more evenly distributed, resulting in more regular thicknesses
325 (Stevens 1990; Milana and Lopez 1998). In shallower waters, the preservation potential
326 of these deposits is very low, due to reworking of sediments by autochthonous agents,
327 such as waves, currents generated by wind, storms, the influence of local sediment supply,
328 and disturbances by biological agents (Smith and Ashley 1985; Zolitschka et al. 2015).
329 However, rhythmites levels in the northern basin, based on ichnological signatures, were
330 interpreted as deposited in very shallow water (Balistieri et al. 2003; Gandini et al. 2007;
331 Ricardi-Branco et al. 2016; Noll and Netto 2018).

332 *Paleorelief insights*

333 Pennsylvanian paleogeography of the southern Paraná Basin was characterized by
334 coastal physiography cut by valleys (palaeodepressions) (Mau 1960; D'Elboux and Paiva
335 1980; Piccoli and Bortuluzzi 1981; Lopes 1995; Santos et al. 1996; Tedesco et al. 2016).
336 Itararé Group corresponds to the basal succession in most of the paleovalleys, like as the
337 Capané, Leão, and Mariana Pimentel (Fig. 7). The paleovalley shape, size, depth, and
338 proximity to the paleocoast have influenced the sediment deposition, resulting in a
339 complex stratigraphy for the Itararé Group.

The isopachs reconstruction of the Itararé Group make paleovalleys visible in Figure 7C (Lopes 1995). Mariana Pimentel is a narrow valley (~2.5 km wide) extending over more than 60 km in the NW-SE direction. It is interpreted as a paleofjord by Paim et al. (1978), Silveira (2000), and Tedesco et al. (2016), and a tectonic valley by Fedorchuk et al. (2018). This valley is connected to the Leão paleovalley (Fig. 7C), a broader valley, reaching 20 km in width in some areas. Leão and Mariana Pimentel paleovalleys are narrower and more confined than the Capané paleovalley (Fig. 7 A and B), which resembles a bay with more than 40 km in width and is separated from the Leão paleovalley by a high in the basement (Fig. 7C).

Mariana Pimentel paleovalley preserves the largest sedimentary succession of the Itararé Group, more than 180 m, while in the Capané paleovalley this unit has about 80 m thick. The restricted environment of Mariana Pimentel paleovalley seems to have contributed to the preservation of the thick sedimentary succession, as seen in the SL-01-RS (Mariana Pimentel Paleovalley, Fig. 5). On the contrary, the HST of the core IB-93-RS (Leão Paleovalley) was totally eroded (Fig. 5).

Mariana Pimentel paleovalley also preserve the thicker rhythmite succession (~40 m). Rhythmites type 1 and sandy facies (mainly fine-grained sandstone) predominate in the Leão-Mariana Pimentel paleovalleys, while the rhythmites type 2 and fine-grained facies (mainly shale) in the Capané paleovalley. This fact can be explained by the source area proximity in the Leão-Mariana Pimentel paleovalley, thus frequent sediments inflow pulses generating rhythmites with variable couplet thicknesses (Fig. 7A). In the more distal environment, Capané paleovalley, there is less influence of the paleocontinent, generating rhythmites with regular and millimeter thickness (Fig. 7B).

Paleovalleys provide the development of a restricted depositional environment, increasing the preservation potential of sediments. According to Dowdeswell et al. (2000)

and Ó Cofaigh and Dowdeswell (2001), rhythmites are more preserved in bays and fjords, than in high-latitude open-marine settings. This palaeogeographic setting explains the absence of higher-energy processes deposits (e.g., Milana and Lopez 1998). Higher preservation potential is also controlled by the increase of accommodation space, which is in turn controlled by subsidence and eustasy. Carboniferous-Permian transition was a period of low tectonic activity (Limarino and Spalletti 2006), marked in the Paraná Basin by a long phase of subsidence (Milani and Ramos 1998). Low subsidence rates during the deposition of the Itararé Group, 9-30 m/Ma (Milani 1997; Milani and Ramos 1998) are likely compensated by the base-level rise during deglaciation in Paraná basin.

CONCLUSIONS

This study provides new sedimentological data that allow a better understanding of the genesis of glacially-influenced fine-grained rhythmites in southern Paraná Basin. From this study, the following conclusions were obtained:

- Rhythmite type 1 records deposition of turbidity currents. Each couplet is the results of a single turbidity current, in which silt laminae is the Bouma division D, and the normal grading to clay is settling of the lofting plume, Bouma division E. Thinning-upward trend suggests decreasing in sedimentation rates, with distance from source due to the transgressive system tract.
- Rhythmites type 2 records deposition of distal hypopycnal flow. Clay laminae was developed during longer periods of scarce or absence of sediment supply, from small particles that remained in suspension.
- Geochemical proxies suggest interglacial conditions during glacial retreat for the rhythmite deposition, with increasing chemical weathering processes, likely

related to milder temperatures and humidity. Rhythmites were deposited in a period of rise of the base level, under marine-brackish-water conditions.

– The preservation of these fine-grained rhythmites is controlled by the paleovalley configuration, which provided a more restricted and protected environment. Low subsidence rates during the deposition of the Itararé Group are compensated by base-level rise during deglaciation in Paraná basin.

ACKNOWLEDGEMENTS

The authors thanks to the project 'Contribution to updating chronostratigraphic knowledge in Sedimentary Basins' coordinated by Prof. Renata G. Netto, for financial support. Authors also thanks to the Geological Survey of Brazil (CPRM), for providing the core samples, and to the Technological Institute of Micropaleontology (ITT Fossil). J. Tedesco thanks to the 'Coordenação de Aperfeiçoamento de Pessoal de Nível Superior (CAPES)' for the scholarship. J. Cagliari thanks to FAPERGS [ARD/PPP 16/2551-000274-6].

REFERENCES

Aboarrage, A.M., and Lopes, R. da C., 1986, Projeto A borda leste da Bacia do Paraná: interpretação geológica e avaliação econômica, DNPM/CPRM, Porto Alegre, 18 p.

Ashley, G.M., 1975, Rhythmic sedimentation in glacial Lake Hitchcock, Massachusetts-Connecticut, Glaciofluvial glaciolacustrine Sediment, p. 304–320.

Balistieri, P.R.M.N., Netto, R.G., and Lavina, E.L.C., 2003, Icnofauna de ritmitos do topo da Formação Mafra (Permo-Carbonífero da Bacia do Paraná) em Rio Negro, Estado do Paraná (PR), Brasil, *in* Buatois, L.A., Mángano, M.G. (Eds.), Icnología: Hacia uma convergencia entre geología y biología. Publicación Especial de la Asociación Paleontológica Argentina 9, Buenos Aires, p. 131–139.

412 Bennett, M.R., Doyle, P., and Mather, A.E., 1996, Dropstones: their origin and
413 significance. Palaeogeogr. Palaeoclimatol. Palaeoecol., v. 121, p. 331–339.
414 https://doi.org/10.1016/0031-0182(95)00071-2

415 Beurlen, K., 1953, Estratigrafia e Paleogeografia das Formações Gondawanicas no sul do
416 Brasil - Notas Preliminares e Estudos da divisão de Geologia e Mineralogia, v. 59, p. 1-
417 9.

418 Bouma, A. H., 1962, Sedimentology of some Flysch deposits: a graphic approach to
419 facies interpretation. Amsterdam; New York: Elsevier Pub. Co.

420 Brandt, D., Franco, D., Ernesto, M., Franco, P.V.P., Zhao, X., Weinschütz, L., and Garza,
421 R.M., 2016, Paleomagnetism and cyclostratigraphy of upper-carboniferous glacial
422 rhythmites of mafra formation, Paraná Basin, Brazil., Latinmag Letters v. 6, p. 1–5.

423 Buatois, L.A., Netto, R.G., Mángano, M.G., and Balistieri, P.R.M.N., 2006, Extreme
424 freshwater release during the late Paleozoic Gondwana deglaciation and its impact on
425 coastal ecosystems. Geology v. 34, p. 1021–1024, https://doi.org/10.1130/G22994A.1

426 Buso, V.V., Aquino, C.D., Paim, P.S.P, Souza, P.A, Mori, A.L., Fallgatter, C., Milana,
427 J.P., and Kneller, B., 2017 (In press), Late Palaeozoic glacial cycles and subcycles in
428 western Gondwana: Correlation of surface and subsurface data of the Paraná Basin,
429 Brazil, Palaeogeography, Palaeoclimatology, Palaeoecology.

430 Caetano-Chang, M.R., Ferreira, S.M., 2006. Ritmitos de itu: Petrografia e considerações
431 paleodeposicionais. Geociencias 25, 345–358.

432 Cai, J., Powell,R. D., Cowan, E.A., Carlson, P.R., 1997, Lithofacies and seismic-
433 reflection interpretation of temperate glacimarine sedimentation in Tarr Inlet, Glacier
434 Bay, Alaska, Marine Geology v. 143, p. 1-4.

435 Cagliari, J., Philipp, R.P., Buso, V.V., Netto, R.G., Klaus Hillebrand, P., da Cunha Lopes,
436 R., Basei, M.A., and Faccini, U.F., 2016, Age constraints of the glaciation in the Paraná
437 Basin: evidence from new U–Pb dates, J. Geol. Soc. London. 173, p. 871–874.
438 https://doi.org/10.1144/jgs2015-161

439 Campbell, F.A., and Williams, G.D., 1965, Chemical composition of shales of Mannville
440 Group Lower Cretaceous of Central Alberta, Canada, AAPG Bulletin v. 49, p. 81–87.

441 CPRM - Serviço Geológico do Brasil, 1982, Programa Carvão energético estado do Rio
442 Grande do Sul – Relatório Final, Porto Alegre, p. 22- 312.

443 Chemale Jr. F. 2000, Evolução geológica do Escudo Sul-rio-grandense, *in* Holz M. and
444 De Ros L.F. (Eds), Geologia do Rio Grande do Sul, Centro de Investigação do Gondwana,
445 Porto Alegre: Universidade Federal do Rio Grande do Sul, p. 13-52.

446 Clift, P.D., Wan, S., and Blusztajn, J., 2014, Reconstructing chemical weathering,
447 physical erosion and monsoonintensity since 25 Ma in the northern South China Sea: A
448 review of competing proxies, Earth-Science Reviews v. 130, p. 86–102.

449 Corrêa da Silva, Z.C., 1978, Observações sobre o Grupo Tubarão no Rio Grande do Sul
450 com especial destaque à estratigrafia da Formação Itararé, Rev. Pesquisas Inst. Geoc.,
451 Universidade Federal do Rio Grande do Sul v. 9, p. 9-61.

452 Cowan, E.A., Cai, J., Powell, R.D., Seramur, K.C., and Spurgeon, V.L., 1998, Modern
453 tidal rhythmites deposited in a deep-water estuary. Geo-Marine Lett. V. 18, p. 40–48.
454 https://doi.org/10.1007/s003670050050

455 Cowan, E.A., and Powell, R.D., 1990, Suspended sediment transport and deposition of
456 cyclically interlaminated sediment in a temperate glacial fjord, Alaska, U.S.S.

457 Glacimarine Enviornments Process, Sediments. Geol. Soc. Spec. Publ. v. 53, p. 1689–
458 1699. https://doi.org/10.1017/CBO9781107415324.004

459 Cowan, E.A., Seramur, K.C., Cai, J., and Powell, R.D., 1999, Cyclic sedimentation
460 produced by fluctuations in meltwater discharge, tides and marine productivity in an
461 Alaskan fjord, Sedimentology v. 46, p. 1109–1126. https://doi.org/10.1046/j.1365-
462 3091.1999.00267.x

463 Crowell, J.C., 1999, Pre-Mesozoic Ice Ages: Their Bearing on Understanding the Climate
464 System, p. 1-79.

465 D'Avila, R.S.F., 2009, Seqüências deposicionais do Grupo Itararé (Carbonífero e
466 Eopermiano), Bacia do Paraná, na área de Dr. Pedrinho e cercanias, Santa Catarina,
467 Brasil: turbiditos, pelitos e depósitos caóticos, Tese de Doutorado, São Leopoldo, p.159-
468 200.

469 Delaney, P. J. V., and Goni, J. 1963, Correlação preliminar entre as formações
470 godwânicas do Uruguai e Rio Grande do Sul, Brasil, Boletim Paranaense de Geografia,
471 Curitiba: AGB v. 9, p. 3-21.

472 D'Elboux, C.V, and Paiva, I.B., 1980, Bacias Residuais: proposição de uma nova unidade
473 prospectiva uranífera no Escudo Sul-Rio-Grandese, *in* Geology brazilian congress 31,
474 Camboriú, SBG. V. 4, p. 2437-2445.

475 De Geer, G., 1912, A geochronology of the last 22,000 years, *in* CONGRÈS International
476 de Géologie, 11, Stockolm, Comptes Rendus, Stockolm, p. 24-258.

477 Dias, M.E.R., 1993, Palinologia do Grupo Itararé no Rio Grande do Sul, Porto Alegre,
478 PhD Thesis, Univ. Federal do Rio Grande do Sul, Porto Alegre, 227 p.

Dowdeswell, J.A., Whittington, R.J., Jennings, A.E., Andrews, J.T., Mackensen, A., and Marienfeld, P., 2000, An origin for laminated glacimarine sediments through sea-ice build-up and suppressed iceberg rafting, Sedimentology v. 47, p. 557–576. https://doi.org/10.1046/j.1365-3091.2000.00306.x

Duff, P. M. D., Hallam, A., and Walton, E. K., 1967, Cyclic sedimentation, Amsterdam, Elsevier.

Einsele, G., and Seilacher, A., 1982, Cyclic and event stratification, Berlin, Springer-Verlag, 536 p.

Einsele, G. and Seilacher, A., 1991, Distinction of tempestites and turbidites, *in* G. Einsele, W. Ricken and A. Seilacher (Editors), Cycles and Events in Stratigraphy, Springer, Berlin, p. 377-382.

Eyles, N., 1993, Earth's glacial record and its tectonic setting, Earth Sci. Rev. v. 35, p. 1–248. https://doi.org/10.1016/0012-8252 (93)90002-O

Eyles, N., Eyles, C., and Miall, A.D., 1988, Geology Glacial facies models, Geology v. 16, p. 374-375. https://doi.org/10.1130/0091-7613 (1988)016<0374

Elrick, M. and Hinnov, L.A., 2007, Millennial-scale paleoclimate cycles recorded in widespread Palaeozoic deeper water rhythmites of North America, Palaeogeography Palaeoclimatology Palaeoecology v. 243, p. 348-372.

Fedorchuck, N.D., Isbell, J.L., Griffis, N.P, Montanez, I. P., Vesely, F.F., Iannuzzi, R., Mundil, R., Yin, Q., Pauls, K.N., and Rosa, L.M., 2018 (In Press), Origin of paleovalleys on the Rio Grande do Sul Shield (Brazil): Implications for the extent of late Paleozoic glaciation in west-central Gondwana, Palaeogeography Palaeoclimatology Palaeoecology. https://doi.org/10.1016/j.palaeo.2018.04.013

Fedorchuck, N.D., Isbell, J.L., Griffis, N.P, Vesely, F.F., Rosa, L.M., Montanez, I. P., Mundil,R., Yin, Q., Iannuzzi, R., Roesler,G., and Pauls, K.N., 2019, Carboniferous glaciotectonized sediments in the southernmost Paraná Basin, Brazil: Ice marginal dynamics and paleoclimate indicators, Sedimentary Geology v. 389, p. 54-72. https://doi.org/10.1016/j.sedgeo.2019.05.006

Franco, D.R., Hinnov, L.A., and Ernesto, M., 2011, Spectral analysis and modeling of microcyclostratigraphy in late Paleozoic glaciogenic rhythmites, Paraná Basin, Brazil, Geochemistry, Geophys. Geosystems v. 12, p. 1–15. https://doi.org/10.1029/2011GC003602

Franco, D.R., Hinnov, L.A., and Ernesto, M., 2012, Millennial-Scale climate cycles in Permian-Carboniferous rhythmites: Permanent feature throughout geologic time? Geology v. 40, p. 19–22. https://doi.org/10.1130/G32338.1

Gama Jr., E.G., Perinotto, J.A.J., Ribeiro, H.J.P.S., and Padula, E.K., 1992, Contribuição ao estudo da ressedimentação no Subgrupo Itararé: tratos de facies e hidrodinâmica deposicional, Revista Brasileira de Geociências v. 22, p. 228-236.

Gandini, R., Netto, R.G., and Souza, P.A., 2007. Paleoicnologia e a palinologia dos ritmitos do Grupo Itararé na pedreira de Águas Claras (Santa Catarina, Brasil), Gaea v. 3, p. 47–59.

Gilbert, R., 1990, Rafting in glacimarine environments, *in* J.A. Dowdeswell and J.D. Scourse (Editors), Glacimarine Environments: Processes and Sediments, Geol. Soc. Spec. Publ. v. 53, p. 105-120.

Goldberg, K., and Humayun, M., 2010, The applicability of the Chemical Index of Alteration as a paleoclimatic indicator: An example from the Permian of the Paraná Basin,

525 Brazil, Palaeogeogr. Palaeoclimatol. Palaeoecol. v. 293, p. 175–183.
526 https://doi.org/10.1016/j.palaeo.2010.05.015

527 Holz, M., 1995, Análise estratigráfica do intervalo gonduanico basal (Eo-Permiano) na
528 região nordeste do Rio Grande do Sul - um exercicio de estratigrafia. Porto Alegre, Tese
529 de Doutorado, UFRGS.

530 Holz, M., 1999, Early Permian sequence stratigraphy and the palaeophysiographic
531 evolution of the Paraná Basin in southernmost Brazil, Journal of African Earth Sciences
532 v. 29, p. 51–61.

533 Holz, M., and Dias-Flor, M.A., 1984, Análise estratigráfica da Formação Rio Bonito
534 (Permiano Inferior) na área de Cachoeira do Sul, *in* SBG, Congresso Brasileiro de
535 Geologia, 33, Anais, Rio de Janeiro, p. 993-1006.

536 Iannuzzi, R., Scherer, C.M.S., Souza, P.A., Holz, M., Caravaca, G., Adami-Rodrigues,
537 K., Tybusch, G.P., Souza, J.M., Smaniotto, L.P., Fischer, T.V., Silveira, A.S., Lykawka,
538 R., Boardman, D.R., and Barboza, E.G. 2010, Afloramento Morro do Papaléo, Mariana
539 Pimentel, RS. Registra ìmpar da sucessão pós-glacial do Paleozóico da bacia do Paraná,
540 *in* Winge, M., et al., (Eds). Sítios Geológicos e paleontologicos do Brasil, v. 2, p. 321-
541 336.

542 Kneller, B. C., and McCaffrey, W. D., 2003, The interpretation of vertical sequences in
543 turbidite beds: the influence of longitudinal flow structure, Journal of Sedimentary
544 Research, v. 73, p. 706-713. https://doi.org/10.1306/031103730706

545 Kochhann, M.V.L., Cagliari, J., Souza, M.K., Aquino, C.D., Tedesco, J. and Vieira, L.,
546 2017, Cyclostratigraphic analysis of reflectance spectroscopy data in the carboniferous
547 rhythmites of the Itararé Group, Paraná Basin, Brazil, *in* X SIMPÓSIO SUL-

548 BRASILEIRO DE GEOLOGIA, 10, Curitiba - PR. Anais, Curitiba. Sociedade Brasileira
549 de Geologia - Núcleo Paraná.

550 Jones, B., and Manning, D.C., 1994, Comparison of geochemical indices used for the
551 interpretation of paleo-redox conditions in Ancient mudstones, Chemical Geology, v.
552 111, p. 111–129.

553 Larsen, E., and Stalsberg, M.K., 2004, Younger Dryas glaciolacustrine rhythmites and
554 cirque glacier variations at Kråkenes, western Norway: Depositional processes and
555 climate, Journal Paleolimnol., v. 31, p. 49–61.
556 https://doi.org/10.1023/B:JOPL.0000013282.14240.e5

557 Lavina, E.L.C., and Lopes, R.d.C., 1987, A transgressão Marinha do Pemiano Inferior e
558 a Evolução Paleogeográfica do Supergrupo Tubarão no estado do Rio Grande do Sul,
559 Paula Coutiana, v. 1, p. 51–103.

560 Lermen, R., 2006, Assinaturas icnológicas em depósitos glaciogênicos do Grupo Itararé
561 no RS. M.S. Thesis, Universidade do vale do Rio dos Sinos São Leopoldo, 84 p.

562 Lima, J. H.D., Netto, R.G., Corrêa, C.G., and Lavina, L.E.C., 2015, Ichnology of
563 deglaciation deposits from the Upper Carboniferous Rio do Sul Formation (Itararé Group,
564 Parana Basin) at central-east Santa Catarina State (southern Brazil), Journal of South
565 American Earth Sciences v. 63, p. 137-148.
566 http://dx.doi.org/10.1016/j.jsames.2015.07.008

567 Limarino, C., Spalletti, L.A., 2006, Paleogeography of the upper Paleozoic basins of
568 southern South America: an overview, Journal of South American Earth Sciences v. 22,
569 p. 134–155. https://doi.org/10.1016/j.jsames.2006.09.011

570 Lopes, R. da C., 1995, Arcabouço Aloestratigráfico para o Intervalo "Rio Bonito-
571 Palermo" (Eopermiano da bacia do Paraná), entre Butiá e São Sepé, Rio Grande do Sul,
572 São Leopoldo, Dissertação de Mestrado, Centro de Ciências Tecnológicas da
573 Universidade do Vale do Rio dos Sinos, São Leopoldo, 254 p.

574 Lowe, D. R., 1982, Sediment gravity flows; 2, Depositional models with special reference
575 to the deposits of high-density turbidity currents, Journal of Sedimentary Petrology, v.
576 52, p. 27-297.

577 Machado, M.A.P., 1994, O Degelo final permiano e o seu registro geológico na borda
578 sudeste da Bacia do Paraná (Paleovale de Candiota-RS), Ph.D. Dissertation, Univ.
579 Federal do Rio Grande do Sul, Porto Alegre, 165 p.

580 Mackiewicz, N.E., Powell, R.D., Carlson, P.R., and Molnia, B.F., 1984, Interlaminated
581 ice-proximal glacimarine sediments in Muir Inlet, Alaska, Mar. Geol. v. 57, p. 113–147.
582 https://doi.org/10.1016/0025-3227 (84)90197-X

583 Mau, H., 1960, Vale Pré-glacial ao Norte de Lavras do Sul, RGB, Boletim da Sociedade
584 Brasileira de Geologia v. 9, p. 79-82.

585 Meiburg, E., and Kneller, B., 2010, Turbidity Currents and Their Deposits, Annu. Rev.
586 Fluid Mech. v. 42, p. 135–156. https://doi.org/10.1146/annurev-fluid-121108-145618

587 Milana, J.P., and Lopez, S., 1998, Solar cycles recorded in Carboniferous glacimarine
588 rhythmites (Western Argentina): Relationships between climate and sedimentary
589 environment, Palaeogeogr. Palaeoclimatol. Palaeoecol. v. 144, p. 37–63.
590 https://doi.org/10.1016/S0031-0182(96)00037-5

591 Milani, E.J., 1997, Evolução Tectono-estratigráfica da Bacia do Paraná e seu
592 Relacionamento com a Geodinâmica Fanerozóica do Gondwana Sul-ocidental, Porto
593 Alegre, M.S. Thesis, Univ. Federal do Rio Grande do Sul, Porto Alegre. 255 p.

594 Milani, E.J., Henrique, J., Melo, G. De, Souza, P.A. De, Fernandes, L.A., and França,
595 A.B., 2007, Bacia do Paraná. Bol. Geociências da Petrobras v. 15, p. 265–287.

596 Milani, E., and Ramos, V.A., 1998, Orogenias paleozoicas no domínio sul-ocidental do
597 Gondwana e os ciclos de subsidência da Bacia do Paraná, Revista Brasileira de
598 Geociências v. 28, p. 527-544. DOI: 10.25249/0375-7536.1998473484

599 Mulder, T., and Alexander, J., 2001. The physical character of subaquaeous sedimentary
600 density flows and their deposits, Sedimentology v. 48, p. 269–299.
601 https://doi.org/10.1046/j.1365-3091.2001.00360.x

602 Nesbitt, H.W., and Young, G.M., 1984, Prediction of some weathering trends of plutonic
603 and volcanic rocks based on thermodynamic and kinetic considerations, Geochimica et
604 Cosmochimica Acta v. 48, p. 1523-1534.

605 Netto, R.G., Balistieri, P.R.M.N., Lavina, E.L.C., and Silveira, D.M., 2009, Ichnological
606 signatures of shallow freshwater lakes in the glacial Itararé Group (Mafra Formation,
607 Upper Carboniferous-Lower Permian of Paraná Basin, S Brazil), Palaeogeogr.
608 Palaeoclimatol. Palaeoecol. v. 272, p. 240–255.
609 https://doi.org/10.1016/j.palaeo.2008.10.028

610 Noll, S.H., and Netto, R.G., 2018, Microbially induced sedimentary structures in late
611 Pennsylvanian glaciais settings: A case study from the Gondwanan Paraná Basin, Journal
612 of South American Earth Sciences v. 88, p. 385-398.
613 https://doi.org/10.1016/j.jsames.2018.09.010

Ó Cofaigh C. O. and Dowdeswell, J.A., 2001, Laminated sediments in glacimarine environments: diagnostic criteria for their interpretation, Quaternary Science Reviews v. 20, p.1411-1436.

Paim, P.S.G., Piccoli, A.E.M., Sarturi, J.A.D., Munaro, P., Holz, M., and Granitoff, W., 1983, Evolução paleogeográfica do Supergrupo Tubarão na área de Mariana Pimentel-Faxinal, Guaíba, RS, SBG, Simp. Sul-Brasileiro Geol. v. 1, p. 121–134.

Phillips, A.C., Smith, N.D., and Powell, R.D., 1991, Laminated sediments in prodeltaic deposits, Glacier Bay, Alaska, *in* Anderson, J. B., and Ashley, G. M., eds., Glacial marine sedimentation, Paleoclimatic significance: Boulder, Colorado, Geological Society of America Special Paper, 261p.

Piccoli, A.E.M., and Bortoluzzi, C.A., 1981, Paleogeografia das Sequências Itararé e Rio Bonito (Permiano inferior) – Região Carbonífera de Santa Maria, RS. *in* Curitiba Regional Symposium, SBG, p. 125-146

Pickering, K.T., Hiscott, R.N., and Hein, F.J., 1989, Deep marine environments: clastic sedimentation and tectonics, Unwin Hyman Ltd, p. 416.

Powell, R.D., 1981, A model for sedimentation by tidewater glaciers, Annals of Glaciology v. 2, p. 129-134.

Powell, R.D., 1983, Glacial marine sedimentation processes and lithofacies of temperate tidewater glaciers, Glacier Bay, Alaska, *in* Molnia, B.F. (ed.) Glacial-Marine Sedimentation, p. 195-232.

Projeto Paraná Sul, 2014, Influência dos lineamentos regionais na organização estratigráfica da Bacia do Paraná no extremo Sul do Brasil: reavaliação dos dados de

superfície e subsuperfície, Universidade do vale do rio dos sinos - PROFEX PETROBRAS.

Reading, H.G. and Collinson, J.D., 1996, Clastic Coasts, *in* Reading, H.G. Ed., Sedimentary Environments: Process, Facies and Stratigraphy, Blackwells, Cornwall, p. 154-231.

Reineck H. E., and Singh I.B., 1980, Depositional Sedimentary Environments, 2° ed. New York, Springer-Verlag, 549 p.

Ricardi-Branco, F., Rohn, R., Longhim, M.E., Costa, J.S., Martine, A.M., and Christiano-DeSouza, I.C., 2016, Rare Carboniferous and Permian glacial and non-glacial bryophytes and associated lycophyte megaspores of the Paraná Basin, Brazil: A new occurrence and paleoenvironmental considerations, Journal of South American Earth Sciences, v. 72, p. 63-75. https://doi.org/10.1016/j.jsames.2016.07.014

Santos, P. R., Rocha-Campos, A.C., and Canuto, J. R., 1996, Patterns of Late Paleozoic deglaciation in the Paraná Basin, Brazil, Palaeogeography Palaeoclimatology Palaeoecology, Amsterdam, v. 125, p. 165-184. https://doi.org/10.1016/S0031-0182(96)00029-6

Schneider, A. W., Muhlmann, H., Tommasi, E., Medeiros, R., Daemon, R.R., and Nogueira, A.A., 1974, Revisão Estratigráfica da Bacia do Paraná, *in* Congresso Brasileiro de Geologia, 28, Porto Alegre, Anais, SBG 1, p. 41-65.

Shanmugam, G., 1995, Deepwater exploration, Conceptual models and their uncertainties, abstr.1, Nigerian Assoc. Pet. ExpIor. (NAPE) Off. Progr., 13th Annu. Int. Conf., Lagos, 45 p.

Shanmugam, G., 1997, The Bouma Sequence and the turbidite mind set, Earth-Science Rev. v. 42, p. 201–229. https://doi.org/10.1016/S0012-8252(97)81858-2

Scheffler, K., Hoernes, S., and Schwark, L., 2003, Global changes during Carboniferous–Permian glaciation of Gondwana: Linking polar and equatorial climate evolution by geochemical proxies, Geology v. 31, p. 605-608. doi: 10.1130/0091-7613(2003)031<0605:GCDCGO>2.0.CO;2.

Scheffler, K., Buehmann, D., and Schwark, L., 2006, Analysis of late Palaeozoic glacial to postglacial sedimentary successions in South Africa by geochemical proxies – Response to climate evolution and sedimentary environment v. 240, p. 184–203. https://doi.org/10.1016/j.palaeo.2006.03.059

Silva, J.G.R., and Azambuja Filho, N.C., 2005a, Cicloestratigrafiado eopermiano - estudo de caso no Grupo Itararé, bacia do Paraná (parte 1): uma metodologia para preparo ao de dados de perfil e rocha, Revista Brasileira de Geociencies, v. 35, p. 63-76.

Silva, J.G.R., and Azambuja Filho, N.C., 2005b, Estudo de caso no Grupo Itarare, Bacia do Parana (parte 2): evidencias de indução astronomica (orbital e solar) no clima e na sedimentação, Revista Brasileira de Geociências v. 35, p. 77-106.

Silveira, A.S., 2000, Estratigrafia de Seqüências e Evolução Paleoambiental da Sucessão Permiana (Sakmariano – Eokazaniano) da Bacia do Paraná, entre Rio Pardo e Mariana Pimentel (RS), M.S. Thesis, Univ. do Vale do Rio dos Sinos, 140 p.

Smaniotto, L.P., Fischer, T. V, Souza, P.A., and Iannuzzi, R., 2006, Palinologia do morro do Papaléo, mariana pimentel (permiano inferior, bacia do paraná), Rio Grande do Sul, Brasil, Distribution v. 9, p. 311–322.

680 Smith, N.D. and Ashley, G.M., 1985, Proglacial lacustrine environments, *in* Ashley,
681 G.M., Shaw, J. and Smith, N.D., editors, Glacial sedimentary environments, SEPM Short
682 Course, No. 16. Tulsa OK, Society of Paleontologists and Mineralogists, p. 135-215.

683 Smith, N.D., Phillips, A.C., and Powell, R.D., 1990, Tidal drawdown: a mechanism for
684 producing cyclic sediment laminations in glaciomarine deltas, Geology, v.18, p. 10-13.

685 Stevens, R.L., 1990, Proximal and distal glacimarine deposits in southwestern Sweden:
686 contrast in sedimentation, *in* J.A. Dowdeswell, J.D. Scourse (Eds.), Glacimarine
687 Environments: Processes and Sediments, Geological Society of London Special
688 Publication v. 53, p. 307-316.

689 Stow, D.A. V., 1979, Distinguishing between fine-grained turbidites and contourites on
690 the Nova Scotian deep-water margin, Sedimentology v. 26, p. 371-87.

691 Stow, D.A. V., and Piper, D.J.W., 1984, Deep-water fine-grained sediments: facies
692 models, Geol. Soc. London, Spec. Publ. v. 15, p. 611–646.
693 https://doi.org/10.1144/GSL.SP.1984.015.01.38

694 Stow, D.A.V., and Shanmugam, G., 1980, Sequences of structures in finegrained
695 turbidites: comparison of recent deep-sea and ancient flysch sediments, Sediment. Geol.
696 v. 25, p. 23–42.

697 Syvitski, J.P.M., Asprey, K.W., Clattenburg, D.A., and Hodge, G.D., 1985, The prodelta
698 environment of a fjord: suspended particle dynamics, Sedimentology v. 32, p. 83–107.
699 https://doi.org/10.1111/j.1365-3091.1985.tb00494.x

700 Talbot, M.R., and Allen, P.A., 1996, Lakes, *in* Reading, H.G., ed., Sedimentary
701 Environments: Processes, Facies and Stratigraphy: London, Blackwell Science, p. 83-
702 125.

Tedesco, J., Cagliari, J., Coitinho, J.D.R., da Cunha Lopes, R., and Lavina, E.L.C., 2016, Late Paleozoic paleofjord in the southernmost Parana Basin (Brazil): Geomorphology and sedimentary fill, Geomorphology v. 269, p. 203-214. https://doi.org/10.1016/j.geomorph.2016.06.035

Tomazelli, L.J., and Soliani Jr., E., 1982, Evidências de atividade glacial no Paleozóico superior do Rio Grande do Sul Brasil, Brazilian Geological Congress, 32, Salvador. SBG. v. 4, p. 1378–1391.

Tomazelli, L.J., and Soliani Jr., E., 1997, Sedimentary Facies and Depositional Environments Gondwana Glaciation in Batovi and Suspiro Regions, Journal of south America Earth Science v. 10, p. 295-303.

Vesely, F.F., 2006, Sistemas subaquosos alimentados por fluxos hiperpicnais glaciogenicos: Modelo deposicional para arenitos do Grupo Itararé, Permocarbonifero da Bacia do Parana, Bol. Geociências da Petrobras v. 15, p. 7–25.

Vesely, F.F., and Assine, M.L., 2004, Seqüências e tratos de sistemas deposicionais do Grupo Itararé, norte do estado do Paraná. Brazilian J. Geol. v. 34, p. 219–230.

Vesely, F.F., and Assine, M.L., 2006, Deglaciation sequences in the Permo-Carboniferous Itararé Group, Paraná Basin, southern Brazil, Journal of South American Earth Sciences v. 22, p. 156-168. https://doi.org/10.1016/j.jsames.2006.09.006.

Vesely, F.F., Trzaskos, B., Kipper, F., Assine, M.L., and Souza, P.A., 2015, Sedimentary record of a fluctuating ice margin from the Pennsylvanian of western Gondwana: Paraná Basin, southern Brazil, Sediment. Geol. v. 326, p. 45–63. https://doi.org/10.1016/j.sedgeo.2015.06.012

725 Vesely F.F., Rodrigues, M.C.N.L., da Rosa, E.L.M., Amato J.A., Trzaskos B., Isbell, J.L.,
726 and Fedorchuk, N.D., 2018, Recurrent emplacement of non-glacial diamictite during the
727 Late Paleozoic Ice Age, Geology, v. 46, p. 615-618. https://doi.org/10.1130/G45011.1.

728 Visser, J.N.J., 1997, Deglaciation sequences in the Permo-Carboniferous Karoo and
729 Kalahari basins of southern Africa: A tool in the analysis of cyclic glaciomarine basin
730 fills, Sedimentology v. 44, p. 507–521. https://doi.org/10.1046/j.1365-3091.1997.d01-
731 35.x

732 Vögeli, N., Najman, Y., Beek, P. V. D., Huyghe, P., Wynn, P. M., Govin, G., Veen, I. V.
733 D., and Sachse, D., 2017, Lateral variations in vegetation in the Himalaya since the
734 Miocene and implications for climate evolution. Earth and Planetary Science Letters v.
735 471, p. 1-9.

736 Wildner, W., Ramgrab, G. E., Lopes, R. da C., and Iglesias, C. M. da F., 2008, Mapa
737 Geológico do Estado do Rio Grande do Sul, Porto Alegre: CPRM, Mapa color, 110x166
738 cm, Escala 1:750.000, (Projeto Mapas Estaduais –PME), CD-ROM.

739 Willians, G.E., 1998, Precambrian tidal and glacial clastic deposits: implications for
740 Precambrian Earth-Moon dynamics and palaeoclimate, Sediment. Geol. v. 120, p. 55–74.
741 https://doi.org/10.1016/S0037-0738 (98)00027-X

742 Yawar, Z., and Schieber, J., 2017, On the origin of silt laminae in laminated shales.
743 Sediment. Geol. v. 360, p. 22–34. https://doi.org/10.1016/j.sedgeo.2017.09.001

744 Zhao, Z., J. Zhao, H. Wang, J. Liao, and C. Liu, 2007, Distribution characteristics and
745 applications of trace elements in Junggar Basin, Nat. Gas Explor, Dev., v. 30, p. 30-33.

746 Zolitschka, B., Francus, P., Ojala, A.E.K., and Schimmelmann, A., 2015, Varves in lake
747 sediments - a review, Quat. Sci. Rev., v. 117, p. 1–41.
748 https://doi.org/10.1016/j.quascirev.2015.03.019

749 **FIGURE CAPTIONS**

750 FIG. 1.--- A) Location of the Paraná Basin in South America and in the Rio Grande do
751 Sul state (black rectangle). B) Study area location in the Rio Grande do Sul state. C)
752 Simplified geological map of the study area (modified from Wildner et al. 2008), showing
753 cores and outcrops location. RS = Rio Grande do Sul State; SC = Santa Catarina State;
754 PB = Paraná Basin.

755 FIG. 2.--- Rhythmite type 1: A) couplets of siltstone and claystone with normal grading
756 and basal sharp contact (core SL-01-RS); B) couplet with normal grading, granules and
757 sand grains arranged in a distinct layer suggesting deposition in a small grain flow (core
758 SL-01-RS); C) couplet with normal grading (core AB-06-RS); D) couplet with normal
759 grading (core IB-93-RS); E) Sand grains and basal sharp contact seen in thin sections
760 (core SL-01-RS); F) granule of the couplet seen in thin sections (core SL-01-RS); G)
761 bioturbation between couplets (core IB-93-RS); H) pebble between couplets (core AB-
762 06-RS); I) sharp contacts between laminae (core IB-93-RS). NG- normal grading; GR-
763 granule; IC-ichnofossil; P-pebble; SG-sand grains.

764 FIG. 3.--- Rhythmites type 2: A) sharp contact within and between couplets, millimetric
765 thicknesses, and presence of pebble (core ST-08-RS); B) sharp contact within and
766 between couplets and granules deforming the lamination (core CA-72-RS); C) pebble
767 deforming lamination (core AC-21-RS); D) sharp contact within and between couplets,
768 millimetric thicknesses (core AC-72-RS); E) pebble deforming lamination in the Capané
769 outcrop sample; F and G) detail of petrographic thin sections showing the sharp contacts

within and between couplets, and the presence of quartz granules (Capané outcrop); AC-abrupt contact; GR-granule; P-pebble.

FIG. 4.---Schematic profile showing the characteristics of the vertical succession of the southern Paraná Basin rhythmites.

FIG. 5.--- Itararé Group vertical succession of facies. Radiometric dating of Cagliari et al. (2016). MFS = maximum flooding surface; HST= highstand system tract; TST= transgressive system tract.

FIG. 6.--- Geochemical proxies: A) C-Value ratio (Zhao et al. 2007); B) CIA - Chemical Index of Alteration (Nesbitt and Young 1982); C, D, E and F) K/Al, Rb/K, V/Sc and Al/Si ratios, respectively (Campbell and Williams 1965; Jones and Manning 1994; Clift et al. 2014). The samples were grouped in the core SL-01-RS according to their occurrence in stratigraphy of the Itararé Group, see Figure 5.

FIG. 7.---A-B) 3D depositional model of the rhythmites type 1 and 2. C) Paleotopography of the study area during the Itararé Group deposition period, formed by extensive paleovalleys (modified from Lopes 1995), with the position of the drill hole records used in this study. Ice-Paleoflow measured in from grooved surfaces (360°) by Tomazelli and Soliani Jr. (1982).

FIGURE

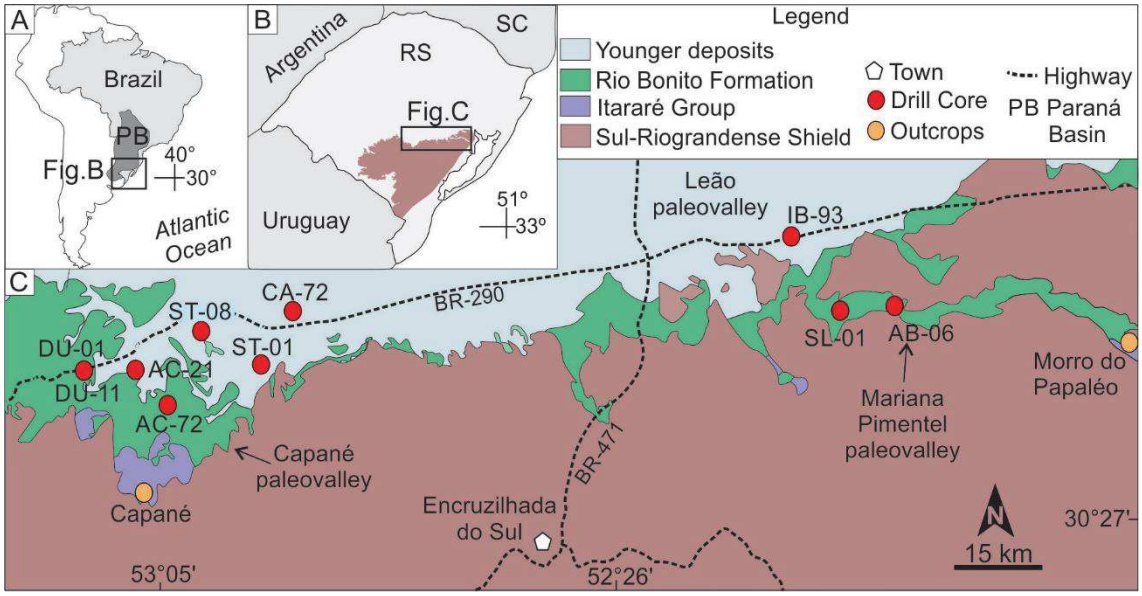

Figure 1

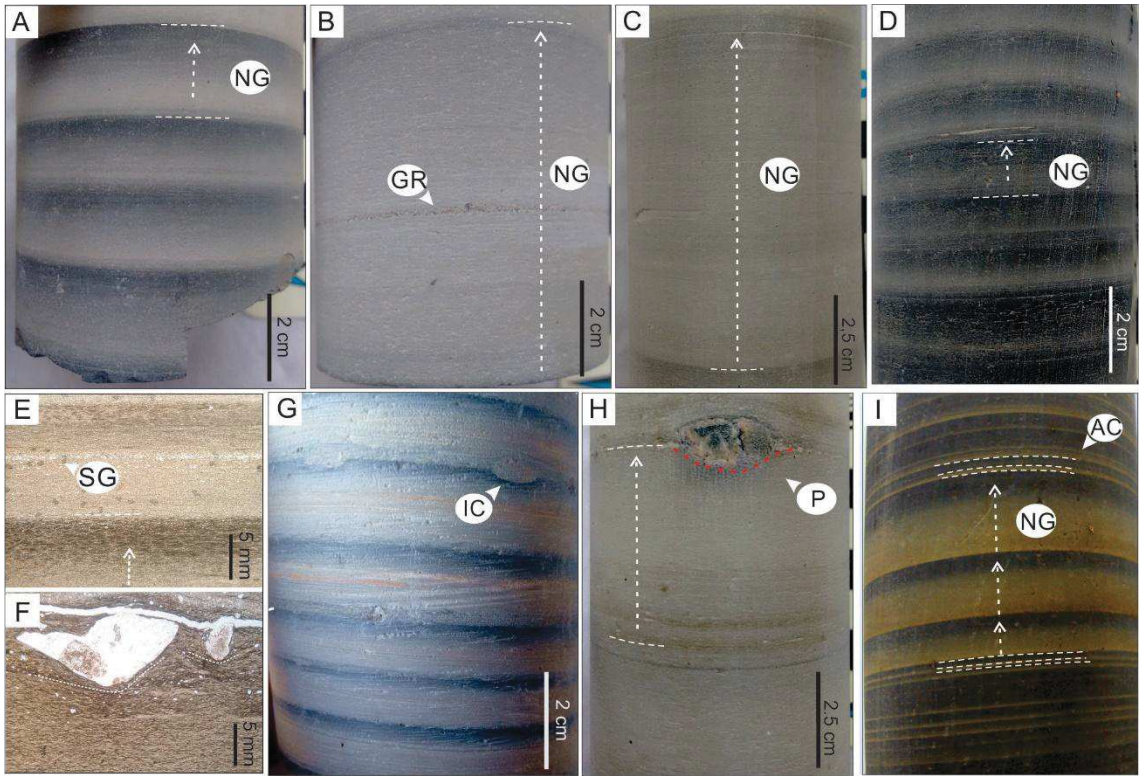

Figure 2

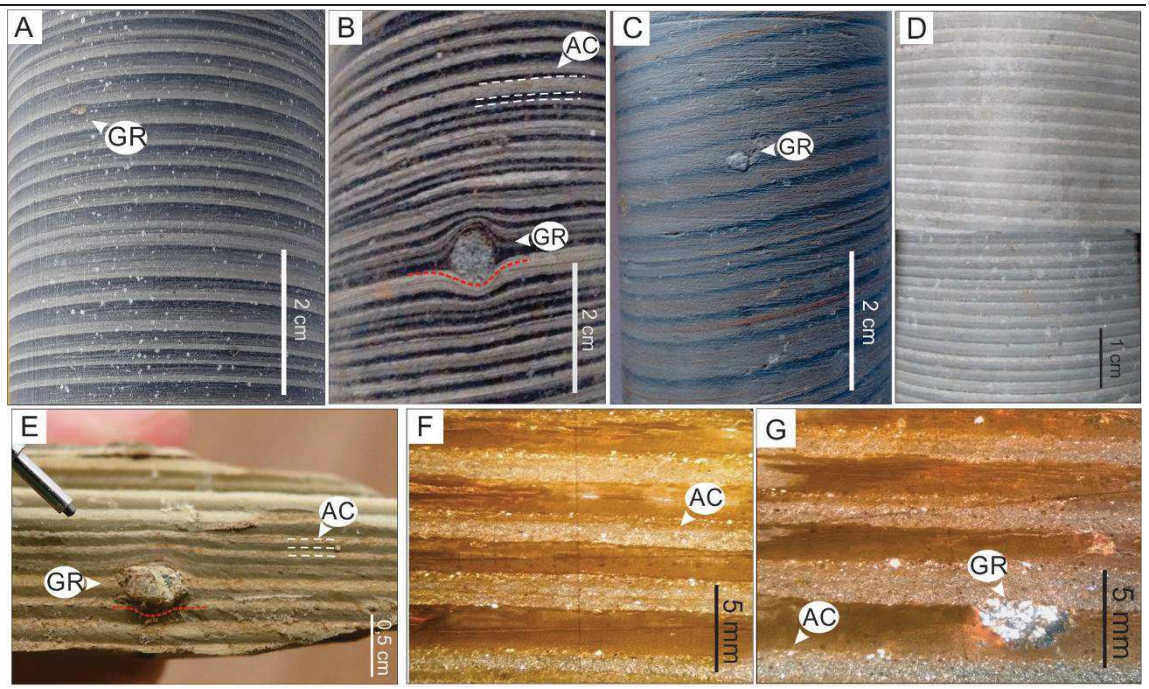

797

798 Figure 3

	Profile	Grain Size	Internal Contact	Couplet Contact	Sedimentary structures	Couplet thickness	Photos
Type 2	Clay / Silt	silt to clay 50% silt 50% clay	sharp	sharp	none	regular 1 - 0.1 cm	8 cm
Type 1		VF sand/ silt to clay 20-90% silt 10-80% clay	normal grading	sharp	subtle plane-parallel lamination at the base	irregular 9.5 - 0.5 cm	10 cm

799

800 Figure 4

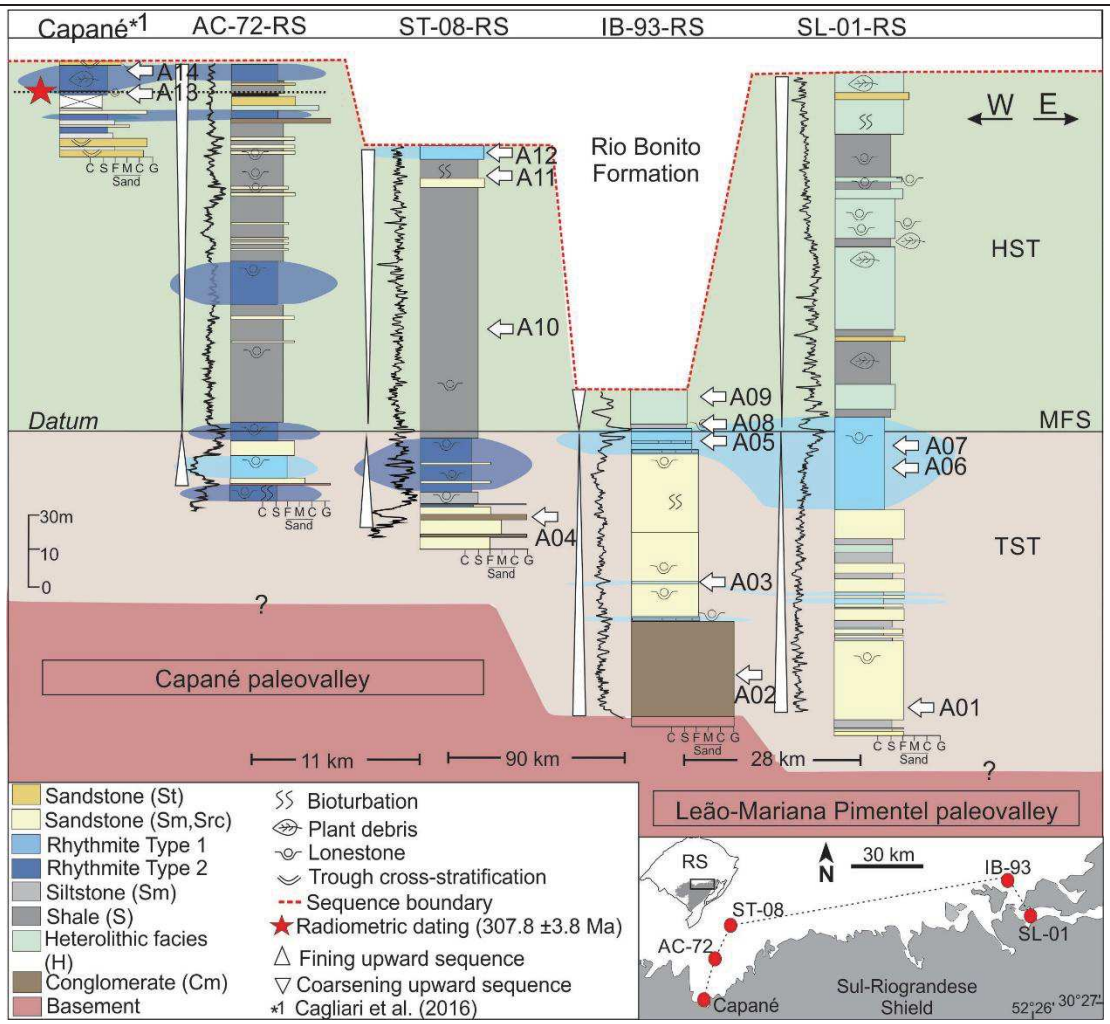

801

802 Figure 5

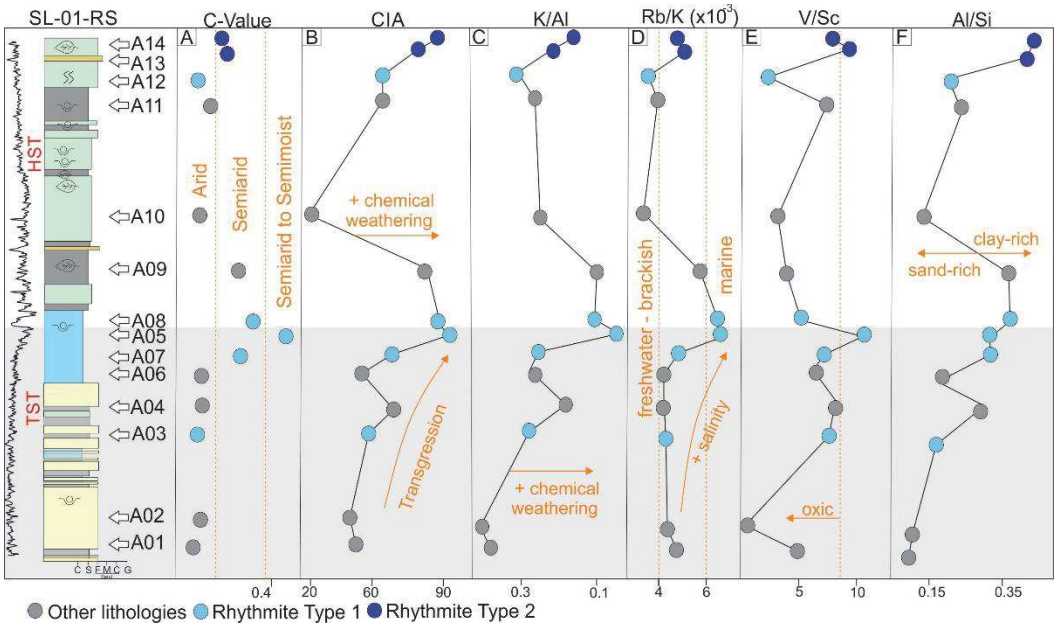

803

804 Figure 6

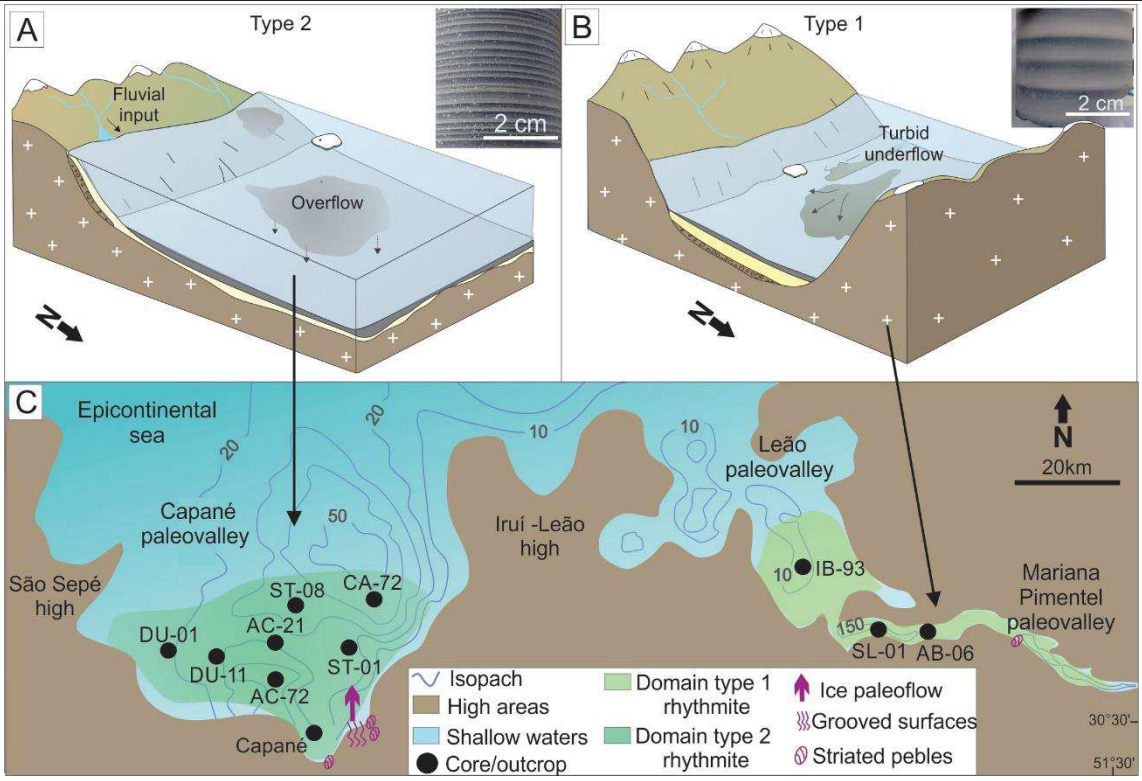

805

806 Figure 7

807

808

3. Comprovante de submissão - manuscrito I

Revista: Journal of Sedimentary Research

Situação: Em revisão

JSR 2019-090 Receipt of New Paper by the Journal of Sedimentary Research

jsedres@allentrack.net
Qua, 10/07/2019 09:48
Você; joiceca@unisinos.br; carol.d.aquino@hotmail.com; juliatedi@gmail.com

Dear Authors,

Manuscript 2019-090 entitled "Late Paleozoic Ice Age rhythmites in the southernmost Paraná Basin: a sedimentological and paleoenvironmental analysis", of which you are listed as a coauthor, has been approved for review by the Journal of Sedimentary Research.

You may check on the status of this manuscript by selecting the "Check Manuscript Status" link at the following URL:

https://sepm-jsr.allentrack.net/cgi-bin/main.plex?el=A5BE7CtJ1A6IER3F7A9ftdWqDvT2C4CTHhmR98D6mVWAZ

(Press/Click on the link above to be automatically sent to the web page. Please note that these links may be too long to fit on one line and may need to be pasted into your browser separately.)

Very sincerely,

Gary Hampson, Peter Burgess
Co-Editors
JSR

4. Manuscrito II

Provenance and paleogeography in Southern Paraná Basin: geochemistry and U-Pb zircon geochronology of the Carboniferous-Permian transition

Julia Tedesco[a]*, Joice Cagliari[a], Farid Chemale Junior[a], Tiago Girelli[a], Cristiano Lana[b]

[a] *Programa de Pós-Graduação em Geologia, Universidade do Vale do Rio dos Sinos, Avenida UNISINOS, 950, 93022-000 São Leopoldo, Rio Grande do Sul, Brazil*

[b]*Departamento de Geologia, Universidade Federal do Ouro Preto, Morro do Cruzeiro, 35400-000 Ouro Preto, Minas Gerais, Brazil*

**Corresponding autor*

E-mail address: julitdsco@hotmail.com (J. Tedesco)

Abstract

The sedimentary succession of the Carboniferous-Permian transition in the Paraná Basin records important information about climatic changes, tectonics, and paleogeographic configurations of SW Gondwana. During this period, the Late Paleozoic Ice Age was in its final phase in the Paraná Basin, giving space to a temperate-tropical climate during the transition to the Permian. With the objective of understanding the patterns of sedimentary dispersal, source area, and changes that occurred during this period, we coupled U-P laser ablation ICP-MS detrital zircon dating and whole-rock geochemistry of rocks of the Itararé Group and the lowermost Rio Bonito Formation in southern Brazil. Data from this study show that the rocks suffered various degrees of weathering, with rocks of the Itararé Group derived from an arid source area, and rocks from the Rio Bonito Formation derived from a hotter and more humid source area. The two units present similar source areas in terms of

composition and age, with principally felsic rocks of Neoproterozoic age. From the obtained data, it was possible to determine that from Late Carboniferous toearly Permian, the Uruguayan Sul-riograndese Shield source areas dominated the system. During the Late Carboniferous the southernmost portion of the Paraná Basin did not receive sediments from the African side as previously described. This suggests a more complex system with ice caps and small ice sheets dominated the glacial environment during the Late Carboniferous in this segment of the SW Gondwana

Keywords: Zircon U-Pb dating, Itararé Group, Rio Bonito Formation, Late Paleozoic Ice Age

1. Introduction

In the period between the Late Carboniferous and the early Permian, the southern hemisphere suffered large tectonic and climatic changes. The Late Paleozoic Ice Age (LPIA), one of the most significant ice ages in the history of Earth, was in its final phase, giving way to temperate and tropical climate conditions. The complex interaction between climatic and tectonic controls is considered responsible for the end of glaciation, including albedo rates, ocean-air circulation pathways, paleolatitude and continental topography changes, and changes in atmospheric CO_2 levels (Visser, 1996; Isbell et al., 2003; Scheffler et al., 2003; Veevers, 2004; Montanez et al., 2007; Goddéris et al., 2017).

The tectonic and climatic changes that occured between the Carboniferous and Permian altered the sedimentary conditions, sea level, paleocurrent patterns, degree and process of weathering and erosion, and the sedimentary provenance of basins in SW Gondwana. (Scheffler et al., 2003, 2006; Goldberg and Humayun, 2010). During this time interval the formation of a mountain chain on the southern margin of Gondwana initiated with the Gondwanides Orogeny (e.g. Trouw and De Wit, 1999; Milani and De

Wit, 2008). The development of this orogeny affected the evolution of peripheral intracratonic basins, altering the patterns of drainage and sedimentary dispersal. (Turner, 1999; Milani, 2007; Ramos et al., 2013, 2014; Canile et al., 2016).

Deposits of the Itararé Group and Rio Bonito Formation register the Carboniferous-Permian transition in the Paraná Basin. In the southern portion of the basin, the paleogeography, paleocurrents, striated pavements, grooved surfaces and the direction of paleovalleys suggest that during glaciation, paleoflow of ice could have contributed sediments from African basins and Precambrian crystalline basement to the Paraná Basin (Frakes and Crowell, 1970; Visser, 1987, 1993; Santos et al., 1996; Vesely et al., 2015, 2018; Tedesco et al., 2016; Assine et al., 2018; Andrews et al., 2019). Recent provenance studies performed on these units (Canile et al., 2016; Griffis et al., 2018; Craddock et al., 2019) defined the major source rocks for the sedimentation of the Itararé Group and Rio Bonito Formation.

In this study, we present new data of whole-rock (WR) geochemistry and U-Pb detrital zircon ages of sedimentary rocks from the Carboniferous-Permian transition, recorded in the Itararé Group and Rio Bonito formations located at southernmost Paraná Basin. The principal objective is to understand the sedimentary evolution and the climatic conditions during this transition in SW Gondwana. From the obtained results, it was possible to recognize the probable source areas of the Paraná Basin during this period, as well as the sedimentary dispersion. We suggest that during the Late Carboniferous there was not sedimentary contribution from African side.

2. Geological setting

Paraná Basin is an intracratonic basin, filled with sedimentary and volcanic rocks with ages from the Ordovician to the upper Cretaceous (Zálan et al., 1990; Milani

et al., 2007) and divided into six depositional supersequences (Milani, 1997). The study interval (Carboniferous-Permian) is part of the the third supersequence, composed of a transgressive-regressive cycle, denoted Gondwana I (Milani et al., 2007).

In the extreme south of the Paraná Basin, the sediments of the Gondwana I supersequence are deposited directly on the basement (Fig. 1). Sedimentation probably initiated during the Pennsylvanian under the influence of an LPIA ice sheet that was evolving with the milder climate in the transition to the Permian.

The Itararé Group records glacially-influenced deposits of the LPIA, principally recorded in glacially-influenced continental system at the base of the succession which evolved to glaciolacustrine and glaciomarine systems toward the top of the unit (Eyles et al., 1993; Santos et al., 1996; Vesely and Assine, 2006; Rocha-Campos et al., 2008). The deposits are predominantly composed of siltstones, rhythmites, shales, fine sandstones, and conglomerates (Schneider et al., 1974).

In the study area, the thickness of the Itararé Group is less than the rest of the basin and corresponds to the final glacial deposits (Schneider et. al., 1974; Machado, 1994; Valdez-Buso et al., 2017) or a post-glaciation phase (Iannuzzi et al., 2010). U-Pb dating in tonstein levels, principally in the Rio Bonito Formation (Frabris de Matos et al., 2001; Matos et al., 2001; Rocha-Campos et al., 2006; Guerra-Sommer et al., 2008; Cagliari et al., 2014, 2016; Griffis et al., 2018) indicate that sedimentation of the Itararé Group in the region was restricted to the Carboniferous (Cagliari et al., 2016).

The Guatá Group was deposited after the end of glaciation, in a marine transgressive context. The Rio Bonito Formation, at the base of the Guatá Group, was deposited in a transitional/shallow marine context, in principally deltaic, estuarine, barrier-lagoon, and shoreface paleoenvironments (Lavina et. al., 1985; Lopes, 1995; Holz et al., 2006). Deposits of this formation are principally composed of sandstones,

siltstones, conglomerates, coals, and quartz sandstones (Lavina and Lopes, 1987; Lopes, 1995). Radiometric dating at the base of the Rio Bonito formation indicates that deposition began in the Early Permian (Frabris de Matos et al., 2001; Matos et al., 2001; Rocha-Campos et al., 2006; Guerra-Sommer et al., 2008; Mori et al., 2012; Cagliari et al., 2014, 2016; Griffis et al., 2018).

3. Materials and methods

A total of 22 samples of sedimentary rocks were collected in the lower, middle, and upper portions of Itararé Group and base of the Rio Bonito Formation along the northern and western margins of the Sul-riograndese Shield, totalling 16 samples from core (CA-53-RS, ST-01-RS, SV-19-RS, IB-93-RS) and 6 from outcrop (Capané, and Morro do Papaléo) (see Fig. 1 and Tab. S1- supplementary material). The sampling levels correspond to rhythmites, siltstones, sandstones, heterolithic facies, and conglomerates.

The samples were ground in a ring mill apparatus. A fraction of the samples were submitted for flourescence spectroscopy (XRF) to the Bureau Veritas Mineral Laboratories (Canada) in order to obtain a WR geochemistry of major, minor , trace, and rare earth elements (REE). Zircon separation was made according to standard techniques, described in Supplementary File 1.

The zircons were dated using a laser ablation microprobe (*Photon-machines Excimer Laser 193*) coupled to a *Thermo-Fisher Element II* (HR-SF-ICP-MS). All of the analyses were made in the Laboratory of Isotope Geology at the Federal University of Ouro Preto (UFOP), Brazil. Five samples were sterile (JT-03, 07, 14, 16, and 17). Samples with few zircons (<35) were not considered, due to their low statistical

representation (see Vermeesch, 2004). A detailed description of methods used in this work is included in Supplementary File 1.

4. Results

4.1. Geochemistry

Geochemical results for rocks of Itararé Group and Rio Bonito Formations are presented in Table S2. The rocks of Itararé Group contain 52-80% SiO_2, while rocks of the Rio Bonito Formation contain higher concentrations of SiO_2 (68-86%), due to the dominance of sandstone lithologies. Siltstones, heterolithic facies, and rhythmites show enrichment in Al_2O_3 (>12%), due to a concentration of aluminous clay minerals. In terms of trace elements, the samples have high concentrations of Zr, Ba, Rb, V, Ni, and Sr, moderate to low concentrations of Hf, Cs, Co, and Nb, and low concentrations of Ta, Sn, and U.

Variable ratios of SiO_2/Al_2O_3 (Fig. 2A) suggests a frequently altered sedimentary environment, resulting in classifications of rocks such as shale, graywacke, subarkose and arkose sandstones. The units shows elevated values (Fig. 2B), with Th/Sc proportions comparable with UCC (~0.75). Elevated proportions of Zr/Sc (~10) suggests a degree of sedimentary reworking and recycling. The enrichment of Zr and Th indicates a felsic provenance (Bauluz et al., 2000). Low values of La/Th (1.59 to 5.06) (Fig. 2C), also suggest a UCC provenance with a dominantly felsic composition. Rocks of the Rio Bonito Formation show minor varation, with the presence of recycled sediments.

Itararé Group source area had a more arid climate (Fig. 2D), while the some of samples from the Rio Bonito Formation indicate a more humid climate. The Itararé Group contains two sets: one set with a moderate degree of weathering (~55), and one

145 set with a high degree of weathering (~80) in the samples closest to the transition
146 between the two units.

147 Four samples of the transition between the Rio Bonito-Itararé show that the arid
148 climate would persisted until the beginning of deposition of the Rio Bonito Formation.
149 Rocks of the Rio Bonito Formation show moderate to high degrees of weathering (Fig.
150 2E). On average, the rocks present moderate to high CIA values (55 to 80), suggesting
151 moderate to intense weathering and recycling in the source areas (Fedo et al., 1995).
152 The A-CN-K plot is also used to restrict the original composition of the source area
153 (Fedo et al., 1995), suggesting source areas felsic and intermediate igneous provinces
154 (granite to granodiorite) (Fig. 2E).

155 Concentration of REE show the units are distinguished in the diagrams (Fig. 2F
156 and Table S2). The rocks of the Rio Bonito Formation are poor in heavy REE (Gd, Tb,
157 Dy, Ho, Er, Tm, Yb, and Lu) and light REE (La, Ce, Nd, Pr, Nd, and Sm) in relation to
158 the UCC and the PAAS, and in the majority do not contain a negative EU anomaly. The
159 rocks of the Itararé Group present higher concentrations of REE in relation to the UCC
160 and the PASS, as well as a negative EU anomaly in almost all of the samples.

161 *4.2. U-Pb Detrital Zircon*

162 1011 detrital zircon grains were analyzed from 17 samples at the Permo-
163 Carboniferous limit (Fig. 3), whose results are presented in Table S3 (supplementary

164 *4.2.1. Itararé Group*

165 Figure 4 presents a general overview of the principal detrital zircon populations
166 found in the Itararé Group. 11 samples were dated, totalling 491 detrital zircon grains.
167 Neoproterozoic zircons were the principal population, representing 74% of the total.
168 The other 26% of zircons were distributed as follows: Cambrian (14%),

Paleoproterozoic (4%), Mesoproterozoic (3%), Archean (2%), Ordovician (2%), Carboniferous (1%), and Devonian (<1%). The peaks of the Neoproterozoic period, correspond predominantly to the Ediacaran, totaling 247 of the zircons of this age (65%). Other zircons of this age are from the Cryogenian (27%) and Tonian (8%).

Archean zircons occur in three samples, in the south of the area (JT-09 to 10), and the conglomerates (JT-9 and 13). Mesoproterozoic ages vary between 1028 and 1589 Ma. Paleoproterozoic zircons present ages between 1664 and 2215 Ma. Age peaks in the Cambrian vary between 507 and 541 Ma. Only one Silurian zircon (441 Ma) and two Devonian zircons (412 and 410 Ma) were encountered. Ordovician zircons vary between 447 and 483 Ma. Carboniferous zircons present minimum ages of 300 Ma.

4.2.2. Rio Bonito Formation

At the base of Rio Bonito Formation (Triunfo Member), five samples were dated totaling 520 zircons. As in the Itararé Group, detrital ages were predominantly Neoproterozoic, composing 79% of the analyzed zircons (Fig. 4). The other age peaks correspond to the Cambrian (7%), Ordovician (4%), Paleoproterozoic (3%), Mesoproterozoic (3%), Carboniferous (2%), Devonian (1%), Silurian (1%), and Archean (<1%). Within the Neoproterozoic, the Ediacaran age dominates, totaling 315 zircons (65% if the Neoproterozoic zircons). Of the remaining Neoproterozoic zircons, 11% present Tonian age and 24% present Cryogenian age.

Two zircons posses Archean ages (2631 to 3350 Ma), found in two samples of the southern area (JT-11 and 12). Mesoproterozoic age peaks vary between 1015 and 1560 Ma. Paleoproterozoic zircons present ages between 1673 and 2217 Ma. Cambrian zircons present ages between 490 and 541 Ma. Ordovician zircons present ages between 448 and 484 Ma. Silurian zircons present ages between 431 and 442 Ma. Devonian

zircons present ages between 370 and 411 Ma. The youngest zircons are from the Carboniferous, with ages between 304 and 358 Ma.

5. Discussion

5.1. Geochemical proxies

After source area, weathering is the principal control over chemical composition of sediments (Taylor and McLennon, 1985). Changes in weathering conditions between the Itararé Group and Rio Bonito Formation (Fig. 2D) reflect the different climatic settings of the two units. Itararé Group in the study region indicates deposition in a cold climate (glacially-influenced) until its top, which was previously established by paleo-humidity (CIA) data obtained by Goldberg and Humayun (2010). The cold, arid climate persisted until the initiation of deposition of the Rio Bonito Formation, was deposited in warm-humid conditions, with a dominance of chemical weathering, resulting in rocks with a high degree of chemical maturity.

The differences in REEs patterns between the Itararé Group and the Rio Bonito Formation may be due: 1) grain size influence REEs values. Sands, which dominate the Rio Bonito Formation, tend to have more variable contents with depletion in REEs, while finer lithologies, like those common in the Itararé Group, tend to present enrichment in REEs, as clay and silt contain the majority of REEs (Cullers et al., 1987); 2) differences in the degree and type of weathering suffered by the rocks, weathering in humid conditions (Rio Bonito Formation) could cause the fractionation of REE, while weathering in arid conditions (Itararé Group) would result in lower fractionation of REEs (Balashov et al., 1964; Cullers et al., 1987).

Negative EU anomaly present in rocks of the Itararé Group is a typical characteristic of detrital sedimentary rocks derived from UCC, indicating a

differentiated silicic (felsic) source (Condie, 1993; McLennan et al., 1993). Some rocks present greater affinity for sediment recycling, indicating the recycling of older sedimentary rocks. Therefore, rocks of the Rio Bonito Formation may be partially composed of sediments of the Itararé Group.

5.2. Rock sources

Zircon grains of Itararé Group and Rio Bonito Formation present similar peaks, and therefore the source areas will be analyzed together. The principal paleocurrents and striated pavements created during deposition of Itararé Group indicate that the most important source areas were located to the south and southeast (Bigarella et al., 1967; Frakes and Crowell, 1969; Tomazelli and Soliani Jr., 1982, 1997; Rocha-Campos et al., 1988; Trosdtorf et al., 2005; Fallgatter and Paim, 2017). Therefore, this analysis will focus on areas located to the south and southeast of the study area.

Archean zircons are present only in the southern region (core SV-19-RS). This distribution is in agreement with the proximity of these possible source areas: Santa Maria Chico granulitic complex (2500 - 3000 Ma) in the Sul-riograndense Shield and Nico Pérez Terrane (2500 - 3404 Ma) in Uruguay (Hartmann et al., 1999; Hartmann et al., 2001; Philipp et al., 2016; Oriolo et al., 2016; Girelli et al., 2018). Zircons of this age occur in some terranes of Africa, such as the Kalahari Craton, Kheis Terrane, Kaapvall Craton and Limpopo Belt (2600 - 2729 Ma.) (Van Niekerk, 2006; Schneiderhan et al., 2011).

Paleoproterozoic rocks are abundant in Sul-riograndense Shield and in Uruguay, including: Seival Metagranite (1750 - 1780 Ma), Arroio dos Ratos Complex (2000 Ma), Vigia Complex (2040 - 2050 Ma), Encantadas Complex (2000 - 2200 Ma), Santa Maria Chico Granulitic Complex (2000 - 2500 Ma) (Hartmann, 1998; Camozzato et al., 2013;

241 Phillipp et al., 2016; Girelli et al., 2018), Piedra Alta Terrane (2053 - 2202 Ma) and
242 Nico Pérez Terrane (1735 - 2500 Ma) (Sánchez Bettucci et al., 2004; Peel and
243 Preciozzi, 2006; Hartmann et al., 2008; Oriolo et al., 2016). Statherian ages may be
244 derived from the Kalahari Craton (1720 - 1800 Ma, Van Schijndel et al., 2014) and
245 Namaqua Province (1700 - 1800 Ma, Barton, 1983).

246 During the Mesoproterozoic there was a period of magmatic quiescence in the
247 region that corresponds to southern Brazil and Uruguay (Hartmann et al., 2008).
248 Therefore, Mesoproterozoic ages are considered strong indicators of an African
249 provenance (Basei et al., 2005, 2008). Mesoproterozoic zircons are common in the
250 Namaqua-Natal Belt (1000 - 1250 Ma), Kheis Sub-Province (1180 Ma) (Becker et al.,
251 2006; Eglington, 2006; Colliston et al., 2015; Bial et al., 2015), and Gariep Belt (1000
252 Ma) (Basei et al., 2005). The presence of few Mesoproterozoic zircons can be explained
253 by regional provenance: zircons of the Calymmian (1550-1570 Ma) may be derived
254 from the Pelotas Batholith or the Tijucas Terrane (Chemale Jr.et al., 2011). Some
255 Mesoproterozoic zircons are present in the metasedimentary sequence of the Dom
256 Feliciano Belt in Brazil (1500 - 1600 Ma, Basei et al., 2008), detrital zircons in
257 Porongos Metamorphic Complex (997 - 1685 Ma, Gruber et al., 2008) and in the
258 metamorphic basement of Dom Feliciano Belt (1400 - 1500 Ma; Gaucher et al., 2011),
259 Punta del Este (900 - 100 Ma), and Nico Pérez Terranes (1429 - 1492 Ma) in Uruguay
260 (Oyhantçabal et al., 2005).

261 Detrital Neoproterozoic ages are abundant in the samples studied in the two
262 units. Dom Feliciano Belt is principally composed of Paleoproterozoic crust that was
263 reworked during the Neoproterozoic, including: the São Gabriel Belt (680 - 880 Ma),
264 Tijucas Terrane (700 - 800 Ma) and Pelotas Batholith (550 – 630 Ma) (Philipp and
265 Machado, 2005; Basei et al., 2011; Pertille et al., 2015). In Uruguay, Neoproterozoic

rocks occur in the granitoids of Nico Pérez Terrane and Isla Cristalina de Rivera (583 - 633 Ma, Hartmann et al., 2002; Oyhantçabal et al., 2009), Dom Feliciano Belt (767 - 800 Ma, Lenz et al., 2012), and granites and metavolcanic rocks of the Punta del Este Terrane (572 - 762 Ma, Hartmann, 2002). During the Neoproterozoic, the Ediacaran age domain was sourced principally from the Pelotas Batholith (550 - 630 Ma) of the Dom Feliciano Belt (Philipp and Machado, 2005). The volcanism in the Camaquã Basin, Hilário Formation (593 Ma) and Acampamento Velho Formation (550 - 570 Ma), also contributed Neoproterozoic zircons (e.g. Oliveira et al., 2016).

Neoproterozoic age domains and Hf signatures are similar between the sedimentary rocks deposited in SW Gondwana (Andersen et al., 2016; Kristoffersen et al., 2016). Neoproterozoic ages were derived from orogenesis during the assembly of western Gondwana, known as the Brazilian-Pan-African Orogeny (Chemale, 2000; Philipp et al., 2016). These Neoproterozoic rocks are spread across SE-Brazil, Uruguay, Congo, Angola, South Africa, and Namibia. Therefore, Neoproterozoic zircons are a common characteristic in these regions (see Supplementary File 2) (Jansson, 2010; Vorster, 2012; Ramos et al., 2014; Uriz et al., 2011, 2016; Craddock et al., 2019) and are not good indicators of sediment provenance (Andersen et al., 2016; Kristoffersen et al., 2016). A lack of isotopic information for this period adds further difficulty to this work.

Cambrian zircons are restricted to the lower Cambrian in the studied units. Zircons of this age were sourced from the Camaquã Basin, which served as the basement for the Itararé Group and Rio Bonito Formation. Cambrian volcanic events in this basin are dated from 535 - 547 Ma (Hartmann et al., 2008; Almeida et al., 2012). In Uruguay, Cambrian ages occur in some granites (532 Ma, Kawashita et al., 1999) and volcanic rocks (520 Ma, Bossi e Gaucher, 2004). Ages younger than 535 Ma are strong

291 indicators of source areas located in Argentina or Africa, such as granites (510 - 520
292 Ma) and metamorphic rocks (505 - 540 Ma) of Damara Belt (Gray et al., 2008; Blanco
293 et al., 2011) and Gariep Belt (514 Ma, Smithies, 1992). In Argentina, they could be
294 derived from the Sierras Pampeanas (515 - 535 Ma, von Gosen et al., 2014; Rapela et
295 al., 2016) and Ventania System (505 - 531 Ma, Rapela et al., 2003).

296 Ordovician, Silurian, and Devonian zircons occur in small quantities in the study
297 area. Rocks of this interval do not exist in the Sul-riograndese Shield and are rare in
298 Africa. However, they are common in Argentina in the Famatinian Arc (466 - 475 Ma),
299 in granites and igneous rocks of the North Patagonian Massif and Sierras Pampeanas
300 (366 - 484 Ma, Pankhurst et al., 1999, 2006; Dahlquist et al., 2018). Sierras Pampeanas
301 had magmatic activity that continued through the Late Devonian to the early
302 Carboniferous (Dahlquist et al., 2018). Due to the proximity of the region, the Asunción
303 Arch could have contributed zircons from igneous rocks (478 - 576 Ma, Comin-
304 Chiaramonti et al., 1996).

305 Some zircons present Carboniferous ages. These Carboniferous zircon may also
306 be sourced from Argentina, from igneous rocks of the North Patagonian Massif (314 -
307 369 Ma, Dahlquist et al., 2013; Pankhurst et al., 2006; Zappettini et al., 2015) and
308 Sierras Pampeanas (341 - 369 Ma, Dahlquist et al., 2013). Youngest zircons have ages
309 between 300 - 308 Ma, corresponding to the age obtained for the deposition of Itararé
310 Group in the southern Paraná Basin, 307.7 ±3.1 Ma (Cagliari et al., 2016). These
311 zircons may be derived from volcanism associated with subduction along the proto-
312 Andean margin (Cawood et al., 2009; Linol et al., 2016).

313 Age populations and the principal paleocurrents and striated pavements of the
314 studied samples indicate regional provenance, from erosion of rocks of the Sul-

315 riograndense Shield and the presently exposed Uruguay Shield. Small amounts of
316 zircons (Ordovician – Carboniferous) were contributed from argentine territories.

317 *5.3. SW-Gondwana Provenance*

318 Comparison between probability density distribution diagrams of dated samples
319 with chrono-correLated units (Supplementary File 2 and Fig. 5) permits the
320 interpretation of provenance patterns during the Carboniferous-Permian transition in
321 SW Gondwana. U-Pb ages (Fig. 5) of the zircons indicate five stages of crustal
322 evolution, connected to large orogenic events.

323 Detrital zircon populations indicate three age domains in the Itararé Group and
324 chrono-correLated units, including: a principal peak in the Cambrian-Neoproterozoic
325 and peaks in the Mesoproterozoic and Paleoproterozoic (Fig. 5A). With the exception of
326 the Kalahari Basin, Archean detrital zircons are scarce, a common characteristic of units
327 deposited in SW Gondwana during the Phanerozoic (Andersen et al., 2016).

328 Analyzed basins of SW Gondwana show important Grenvilian
329 (Mesoproterozoic) peaks, with the exception of the southern region of the Paraná Basin.
330 Archean zircons are also scarce in the study region, but they form a principal peak with
331 ages similar to those of the Kalahari Basin. The lack of important peaks in the
332 Mesoproterozoic and Archean indicate that the southern Paraná Basin was not
333 influenced by African basins in this period.

334 Itararé Group, to the north of the study region (state of Santa Catarina), presents
335 peaks in the Grenvilian and Paleoproterozoic (Fig. 5A) (Canile et al., 2016), that are not
336 observed in the study area. The difference in provenance is in part explained by rocks
337 that occur in the region of Santa Catarina. However, Grenvilian ages were sourced from
338 areas outside of the basin, Africa (Canile et al., 2016). Different sources areas suggest

339 that in the study region, the Itararé Group was fed by different source areas when
340 compared with the rest of Paraná Basin.

341 Comparison of detrital ages of Rio Bonito Formation, with the Superior Lukuga
342 Group (Congo Basin), resulted in three age domain peaks: Neoproterozoic-Cambrian,
343 Paleoproterozoic, and Mesoproterozoic (Fig. 7B). In comparison with the Itararé Group,
344 it presents the same Neoproterozoic age domain and few Grenvilian ages, but it has a
345 smaller population of Cambrian zircons. The beginning of deposition of Rio Bonito
346 Formation shows differences in source areas between the studied region and more
347 northern areas of the basin, observed through the Grenvilian, Paleoproterozoic, and
348 Archean age peaks. This suggests, as with the Itararé Group, the occurrence of different
349 source areas for different regions of the Paraná Basin during this period.

350 *5.4. Paleogeographic implications*

351 In the extreme south of the Paraná Basin, glacial striations and paleocurrents
352 indicate that the paleoflow of ice in the Late Carboniferous was towards the NW-N
353 (Tomazelli and Soliani Jr., 1982, 1997; Assine et al., 2018) (Fig. 6A). Paraná Basin
354 extends to Uruguay, where the San Gregório Formation is the equivalent of the Itararé
355 Group. The proximity between the areas, the direction of ice paleoflow lines and the
356 facies succession suggest a paleogeographic connection between these areas (Assine et
357 al., 2018). Therefore, paleo-glaciers could have moved from Uruguay to the extreme
358 south of Brazil (Frakes and Crowell 1970; Assine et al., 2018). Sul-riograndense and
359 Uruguay highlands nucleated the glaciers, denominated the Uruguay ice lobe (Frakes
360 and Crowell, 1972; Crowell, 1999; Assine et al., 2018), and served as the principal
361 source area for sediments in the extreme south of the basin during the Late
362 Carboniferous.

Although the deposits of the LPIA are asynchronous (Isbell et al., 2012; Cagliari et al., 2016), dating of a tonstein layer in southern Namibia (302 Ma, Stollhofen et al., 2008) shows that glacially-influenced deposits of Namibia existed in periods correlated with the deposits in the study region (307 Ma, Cagliari et al., 2016). The lack of important Grenvilian (Mesoproterozoic) peaks in the study area shows that African basins did not interact with the southern Paraná Basin during this period. Restriction of ice centers, geographic restriction to the highlands, and reduced size are some of the reasons why African ice flows did not reach the study region. There is no consensus as to whether or not the extreme south of Brazil still had ice centers during this period, since glaciation was already in its final phase in the region, and the upper deposits of the Itararé Group show no evidence of the ice-proximal, interpreted by some authors as post-glaciation phase (Iannuzzi et al., 2010). Another explanation is the presence of topographic barriers between the study region and the Kalahari Basin, which served as divisions between ice centers and blocked the entrance of sediments into the region. Study region does not present a significant quantity of detrital African zircons, even in the basal deposits of the Itararé Group, suggesting that African glaciers never reached the basin or that their deposits were eroded.

Similar provenance data indicate that during the deposition of the Itararé Group and the beginning of Rio Bonito Formation, the source areas did not change in the region. Paleovalleys, ancient routes followed by the glaciers, and fluvial-deltaic systems fed by melt-water during the deposition of the Itararé Group continued to distribute sediments in the post-glacial phase.

Zircons grains fromArgentina were likely transported by the wind (igneous zircons) and through an epicontinental sea that connected the Paraná Basin to the Chaco Basin. Small contributions of Ordovician-Carboniferous zircons came from the

388 epicontinental sea and were also observed in the southeast of the basin (Canile et al.,
389 2016). The connection with the sea could have also permitted the introduction of
390 material into the region from the Asunción Arch, a proximal elevated area (Veevers et
391 al., 1994; Santos et al., 1996).

392 Paleoflow directions of ice and paleovalleys have a general direction to the west
393 (Fig. 6A). This is the same paleoflow direction of ice as in the southeast of the Paraná
394 Basin (Barbosa, 1940; Rocha-Campos et al., 1988; Santos et al., 1992; Puigdomenech et
395 al., 2014; Fallgatter and Paim, 2018). Contributions of African zircons in the southeast
396 of the basin (Santa Catarina) were observed by Canile et al. (2016) at the top of Itararé
397 Group, suggesting connections between the basins during the Pennsylvanian. These
398 zircons would be transported by glaciers or through fluvial-deltaic systems fed by melt-
399 water, as was proposed for an older interval (Vesely et al., 2018). An ice sheet located
400 in the Windhoek Highlands (NW-Namibia), denominated the Windhoek Ice Sheet
401 (Visser, 1987; Santos et al., 1996; Rocha-Campos et al., 2008) or the Kaokoveld Ice
402 Sheet (Frakes and Crowell, 1970; Eyles, 1993; Andrews et al., 2019) would have been
403 responsible for the distribution of African sediments.

404 In the basins of SE Africa, provenance differences between the Kalahari Basin
405 and the Karoo, indicated by Archean and Paleoproterozoic-aged peaks (Fig. 5), suggests
406 that the basins had different source areas. The Cargonian Highlands were between these
407 basins in this period, and probably served as a division between ice centers (Craddock et
408 al., 2019) (Fig. 6B). Similarities in the peaks of detrital zircons (Fig. 5) indicate a
409 connection between the Karoo Basin (South Africa) and the Sauce-Grande Basin
410 (Argentina), as was already established in other works (Van Lente, 2004; Vorster, 2013;
411 Ramos et al., 2014).

Differences in zircon age populations between the basins of SW Gondwana suggests that in the middle-upper Pennsylvanian there was not a continental ice sheet connecting the basins, as was suggested for older deposits (lower Pennsylvanian) of the Itararé Group (Rosa et al., 2019). Therefore, the idea of a large polar ice sheet (e.g. Craddock et al., 2019) is not adequate to explain the LPIA in the Paraná Basin during the end of the Late Carboniferous. Relatively small ice sheets and ice caps likely existed (Isbell et al., 2012; Griffis et al., 2018; Vesely et al., 2018), confined to more elevated areas.

5.4. Tectonic controls

Topographically controlled ice-spreading centers suggest a significant role of tectonics in the nucleation of glaciers of the LPIA (Eyles, 1993; Isbell et al., 2012; Vesely et al., 2015). Important tectonic events occurred in SW Gondwana in this period, known as the Famatinian and Gondwanides Orogenies.

Deposition of Itararé Group was preceded by a depositional hiatus of about 50 Ma, known as the ¨Pre-Itararé Discordance¨ (Milani, 1997; Milani et al., 2007). In the extreme south of the basin, this hiatus is much larger. Between the final deposition of the Camaquã Basin (Middle Cambrian) and the beginning of the deposition of Itararé Group (Late Carboniferous), the hiatus is estimated to be about 190 Ma (Fig. 7). Due to its large extension, the depositional gap cannot be explained only by a period of non-deposition due to erosion caused by glaciers.

Initial subsidence caused by the Famatinian Orogeny in the Paraná Basin (Ordovician and Devonian, Milani and Ramos, 1998; Pinto and Vidotti, 2019), seems to not have reached the extreme south of the basin. Sul-riograndense Shield suffered uplift during this period, principally in the most occidental units (Oliveira et al., 2016).

Estimate of denudation for the period between 445 and 300 Ma is 1560 to 3380 m for the region (Oliveira et al., 2016). Isopachs of anterior units of the Itararé Group show that the south of the basin was an elevated area during this period, with the margin of the Paraná Basin about 200 km to the north (Milani et al., 1998) (Fig. 7).

In the early Carboniferous, the tectonic activity of the Chanic phase of the Gondwanides Orogeny (Milani and De Wit, 2008) resulted in a lack of significant sedimentation in the basins of southern South America (Limarino and Spalletti, 2006). In the Sul-riograndense Shield, at about 350 Ma, the Chanic phase caused uplift of the basement (Oliveira et al., 2016) (Fig. 7). Elevation of the region by the Gondwanide Orogeny made the nucleation and development of glaciers possible in elevated areas.

During the lower Pennsylvanian, subsidence occurred in the eastern portion of South America (Limarino and Spalletti, 2006). The reasons are not well understood, but may be connected to post-orogenic relaxation (Limarino and Spalletti, 2006) inside of a large interval of subsidence due to regional flexure (Milani, 2007). This subsidence event resulted in the accumulation of sediments in the extreme south of the Paraná Basin. The Itararé Group began its deposition from the Moscovian.

Influence of the same source areas for the Itararé Group and the beginning of sedimentation in Rio Bonito formation in the extreme south of basin indicates that no great tectonic event occurred or influenced the region during this period. Carboniferous-Permian transition was a period of low tectonic activity (Limarino and Spalletti, 2006), marked in the Paraná Basin by a long phase of subsidence, that extended until the lower Triassic (Milani and Ramos, 1998).

6. Conclusions

Geochemical and U-Pb isotope data of detrital zircons from rocks of Itararé Group and Rio Bonito Formation during the Carboniferous-Permian transition allow for the following conclusions:

- Rocks suffered various degrees of weathering. Sediments of the Itararé Group derived from more arid source areas, and those of Rio Bonito Formation derived from source areas that had a hot and humid climate. This suggest that the Itararé Group in the region was deposited in a cold climate until its top.
- Two units present similar source areas, with a dominance of Neoproterozoic ages. This indicates regional provenance due to the erosion of rocks in the Sul-riograndense and uruguaian shield. Zircons from Ordovician-Carboniferous indicate small contributions from source areas located in Argentina. Youngest zircons, 300-308 Ma, correspond to the final depositional age estimated for the the Itararé Group in the southern Paraná Basin.
- Lack of important Mesoproterozoic and Archean peaks indicate that the south of the Paraná Basin did not interact with basins of SW Africa during the Late Carboniferous. Different detrital zircon populations between the study area and Santa Catarina state suggests that the study area had different sediment source areas than the rest of the Paraná Basin.
- Paleocurrent and provenance data and the comparison of probability density distribution plots for the basins of Africa and South America suggest an ice center that connected Uruguay and Brazilian state of Rio Grande do Sul (Uruguay Ice Sheet). Glaciers were nucleated in the Sul-riograndense and Uruguayan highlands. Santa Catarina region was not connected to the study region, and was instead linked to an ice center in northern Namibia.

- Epicontinental sea served as a connection between source areas in Argentina and the Chaco and Paraná Basins. Asunción Arch was also connected with the Paraná Basin by the epicontinental sea, and could have contributed zircons to the south of the basin, which was an elevated region proximal to the study area.
- In the Late Carboniferous, there were not ice sheets connected the basins. Ice caps and small ice sheets dominated during the Late Carboniferous, linked to the period of final retraction of the Late Paleozoic Ice Sheet in the south of the basin.
- Extreme southern region of the Paraná Basin was likely an elevated region during the Ordovician-Devonian. Due to the elevation of the region by the Gondwanides Orogeny (Chanic phase), ice sheets nucleated and evolved in elevated areas. Starting in the early Pennsylvanian, there was subsidence in the southern region of the basin, allowing for the accumulation of sediments of the Itararé Group.

Acknowledgments

The authors are grateful to the project 'Contribution to updating chronostratigraphic Knowledge in Sedimentary Basins' coordinated by Prof. Renata G. Netto and FAPERGS/CAPES (03/2018) - PRÓ-EQUIPAMENTOS (proc. 18/2551-0000429-4), FAPERGS [ARD/PPP 16/2551-000274-6] for financial support. We acknowledge the mineral analyses and cathodoluminescence images the Microanalysis Laboratory of Universidade Federal de Ouro Preto. We are grateful to CPRM – Geological Survey of Brazil, for the material for study and collection, to, and the CAPES for the scholarship to the first author.

References

Andrews, G.D.A., Mcgrady, A.T., Brown, S.R., Maynard, S.M., 2019. First description of subglacial megalineations from the late Paleozoic ice age in southern Africa. PLoS ONE 14(1): e0210673. https://doi.org/10.1371/journal.pone.0210673

Almeida, D.P.M., Chemale Jr., F., Machado, A., 2012. Late to Post-Orogenic Brasiliano-Pan- African Volcano-Sedimentary Basins in the Dom Feliciano Belt Southernmost Brazil. In: Al-Juboury, A.I. (Ed.), Petrology—NewPerspectives and Applications. InTech—Open Acess Publisher, Rijeka, pp. 73–135.

Andersen, T., Kristoffersen, M., Elburg, M.A., 2016. How far can we trust provenance and crustal evolution information from detrital zircons? A South African case study. Gondwana Res. 34, 129–148. https://doi.org/10.1016/j.gr.2016.03.003

Assine, M.L., de Santa Ana, H., Veroslavsky, G., Vesely, F.F., 2018. Exhumed subglacial landscape in Uruguay: Erosional landforms, depositional environments, and paleo-ice flow in the context of the late Paleozoic Gondwanan glaciation. Sediment. Geol. 369, 1–12. https://doi.org/10.1016/j.sedgeo.2018.03.011

Babinski, M., Chemale Jr., F., Van Schmus, W. R., Hartmann, L.A., Silva, L.C., 1997. U-Pb and Sm-Nd geochronology of the Neoproterozoic granitic-gneissic Dom Feliciano Belt, Southern Brazil. Journal of South American Earth Sciences 10, 263–274.

Balashov, Y.A., Ronov, A.B., Migdisov, A.A., Turanskaya, N.V., 1964. The effect of climate and facies environment on the fractionation of the rare-earths during sedimentation. Geochem. Int. 2, 951-969.

528 Barbosa, O., 1940. Estrias produzidas por gelo permi-carbonífero: Mineração e
529 Metalurgia 4, 272–273 (in Portuguese).

530 Basei, M.A.S., Frimmel, H.E., Nutman, A.P., Preciozzi, F., Jacob, J., 2005. A
531 connection between the Neoproterozoic Dom Feliciano (Brazil /Uruguay) and
532 Gariep (Namibia/South Africa) orogenic belts – evidence from a reconnaissance
533 provenance study 139, 195–221. https://doi.org/10.1016/j.precamres.2005.06.005

534 Basei, M.A.S., Frimmel, H.E., Nutman, A.P., Preciozzi, F., 2008. West Gondwana
535 amalgamation based on detrital zircon ages from Neoproterozoic Ribeira and Dom
536 Feliciano belts of South America and comparison with coeval sequences from SW
537 Africa. Geological Society of London Special Publications 294, 239–256.

538 Bauluz, B., Mayayo, M.J., Fernandez-Nieto, C., Lopez, J.M.G., 2000. Geochemistry of
539 Precambrian and Paleozoic siliciclastic rocks from the Iberian Range (NE Spain):
540 implications for source-area weathering, sorting, provenance, and tectonic setting.
541 Chemical Geology 168, 135-150.

542 Blanco, G., Germs, G.J.B., Rajesh, H.M., Chemale Jr., F., 2011. Provenance and palae-
543 ogeographic evolution of the Nama Group (Ediacaran-early Palaeozoic, Namibia):
544 petrography, geochemistry and U-Pb zircon ages. Precambrian Res. 187, 15-32.

545 Becker, T., Schreiber, U., Kampunzu, A.B., Armstrong, R., 2006. Mesoproterozoic
546 rocks of Namibia and their plate tectonic setting. Journal of Earth Science 46, 112–
547 140.

548 Bial, J., Büttner, S.H., Frei, D., 2015. Lithos Formation and emplacement of two
549 contrasting late-Mesoproterozoic magma types in the central Namaqua

Metamorphic Complex (South Africa, Namibia): Evidence from geochemistry and geochronology 225, 272–294.

Bigarella, J.J., Salamuni, R., Fuck, R.A., 1967. Striated surfaces and related features developed by the Gondwana ice sheets (state of Parana, Brazil). Palaeogeography Palaeoclimatology Palaeoecology 3, 265–276.

Boynton, W.V., 1984. Cosmochemistry of the rare earth elements; meteorite studies. In: Rare earth element geochemistry. Henderson, P. (Editors), Elsevier Sci. Publ. Co., Amsterdam. pp. 63-114.

Bossi, J., Gaucher, C., 2004. The Cuchilla Dionisio terrane, Uruguay: an allochthonous block accreted in the Cambrian to SW-Gondwana. Gondwana Research 7, 661–674.

Cagliari, J., Lavina, E.L.C., Philipp, R.P., Tognoli, F.M.W., Basei, M.A.S., Faccini, U.F., 2014. New Sakmarian ages for the Rio Bonito formation (Paraná Basin, southern Brazil) based on LA-ICP-MS U-Pb radiometric dating of zircons crystals. J. South Am. Earth Sci. 56, 265–277. https://doi.org/10.1016/j.jsames.2014.09.013

Cagliari, J., Philipp, R.P., Buso, V.V., Netto, R.G., Klaus Hillebrand, P., da Cunha Lopes, R., Stipp Basei, M.A., Faccini, U.F., 2016. Age constraints of the glaciation in the Paraná Basin: evidence from new U–Pb dates. J. Geol. Soc. London. 173, 871–874. https://doi.org/10.1144/jgs2015-161

Canile, F.M., Babinski, M., Rocha-Campos, A.C., 2016. Evolution of the Carboniferous-Early Cretaceous units of Paraná Basin from provenance studies

based on U-Pb, Hf and O isotopes from detrital zircons. Gondwana Res. 40, 142–169. https://doi.org/10.1016/j.gr.2016.08.008

Cawood P.A., Kröner A., Collins W.J., Kusky T.M., Mooney W.D., Windley B.F., 2009. Accretionary orogens through Earth history. Geol Soc Lond Spec Publ 318, 1–36

Chemale Jr. F., 2000. Evolução Geológica do Escudo Sul-rio-grandense. In: Holz, M. & De Ros, L.F. (Ed.): Geologia do Rio Grande do Sul. Porto Alegre: CIGO/Universidade Federal do Rio Grande do Sul, p. 13-52. (in Portuguese)

Chemale Jr., F., Philipp, R. P., Dussin, I. A. , Formoso, M.L.L., Kawashita, K., Berttotti, A. L. 2011 Lu-Hf and U-Pb age determination of Capivarita Anorthosite in the Dom Feliciano Belt, Brazil. Precambrian Research. , 186, 117 - 126

Chemale, F., Scheepers, R., Gresse, P.G., Schmus, W.R., 2011. Geochronology and sources of late Neoproterozoic to Cambrian granites of the Saldania Belt. Int. J. Earth Sci. 100, 431e444.

Craddock, J.P., Ojakangas, R.W., Malone, D.H., Konstantinou, A., Mory, A., Bauer, W., Thomas, J., Affinati, S.C., Pauls, K., Botha, G., Rochas-Campos, A., Tohver, E., Riccomini, C., Martin, J., Redfern, J., Gehrels, G., 2019. Detrital zircon provenance of Permo-Carboniferous glacial diamictitesacross Gondwana. Earth-Science Rev. 192, 285-316. https://doi.org/10.1016/j.earscirev.2019.01.014

Crowell, J.C., 1999. Pre-Mesozoic Ice Ages: Their Bearing on Understanding the Climate System: Geological Society of America Memoir 192, p.106.

592 Comin-Chiaramonti, C., Cundari, A., De Min, A., Gomes, C.B., Velázquez, V.F., 1996.
593 Magmatism in Eastern Paraguay: occurrence and petrography. In: Comin-
594 Chiaramonti, P., Gomes, C.B. (Eds.), Alkaline Magmatism in Central-Eastern
595 Paraguay. Relationships with Coeval Magmatism in Brazil, 1996. São Paulo, pp.
596 103–122.

597 Condie, K. C., 1993. Chemical composition and evolution of the upper continental
598 crust: contrasting results from surface samples and shales. Chemical Geology 104,
599 pp. 1-37.

600 Costa, T.D.E., 2016. A proveniência dos sedimentos e cinzas vulcânicas dos sedimentos
601 Permianos da Bacia do Paraná: implicações para a história geológica do sul-
602 sudoeste de Gondwana. Tese de doutorado. Universidade de Brasília.

603 Cullers, R. L., Barrett, T., Carlson, R. and Robinson, B., 1987. Rare-earth element and
604 mineralogic changes in Holocene soil and stream sediment: a case study in the Wet
605 Mountains, Colorado, U.S.A. Chemical Geology 63, 275-297.

606 Dahlquist, J.A.; Pankhurst, R.J.; Gaschnig, R.M.; Rapela, C.W.; Casquet, C.; Alasino,
607 P.H.; Galindo, C.; Baldo, E.G. 2013. Hf and Nd isotopes in Early Ordovician to
608 Early Carboniferous granites as monitors of crustal growth in the Proto-Andean
609 margin of Gondwana. Gondwana Research 23, 1617-1630.

610 Dahlquist, J.A., Alasino, P.H., Basei, M.A.S., Morales Cámera, M.M., Macchioli
611 Grande, M., da Costa Campos Neto, M., 2018. Petrological, geochemical, isotopic,
612 and geochronological constraints for the Late Devonian–Early Carboniferous
613 magmatism in SW Gondwana (27–32°LS): an example of geodynamic switching.
614 Int. J. Earth Sci. 107, 2575–2603. https://doi.org/10.1007/s00531-018-1615-9

615 Eglington, B.M., 2006. Evolution of the Namaqua-Natal Belt, southern Africa –
616 ageochro- nological and isotope geochemical review. Journal of African Earth
617 Sciences 46, 93–111.

618 El-Bialy, M.Z., 2013. Lithos Geochemistry of the Neoproterozoic metasediments of
619 Malhaq and Um Zariq formations, Kid metamorphic complex, Sinai, Egypt :
620 Implications for source-area weathering , provenance , recycling , and depositional
621 tectonic setting 176, 68–85. https://doi.org/10.1016/j.lithos.2013.05.002

622 Eyles, N., 1993. Earth's glacial record and its tectonic setting. Earth Sci. Rev. 35, 1–
623 248. https://doi.org/10.1016/0012-8252(93)90002-O

624 Eyles, C.H., Eyles, N., Franca, A.B., 1993. Glaciation and tectonics in an active
625 intracratonic basin: the late Palaeozoic Itarare Group, Parana Basin, Brazil.
626 Sedimentology 40, 1–25.

627 Fabris de Matos, S.L.F., Yamamoto, J.K., Riccomini, C., Hachiro, J., and Tassinari,
628 C.C.G., 2001. Absolute dating of Permian ash-fall in the Rio Bonito Formation,
629 Paraná Basin: Gondwana Research 4, 421–426, doi: 10.1016/S1342-
630 937X(05)70341-5.

631 Fallgatter, C., Paim, P.S.G., 2016. On the origin of the Itararé Group basal
632 nonconformity and its implications for the Late Paleozoic glaciation in the Paraná
633 Basin, Brazil. Palaeogeogr. Palaeoclimatol. Palaeoecol.
634 https://doi.org/10.1016/j.palaeo.2017.02.039

635 Fanning, C.M., Hervé, F., Pankhurst, R.J., Rapela, C.W., Kleiman, L.E., Yaxley, G.M.,
636 Castillo, P., 2011. Lu-Hf isotope evidence for the provenance of Permian detritus

637 in accretionary complexes ofwestern Patagonia andthenorthernAntarctic Peninsula
638 region. Journal of South American Earth Sciences 32, 485–496.

639 Fedo, C.M., Nesbitt, H.W., Young, G.M., 1995. Unravelling the effects of potassium
640 metasomatism in sedimentary rocks and paleosols, with implications for
641 paleoweathering conditions and provenance. Geology 23, 921-924.

642 Fedorchuk, N.D., Isbell, J.L., Griffis, N.P., Montañez, I.P., Vesely, F.F., Iannuzzi, R.,
643 Mundil, R., Yin, Q.Z., Pauls, K.N., Rosa, E.L.M., 2018. Origin of paleovalleys on
644 the Rio Grande do Sul Shield (Brazil): Implications for the extent of late Paleozoic
645 glaciation in west-central Gondwana. Palaeogeogr. Palaeoclimatol. Palaeoecol.
646 https://doi.org/10.1016/j.palaeo.2018.04.013

647 Floyd P.A., Leveridge B.E.,1987. Tectonic environment of the Devonian Gramscatho
648 basin, south Cornwell: framework mode and geochemical evidence from turbidite
649 sandstones. J. Geo.l Soc. Lond. 144, 531–542

650 Frakes, L.A. and Crowell, J. C., 1969. Late Paleozoic glaciation. I, South America.
651 Geol. Soe. Amer., BulI., 80.

652 Frakes, L.A., and Crowell, J.C., 1970. Late Paleozoic glaciation: II. Africa, exclusive of
653 the Karoo Basin: Geological Society of America Bulletin 81, 2261–2286. doi:
654 10.1130/0016-7606(1970)81[2261:LPGIAE] 2.0.CO;2.

655 Frakes, L.A., Crowell, J.C., 1972. Late Paleozoic glacial geography between the Paraná
656 Basin and the Andean geosyncline. Anais da Academia Brasileira de Ciências 44,
657 139–145.

Gray, D.R., Foster, D.A., Meert, J.G., Goscombe, B.D., Armstrong, R., Trouw, R.A.J., Passchier, C.W., 2008. A Damara orogen perspective on the assembly of southwestern Gondwana. Geol. Soc. London, Spec. Publ. 294, 257–278. https://doi.org/10.1144/sp294.14

Gao, S., Ling, W., Qiu, Y. Zhou, L., Hartmann, G., Simon, K., 1999. Contrasting geochemical and Sm–Nd isotopic compositions of Archean metasediments from the Kongling high-grade terrain of the Yangtze Craton; evidence for cratonic evolution and redistribution of REE during crustal anatexis Geochim. Cosmochim. Acta 63, 2071-2088.

Gaucher, C.; Frei, R.; Chemale Jr., F.; Frei, D.; Bossi, J.; Martinez, G.; Chiglino, L.; Cernuschi, F., 2011. Mesoproterozoic evolution of the Rio de la Plata Craton in Uruguay: at the heart of Rodinia? Int. J. Earth Sci. 100, 273-288 doi:10.1007/s00531- 010-0562-x

Gesicki, A.L.D., Riccomini, C., and Boggiani, P.C., 2002. Ice flow direction during late Paleozoic glaciation in western Paraná Basin, Brazil: Jour- nal of South American Earth Sciences 14, 933–93. https://doi .org /10.1016 /S0895-9811 (01) 00076-1.

Girelli, T. J., Chemale, F., Lavina, L.E.C., Laux, J.H., Bongiolo, E.M., Lana, C., 2018. Granulite accretion to Rio de la Plata Craton, based on zircon U-Pb-Hf isotopes: Tectonic implications for Columbia Supercontinent reconstruction. Gondwana Res. 56, 105–118. https://doi.org/10.1016/j.gr.2017.12.010

Goldberg, K., Humayun, M., 2010. The applicability of the Chemical Index of Alteration as a paleoclimatic indicator: An example from the Permian of the Paraná

680 Basin, Brazil. Palaeogeogr. Palaeoclimatol. Palaeoecol. 293, 175–183.
681 https://doi.org/10.1016/j.palaeo.2010.05.015

682 Goddéris, Y., Donnadieu, Y., Carretier, S., Aretz, M., Dera, G., MacOuin, M., Regard,
683 V., 2017. Onset and ending of the late Palaeozoic ice age triggered by tectonically
684 paced rock weathering. Nat. Geosci. 10, 382–386.
685 https://doi.org/10.1038/ngeo2931

686 Griffis, N.P., Montañez, I.P., Fedorchuk, N., Isbell, J., Mundil, R., Vesely, F.,
687 Weinshultz, L., Iannuzzi, R., Gulbranson, E., Taboada, A., Pagani, A., Sanborn,
688 M.E., Huyskens, M., Wimpenny, J., Linol, B., Yin, Q.Z., 2018. Isotopes to ice:
689 Constraining provenance of glacial deposits and ice centers in west-central
690 Gondwana. Palaeogeogr. Palaeoclimatol. Palaeoecol. 1–14.
691 https://doi.org/10.1016/j.palaeo.2018.04.020

692 Gu, X.X., Liu, J.M., Zheng, M.H., Tang, J.X., Qi, L., 2002. Provenance and tectonic
693 setting of the Proterozoic turbidites in Hunan South China: geochemical evidence.
694 Journal of Sedimentary Research 72, 393-407.

695 Guerra-Sommer, M., Cazzulo-Klepzig, M., Santos, J.O.S., Hartmann, L.A., Ketzer,
696 J.M., Formoso, M.L.L., 2008c. Radiometric age determination of tonsteins and
697 strat- igraphic constrains for the Lower Permian coal succession in southern Parana
698 Basin, Brazil. Int. J. Coal Geol. 74, 13-27.

699 Gruber, L., Poercher, C.C. Lenz, C., Dussin, I. Chemale Jr., F., 2008. Mesoproterozoic
700 Detrital Zircons in the Dom Feliciano Belt: zircon ages for the Porongos
701 Metamorphic Complex. VI South American Symposium on Isotope Geology. San
702 Carlos de Bariloche, Argentina.

Hartmann, L.A. 1998. Deepest exposed crust of Brazilgeochemistry of Paleoproterozoic depleted Santa Maria Chico granulites. Gondwana Res. 1, 331-341.

Hartmann L.A., Nardi L.V.S., Formoso M.L.L., Remus M.V.D., Lima E.F., Mexias A.S. 1999. Magmatism and metallogeny in the crustal evolution of Rio Grande do Sul Shiel, Brazil. Pesquisas 26. https://doi.org/10.22456/1807-9806.21123

Hartmann, A.A., Orestes, A., Santos, S., Mcnaughton, N.J., 2001. Archean crust in the Rio de la Plata Craton, Uruguay. SHRIMP U ± Pb zircon reconnaissance geochronology 14, 557–570.

Hartmann, Â.A., Campal, Â., Schipilov, A., Orestes, Ä., Santos, S., Bossi, J., Pe, N., 2002. Zircon and titanite U ± Pb SHRIMP geochronology of Neoproterozoic felsic magmatism on the eastern border of the Rio de la Plata Craton. Uruguay 15, 229-236

Hartmann, L.A., Santos, J.O.S., McNaughton, N.J., 2008. Detrital zircon U–Pb age data, and Precambrian Provenance of the Paleozoic Guaritas Formation, Southern Brazilian Shield. Int. Geol. Rev. 50, 364–374.

Hanson, R.E., Rioux, M., Bowring, S.A., Gose, W.A., Bartholomew, L.T., Kilian, T.M., Evans, D.A.D., Panzik, J., Hoffmann, K.H., Reid, D.L., 2011. Constraints on the Neoproterozoic intraplate magmatism in the Kalahari craton: geochronology and paleomagnetism of 890–795 Ma extension-related igneous rocks in SW Namibia and adjacent parts of South Africa. Geological Society of America Abstractswith Programs 43, 371.

724 Herron, M.M., 1988. Geochemical classification of terrigenous sands and shales from
725 core or log data. Journal of Sedimentary Petrology 58, 820-829.

726 Holz, M., Küchle, J., Philipp, R.P., Bischoff, A.P., Arima, N., 2006. Hierarchy of
727 tectonic control on stratigraphy signatures: base-level changes during the Early
728 Permian in the Parana Basin, southernmost Brazil. J. South Am. Earth Sci. 22, 185-
729 204.

730 Kawashita K., Gaucher C., Sprechmann P., Teixeira W., Victória R. 1999. Preliminary
731 chemostratigraphic insights on carbonate rocks from Nico Pérez Terrane
732 (Uruguay) Actas, II South American Symposium on Isotope Geology, Córdoba,
733 Argentina, 399–402

734 Kristoffersen, M., Andersen, T., Elburg, M.A., Watkeys, M.K., 2016. Detrital zircon in
735 a supercontinental setting: locally derived and far-transported components in the
736 Ordovician Natal Group, South Africa. Journal of the Geological Society 173,
737 203–215. http://dx.doi.org/10.1144/jgs2015-012.

738 Iannuzzi, R., Souza, P.A., Holz, M., 2010. Post-glacial succession in the Southern
739 Brazilian Paraná Basin. Society 2468, 113–132.
740 https://doi.org/10.1130/2010.2468(05).

741 Isbell, J.L., Lenaker, P.A., Askin, R.A., Miller, M.F., Babcock, L.E., 2003.
742 Reevaluation of the timing and extent of late Paleozoic glaciation in Gondwana:
743 Role of the Transantarctic Mountains. Geology 31, 977–980.
744 https://doi.org/10.1130/G19810.1

745 Isbell, J.L., Henry, L.C., Gulbranson, E.L., Limarino, C.O., Fraiser, M.L., Koch, Z.J.,
746 Ciccioli, P.L., Dineen, A.A., 2012. Evaluations of glacial paradoxes during the late
747 Paleozoic Ice Age using the concept of the equilibrium line altitude (ELA) as a
748 control on gla- ciations. Gondwana Research 22, 1–19.

749 Jansson, M.D., 2010. What lies under the Kalahari sand? U/Pb dating of Dwyka tillites,
750 South Africa. Master of Science thesis. University of Gothenburg.

751 Lavina, E.L., Nowatzki, C.H., Santos, M.A.A., Leao, H.Z., 1985. Ambientes de
752 sedimentaçao do Super-Grupo Tubarão na região de Cachoeira do Sul. Acta
753 Geolog. Leopoldensia 9, 5-75.

754 Lavina, E.L., Lopes, R.C., 1987. A transgressão marinha do Permiano Inferior e a
755 evolução paleogeografica do Super-Grupo Tubarao no Estado do Rio Grande do
756 Sul. Paula Coutiana 1, 51-103.

757 Lenz, C., Porcher, C.C., Fernandes, L.A.D., Masquelin, H., Koester, E., Conceição,
758 R.V., 2012. Geochemistry of the Neoproterozoic (800–767 Ma) Cerro Bori
759 orthogneisses, Dom Feliciano Belt in Uruguay: tectonic evolution of an ancient
760 continental arc. Mineralogy and Petrology Special Issue Gondwana Collision.

761 Limarino, C.O., Spalletti, L.A., 2006. Paleogeography of the upper Paleozoic basins of
762 southern South America: An overview. J. South Am. Earth Sci. 22, 134–155.
763 https://doi.org/10.1016/j.jsames.2006.09.011

764 Linol, B., de Wit, M.J., Barton, E., de Wit, M.M.J.C., Guillocheau, F., 2016. U-Pb
765 detrital zircon dates and source provenance analysis of Phanerozoic sequences of

the Congo Basin, central Gondwana. Gondwana Res. 29, 208–219. https://doi.org/10.1016/j.gr.2014.11.009

Lopes, R. da C., 1995. Arcabouço aloestratigrafico para o intervalo "Rio Bonito-Palermo" (Eopermiano da Bacia do Parana), entre Butia e São Sepé, Rio Grande do Sul. Dissertação de mestrado. Programa de Pós-graduação em Geologia. Universidade do Vale do Rio dos Sinos. (In Portuguese)

Luft Jr., J.L. 2005. Evolução Crustal do Vale do Rio Hoanib, Cinturão Kaoko, NW da Namíbia. Doctorade Thesis, UFRGS, Poroto Alegre.

Machado, Marco Antonio Pinheiro. 1994. 0 degelo final permiano e 0 seu registro geologico na borda sudeste da Bacia do Parana (Paleovale de Candiota - RS). Porto Alegre, 165p. Dissertacao de Mestrado em Geociencias, Instituto de Geociencias, Universidade Federal do Rio Grande do SuI.

Matos, S.L.F. de, Yamamoto, J.K., Riccomini, C., Hachiro, J., Tassinari, C.C.G., 2001. Absolute dating of permian ash-fall in the Rio bonito formation, Paraná Basin, Brazil. Gondwana Res. 4, 421-426.

Mclennan, S.M., Hemming, S., Mcdaniel, D.K., Hanson, G.N., 1993. Geochemical approaches to sedimentation, provenance, and tectonics. https://doi.org/10.1130/SPE284-p21.

McLennan, S.M., Taylor, S.R., Hemming, S.R., 2006. In: Brown, M., Rushmer, T. (Eds.), Composition, Differentiation, and Evolution of Continental Crust: Constraints from Sedimentary Rocks and Heat Flow. Cambridge University Press, pp. 92–134.

788 Milani, E.J., and Ramos, V., 1998, Orogenias Paleozóicas no domínio sul- ocidental do
789 Gondwana e os ciclos de subsidência da Bacia do Paraná: Revista Brasileira de
790 Geociências 28, 527–544.

791 Milani, E. J., 1997. Evolução tectno-estratigráfica da Bacia do Paraná e seu
792 relacionamento com a geodinâmica fanerozóica do gondwana sul- ocidental. Porto
793 Alegre. Tese de Doutorado em Geociências. Universidade Federal do Rio Grande
794 do Sul.

795 Milani, E.J., de Souza, P.A., Melo, J.H.G., 2007. Bacia do Paraná. Bol. Geociências -
796 Petrobras 15, 265–287.

797 Milani, E.J., De Wit, M.J., 2008. Correlations between the classic Paraná and Cape–
798 Karoo sequences of South America and southern Africa and their basin infills
799 flanking the Gondwanides: du Toit revisited. Geol. Soc. London, Spec. Publ. 294,
800 319–342. https://doi.org/10.1144/sp294.17

801 Montañez, I.P., Tabor, N.J., Niemeier, D., DiMichele, W.A., Frank, T.D., Fielding,
802 C.R., Isbell, J.L., Birgenheier, L.P., and Rygel, M.C., 2007. $C0_2$-forced climate and
803 vegetation instability during late Paleozoic deglaciation. Science 315, 87-91.

804 Mori, A.L.O., de Souza, P.A., Marques, J.C., Lopes, R. da C., 2012. A new U-Pb zircon
805 age dating and palynological data from a Lower Permian section of the
806 southernmost Paraná Basin, Brazil: Biochronostratigraphical and geochronological
807 implications for Gondwanan correlations. Gondwana Res. 21, 654–669.
808 https://doi.org/10.1016/j.gr.2011.05.019

809 Nance, W.B., Taylor, S.R., 1976. Rare earth element patterns and crustal evolution I.
810 Australian post-archean sedimentary rocks. Geochimica et Cosmochimica Acta 40,
811 1539–1551.

812 Nesbitt, H.W., Young, G.M., 1984. Prediction of some weathering trends of plutonic
813 and volcanic rocks based on thermodynamic and kinetic considerations.
814 Geochimica et Cosmochimica Acta 48, 1523-1534.

815 Oyhantçabal P., 2005. The Sierra Ballena shear zone: Kinematics, timing and its
816 significance for the geotectonic evolution of southeast Uruguay. Diss. z. Erlangung
817 des Doktorgrades. Georg August-University, Gottingen, pp. 139-145.

818 Oyhantçabal P, Siegesmund S, Wemmer K, Presnyakov S, Layer P., 2009.
819 Geochronological constraints on the evolution of the southern Dom Feliciano Belt
820 (Uruguay). J. Geol. Soc. 166, 1075–1084

821 Oliveira, C. H. E., De Ritter, A., Chemale, F., Bernet, M., 2016. Tectonophysics
822 Evidence of post-Gondwana breakup in Southern Brazilian Shield: Insights from
823 apatite and zircon fi ssion track thermochronology. Tectonophysics 666, 173–187.
824 https://doi.org/10.1016/j.tecto.2015.11.005

825 Oriolo, S., Oyhantçabal, P., Basei, M.A.S., Wemmer, K., Siegesmund, S., 2016a. The
826 Nico Pérez Terrane (Uruguay): From Archean crustal growth and connections with
827 the Congo Craton to late Neoproterozoic accretion to the Río de la Plata Craton.
828 Precambrian Res. 280, 147–160. doi:10.1016/j.precamres.2016.04.014

Pankhurst, R.J., Weaver, S.D., Hervé, F., Larrondo, P. 1999. Mesozoic-Cenozoic evolution of the North Patagonian Batholith in Aysén, Southern Chile Journal of the Geological Society, London 156, 673-694.

Pankhurst, R.J., Rapela, C.W., Fanning, C., Márquez, M., 2006. Gondwanide continental collision and the origin of Patagonia. Earth Sci. Rev. 76, 235–257.

Peel, E., Preciozzi, F., 2006. Geochronologic synthesis of the Piedra Alta Terrane, Uruguay. V SouthAmerican Symposiumon Isotope Geology. Short Papers - V South American Symposium on Isotope Geology, pp. 234–237.

Pertille J., Hartmann L.A., Philipp R.P. 2015. Zircon U-Pb age constraints on the Paleoproterozoic sedimentary basement of the Ediacaran Porongos Group, Sul-Riograndense Shielf, southern Brazil: Journal of South American Earth Sciences, 63, 334-345.

Philipp, R.P., Machado, R., 2005. The late Neoproterozoic granitoid magmatism of the Pelotas Batholith, southern Brazil. J. S. Am. Earth Sci. 19, 461–478.

Philipp, R.P., Pimentel, M.M., 2016. Tectonic evolution of the Dom Feliciano Belt in Southern Brazil: Geological relationships and U-Pb geochronology 46, 83–104. https://doi.org/10.1590/2317-4889201620150016

Pinto, M.L., Vidotti, R.M., 2019. Tectonic framework of the Paraná basin unveiled from gravity and magnetic data. J. South Am. Earth Sci. 90, 216–232. https://doi.org/10.1016/j.jsames.2018.12.006

Powell, C. Mc.A., Li, Z.X., 1994, Reconstruction of the Panthalassan margin of Gondwanaland, in Veevers, J.J., and Powell, C.M., eds., Permian-Triassic Pangean

basins and foldbelts along the Panthalassan margin of Gondwana- land: Boulder, Colorado, Geological Society of America Memoir 184, 5–9.

Puigdomenech, C.G., Carvalho, B., Paim, P.S.G., Faccini, U.F., 2014. Lowstand Turbidites and Delta Systems of the Itararé Group in the Vidal Ramos region (SC), southern Brazil. Brazilian J. Geol. 44, 529–544. https://doi.org/10.5327/Z2317488920140004002

Ramos, V.A., 2008. The basement of the Central Andes: the Arequipa and related terranes. Annual Review of Earth and Planetary Sciences 36, 289–324.

Ramos, V.A., Naipauer, M., 2013. Patagonia: where does it come from? Journal of Iberian Geology 40, 367-379.

Ramos, V.A., Chemale, F., Naipauer, M., Pazos, P.J., 2014. A provenance study of the Paleozoic Ventania System (Argentina): Transient complex sources from Western and Eastern Gondwana. Gondwana Res. 26, 719–740. https://doi.org/10.1016/j.gr.2013.07.008

Rapela, C.W., Pankhurst, R.J., Fanning, C.M., Grecco, L.E., 2003. Basement evolution of the Sierra de la Ventana Fold Belt: new evidence for Cambrian continental rifting along the southern margin of Gondwana. Journal of the Geological Society, London, 160, 613–628.

Rapela, C.W., Verdecchia, S.O., Casquet, C., Pankhurst, R.J., Baldo, E.G., Galindo, C., Murra, J.A., Dahlquist, J.A., Fanning, C.M., 2016. Identifying Laurentian and SW Gondwana sources in the Neoproterozoic to Early Paleozoic metasedimentary

rocks of the Sierras Pampeanas: Paleogeographic and tectonic implications. Gondwana Res. 32, 193–212. https://doi.org/10.1016/j.gr.2015.02.010

Ryan W.B.F., Carbotte S.M., Coplan J.O., O'Hara S., Melkonian A., Arko R., Weissel R.A., Ferrini V., Goodwillie A., Nitsche F., Bonczkowski J., Zemsky R., 2009. Global multiresolution topography synthesis. Geochem. Geophys. Geosyst., 10.

Rocha-Campos, A.C., Machado, L.C.R., dos Santos, P.R., Canuto, J.R., Castro, J.C., 1988. Pavimento Estriado da Glaciação Neopaleozoica em Alfredo Wagner, Santa Catarina, Brazil. Série Científica 19. Bol. IG Inst. Geociênc. Univ. São Paulo, pp. 39–46. (In portuguese).

Rocha-Campos, A.C., Basei, M.A.S., Nutman, A.P., Santos, P.R dos, 2006. SHRIMP U-Pb zircon geochronological calibration of the paleozoic supersequence, paraná Basin, Brazil. In: V South American Symposium on Isotope Geology. Short Papers, Punta del Este, 1.

Rocha-Campos, A.C., dos Santos, P.R., Canuto, J.R., 2008. Late Paleozoic glacial deposits of Brazil: Paraná Basin. Resolv. Late Paleoz. Ice Age Time Sp. 441, 97–114. https://doi.org/10.1130/2008.2441(07)

Rocha-Campos, A.C., Basei, M.A.S., Nutman, A.P., Kleiman, L.E., Varela, R., Llambias, E., Canile, F.M., da Rosa, O.C.R., 2011. 30 million years of Permian volcanism recorded in the Choiyoi igneous province (W Argentina) and their source for younger ash fall deposits in the Paraná Basin: SHRIMPU-Pb zircon geochronology evidence. Gondwana Research 19, 509–523.

Rosa, E.L.M., Vesely, F.F., Isbell, J.L., Kipper, F., Fedorchuk, N.D., Souza, P.A., 2019. Constraining the timing, kinematics and cyclicity of Mississippian-early Pennsylvanian glaciations in the Paraná Basin, Brazil. Sediment. Geol. 384, 29-49. https://doi.org/10.1016/j.sedgeo.2019.03.001

Roser, B.P., Korsch, R.J., 1988. Provenance signature of sandstone- mudstone suites determined using discriminant function analysis of major element data. Chemical Geology 67, 119-139.

Sánchez Bettucci L., Oyhantçabal P, Loureiro J., Ramos V.A., Preciozzi F., Basei M.A.S. 2004. Mineralizations of the Lavalleja Group (Uruguay), a probable Neoproterozoic volcano-sedimentary sequence. Gondwana Res. 7, 745-751.

Santos, P.R., Rocha-Campos, A.C., Canuto, J.R., 1992. Estruturas de arrasto de icebergs em ritmitos do Subgrupo Itararé (Neopaleozoico) Trombudo Central, SC, Boletim IGUSP, Serie Cientıfica 23, 1–18. (in portuguese).

Santos, P.R., Rocha-Campos, A.C., Canuto, J.R., 1996. Patterns of late Palaeozoic deglaciation in the Parana Basin, Brazil. Palaeogeogr. Palaeoclimatol. Palaeoecol. 125, 165–184. https://doi.org/10.1016/S0031-0182(96)00029-6

Schneider, R.L., Muhlmann, H., Tommazi, E., Medeiros, R.A., Daemon, R.F., Nogueira, A.A., 1974. Revisão estratigráfica da bacia do Paraná. Anais 27° Congresso Brasileiro de Geologia, vol. 1. Sociedade Brasileira de Geologia, Porto Alegre, pp. 41–66. (in portuguese).

Schneiderhan, E., Zimmermann, U., Gutzmer, J., Mezger K, Armstrong, R., 2011. Sedimentary provenance of the Neoarchean Ventersdorp Supergroup, Southern

915 Africa: Shedding light on the evolution of the Kaapvaal Craton during the
916 Neoarchean. The Journal of Geology 119, 575-596.

917 Scheffler, K., Hoernes, S., and Schwark, L., 2003, Global changes during
918 Carboniferous–Permian glaciation of Gondwana: Linking polar and equa- torial
919 climate evolution by geochemical proxies: Geology 31, 605-608, doi:
920 10.1130/0091-7613(2003)031<0605:GCDCGO>2.0.CO;2.

921 Scheffler, K., Buehmann, D., Schwark, L., 2006. Analysis of late Palaeozoic glacial to
922 postglacial sedimentary successions in South Africa by geochemical proxies –
923 Response to climate evolution and sedimentary environment 240, 184–203.
924 https://doi.org/10.1016/j.palaeo.2006.03.059

925 Smith, J.M., 1984. Experiments relating to the fracture of bedrock at the ice-rock
926 interface. Journal of Glaciology 30, 123–125.

927 Smithies, R.H., 1992. The geochemical evolution of three alkaline complexes in the
928 Kuboos-Bremen igneous province, southern Namibia. PhD Thesis (Unpublished),
929 Rhodes University, Grahamstown, 197 p.

930 Stollhofen, H., Stanistreet, I.G., Bangert, B., Grill, H., 2000. Tuffs, tec- tonism and
931 glacially related sea-level changes, Carboniferous-Permian, southern Namibia:
932 Palaeogeog., Palaeoclimat., Palaeoec. 161, 127–150. doi: 10.1016/S0031-
933 0182(00)00120-6.

934 Stollhofen, H., Werner, M., Stanistreet, I.G., Armstrong, R.A., 2008. Single-zircon U-
935 Pb dating of Carboniferous-Permian tuffs, Namibia, and the intercontinental

deglaciation cycle framework. Spec. Pap. 441 Resolv. Late Paleoz. Ice Age Time. pp. 83–96. https://doi.org/10.1130/2008.2441(06)

Suttner, L.J., Dutta, P.K., 1986. Alluvial sandstone composition and paleoclimate, I. Framework mineralogy. Journal of Sedimentary Petrology 56, 329–345.

Taylor, S.R., McLennan, S.M., 1985. The Continental Crust: Its Composition and Evolu- tion. Blackwell Scientific, Oxford 312.

Tedesco, J., Cagliari, J., Coitinho, J.D.R., da Cunha Lopes, R., Lavina, E.L.C., 2016. Late Paleozoic paleofjord in the southernmost Parana Basin (Brazil): Geomorphology and sedimentary fill. Geomorphology 269, 203-214. https://doi.org/10.1016/j.geomorph.2016.06.035

Tomazelli. L. 1. and Soliani Jr., E., 1982. Evidencias de atividade glacial no Paleozoico Superior do Rio Grande do Sul, Brasil. I Congresso Brasileiro de Geologia, Salvador 4, 1378-1389.

Tomazelli, L.J., Soliani, E., 1997. Sedimentary facies and depositional environments related to Gondwana glaciation in Batovi and Suspiro regions, Rio Grande Do Sul, Brazil. J. South Am. Earth Sci. 10, 295–303. https://doi.org/10.1016/S0895-9811(97)00019-9

Trosdtorf, I., Rocha-Campos, A.C., dos Santos, P.R., Tomio, A., 2005. Origin of Late Paleozoic, multiple, glacially striated surfaces in northern Paraná Basin (Brazil): Some implications for the dynamics of the Paraná glacial lobe. Sediment. Geol. 181, 59–71. https://doi.org/10.1016/j.sedgeo.2005.07.006

957 Turner, B.R., 1999. Tectonostratigraphical development of the Upper Karoo foreland
958 basin: orogenic unloading versus thermally induced Gondwana rifting. J. Afr.
959 Earth Sci. 28, 215-238.

960 Trouw, R. A.J., De Wit, M. J., 1999. Relation between the Gondwanide Orogen and
961 contemporaneous intra- cratonic deformation. Journal of African Earth Sciences
962 28, 203–213.

963 Uriz, N.J., Cingolani, C.A., Armstrong, R., 2011. Isotopic studies on detrital zircons of
964 Silurian – Devonian siliciclastic sequences from Argentinean North Patagonia and
965 Sierra de la Ventana regions: comparative provenance, pp. 571–589.
966 https://doi.org/10.1007/s00531-010-0597-z

967 Uriz, N.J., Cingolani, C.A., Basei, M.A.S., Blanco, G., Abre, P., Portillo, N.S., 2016.
968 Journal of South American Earth Sciences Provenance and paleogeography of the
969 Devonian Durazno Group, southern Parana Basin in Uruguay. J. South Am. Earth
970 Sci. 66, 248–267. https://doi.org/10.1016/j.jsames.2016.01.002

971 Valdez-Buso, V.., Milana, J.P., Paim, P.S.G., Aquino, C.D., Faccini, U.F., 2016. Facies
972 and depositional architecture according to a jet efflux model of a late Paleozoic
973 tidewater grounding-line system from the Itararé Group (Paraná Basin), southern
974 Brazil. J. South Am. Earth Sci. 67, 180–200.
975 https://doi.org/10.1016/j.jsames.2016.02.008

976 Van Lente, V., 2004. Chemostratigraphic trends and provenance of the Permian Tanqua
977 and Laingsburg depocentre, southwestern Karoo Basin, South Africa. Dissertation
978 of Doctor. University of Stellenbosch.

Van Niekerk, H.S. 2006. The origin of the Kheis Terrane and its relationship with the Archean Kaapvaal Craton and the Grenville Namaqua Province in southern Africa. PhD Thesis (unpubl.), University of Johannesburg.

Van Schijndel, V., Cornell, D.H., Frei, D., Simonsen, S.L., Whitehouse, M.J., 2014. Crustal evolution of the Rehoboth Province fromArchean toMesoproterozoic times: insights from the Rehoboth basement inlier. Precambrian Research 240, 22–36

Veevers, J.J., 1994. Case for the Gamburtsev Subglacial Mountains of East Antarctica originating by mid-Carboniferous shortening of an intracratonic basin: Geology 22, 593–596.

Veevers, J.J., 2004. Gondwanaland from 650–500 Ma assembly through 320 Mamerger in Pangea to 185–100 Ma breakup: supercontinental tectonics via stratigraphy and radiometric dating. Earth-Science Reviews 68, 1–132.

Vesely, F.F., Assine, M.L., 2006. Deglaciation sequences in the Permo-Carboniferous Itararé Group, Paraná Basin, southern Brazil. J. South Am. Earth Sci. 22, 156–168. https://doi.org/10.1016/j.jsames.2006.09.006

Vesely, F.F., Trzaskos, B., Kipper, F., Assine, M.L., Souza, P.A., 2015. Sedimentary record of a fluctuating ice margin from the Pennsylvanian of western Gondwana: Paraná Basin, southern Brazil. Sediment. Geol. 326, 45–63. https://doi.org/10.1016/j.sedgeo.2015.06.012

Vesely, F.F., Rodrigues, M.C.N.L., Rosa, E.L.M., Amato, J.A., Trzaskos, B., Isbell, J.L., Fedorchuk, N.D., 2018. Recurrent emplacement of non-glacial diamictite during the late Paleozoic ice age 46, 615–618.

Visser, J.N.J., 1987. The palaeogeography of part of southwestern Gondwana during the Permo-Carboniferous glaciation. Palaeogeogr. Palaeoclimatol. Palaeoecol. 61, 205–219. https://doi.org/10.1016/0031-0182(87)90050-2

Visser, J.N.J., 1996. Controls on Early Permian shelf deglaciation in the Karoo Basin of South Africa. Palaeogeogr. Palaeoclimatol. Palaeoecol. 125, 129–139. https://doi.org/10.1016/S0031-0182(96)00027-2

Vorster, C., 2013. Laser ablation ICP-MS age determination of detrital zircon populations in the Phanerozoic Cape and lower Karoo Supergroups (South Africa) and correlatives in Argentina. Unpublished PhD thesis, University of Johannesburg, South Africa.

Von Gosen, W., McClelland, W.C., Loske, W., Martinez, J.C., Prozzi, C., 2014. Geochronology of igneous rocks in the Sierra Norte de Cordoba (Argentina): Implications for the Pampean evolution at the western Gondwana margin. Lithosphere 6, 277–300. https://doi.org/10.1130/L344.1

Zalán, P.V., Wolff, S., Conceição, J.C.J., Marques, A., Astolfi, M.A.M., Vieira, I.S., Appi, V.T., Zanotto, G.A., 1990. Bacia do Paraná. In: Raja Gabaglia, G.P. e Milani, E.J. (coords.), Origem e Evolução das Bacias Sedimentares. CENPES-PETROBRAS, pp.135–168.

Ziegler, A.M., Hulver, M.L., and Rowley, D.B., 1997. Permian world topography and climate. In: Martini, I.P. (ed.). Late glacial and postglacial environmental changes, Oxford Univ. Press, 111-146.

Figure captions

Fig. 1. (A) Location of study area in south of Brazil; (B) Geological map of the study area (modified by Oliveira et al., 2016) showing the drill core (IB-93-RS, CA-53-RS, ST-01-RS, and SV-19-RS) locations and in the U-Pb-Hf analysis collection of samples. DC – Dorsal de Canguçu Shear Zone; PE – Passo dos Enforcados Shear Zone; PM – Passo do Marinheiro Shear Zone.

Fig. 2. Geochemical diagrams: (A) Diagram for lithological classification of siliciclastic rocks (Herron, 1988); (B) Th/Sc versus Zr/Sc diagram after McLennan et al. (1993); (C) La/Th vs Hf diagram (Floyd and Leveridge, 1987; Gu et al., 2002); (D) Bivariate plot of SiO_2 versus $Al_2O_3+K_2O+Na_2O$ (Suttner and Dutta, 1986). (E) A-CN-K diagram (Nesbitt and Young, 1984), dashed lines represent weathering trends of different igneous rocks. (F) Upper continental crust-normalized REE patterns. PAAS: Post Archaean Australian Shales (Nance and Taylor, 1976) and UCC: Upper continental crust (Taylor and McLennan, 1985; McLennan et al., 2006), after Boynton (1984).

Fig. 3. Stratigraphic correlations showing the core-samples with detrital zircon dates. Radiometric dating of Cagliari et al. (2016). SRGS - Sul-Riograndense Shield.

Fig. 4. Distribution between the main detrital zircon groups for each studied unit.

Fig. 5. (A) Comparison of probability density distribution diagrams of Itararé Group and correLated units. 1- Ramos et al. (2014), Vorster (2013); 2- Linol et al. (2016); 3- Jansson (2010); 4- Vorster (2013), Andersen et al. (2016); 5- Canile et al. (2016),

Griffis et al. (2018), Craddock et al., (2019); 6- Griffis et al. (2018), Fedorchuck et al. (2018) and this study. (B) Rio Bonito formation and correLated units. 7- Linol et al. (2016); 8- Canile et al. (2016), Costa (2016); 9- Canile et al. (2016), Costa (2016), Fedorchuck et al. (2018); 10-This study. RS-Rio grande do Sul State; SC-Santa Catarina State.

Fig. 6. (A) Paleogeography configuration of the SW-Gondwana no upper Paleozoic. Africa paleo-ice flow (subglacial erosional landforms) and paleocurrents of Smith (1984), Visser (1987), Stollhofen et al. (2000) and Andrews et al. (2019). Uruguay paleo-ice flow of Assine et al. (2018). Brazil paleo-ice flow and paleocurrents of Barbosa (1940), Tomazelli and Soliani Jr. (1982), (1997), Rocha-Campos et al. (1988), Santos et al. (1992), Puigdomenech et al. (2014), Fallgatter and Paim (2018). Argentina paleocurrents of Ramos et al., (2014). (B) Distribution of major depositional Basins in SW-Gondwana, and proposed paleo-ice lobe (Gesicki et al., 2002; Andrews et al., 2019) modificado de Limarino and Spalletti (2006). Relief taken from GeoMapApp program (Ryan et al., 2009).

Fig. 7. Chart comparing glacial deposits and tectonic ccles in Gondwana. 1- Cagliari et al. (2016); 2- Cagliari et al. (2016), Griffis et al. (2018); Rocha-Campos et al. (2006. Modified from Isbell et al. (2003) Milani et al. (1997, 2007), Powel and Li (1994). LPIA - Late Paleozoic Ice Age.

1067 **Figures**

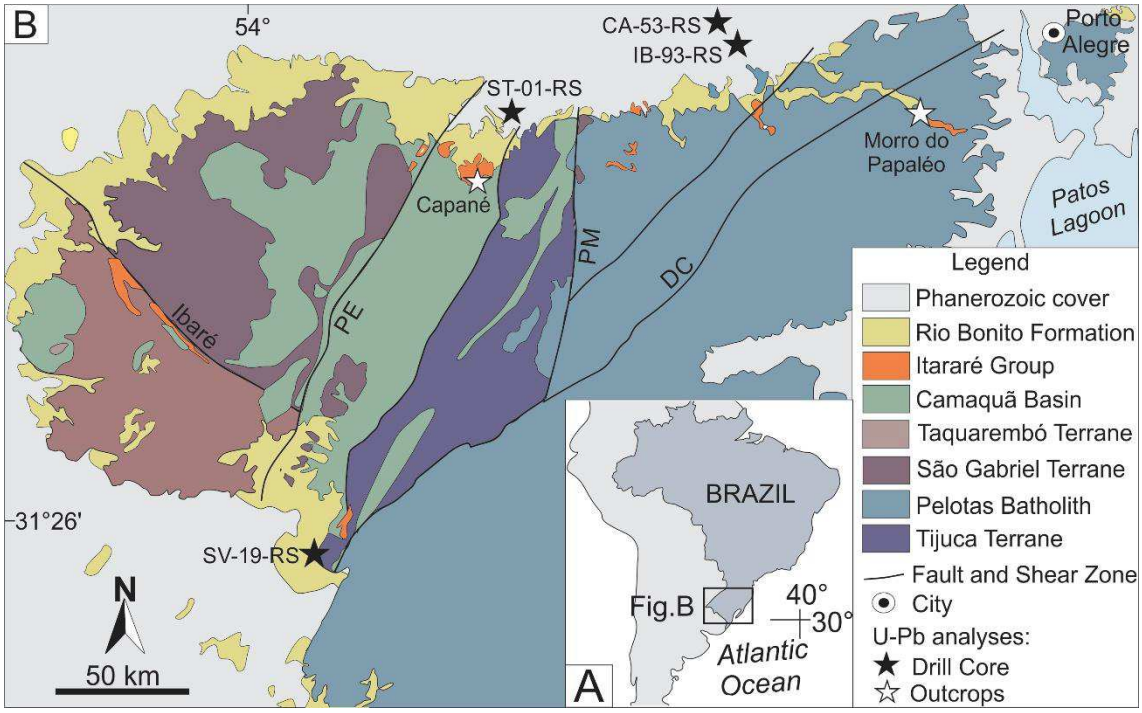

1068

1069 Figure 1

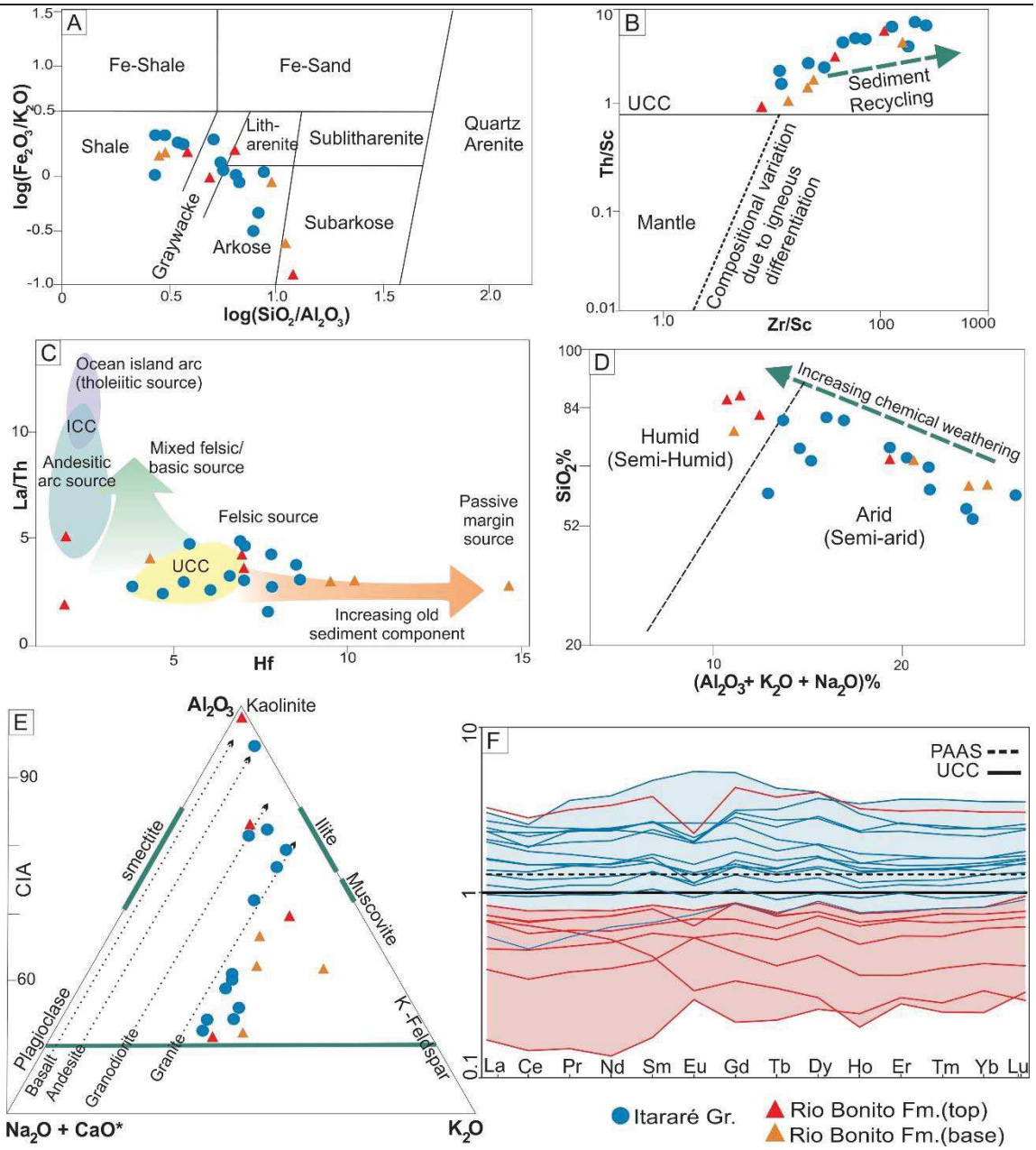

1070

1071 Figure 2

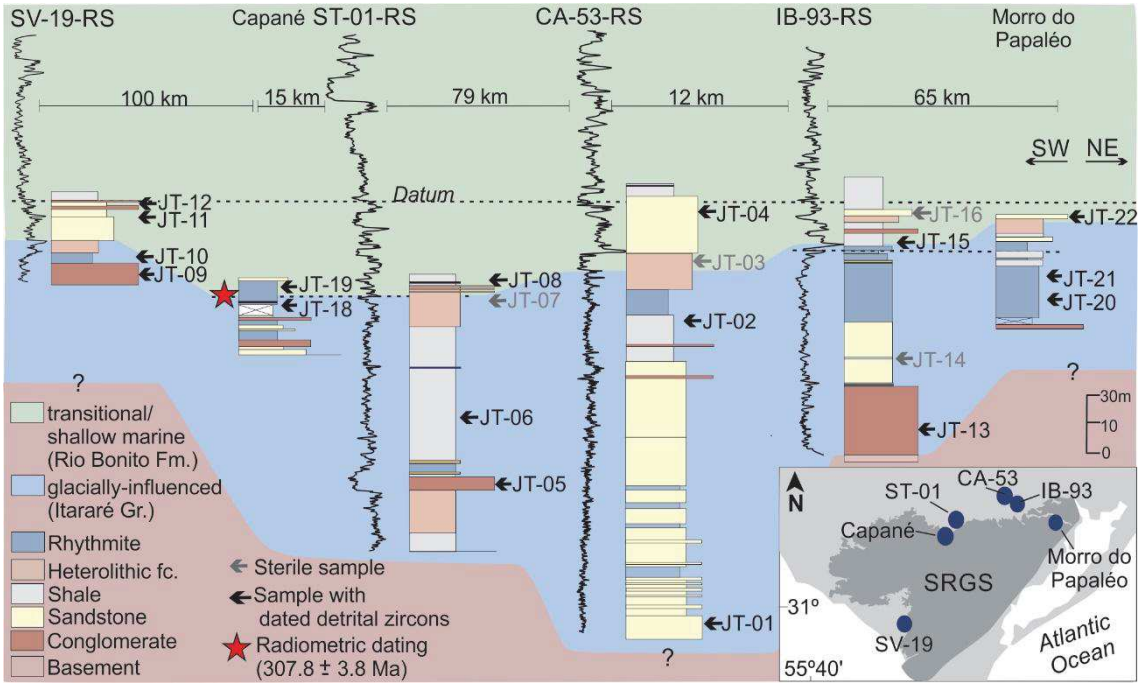

1072

1073 Figure 3

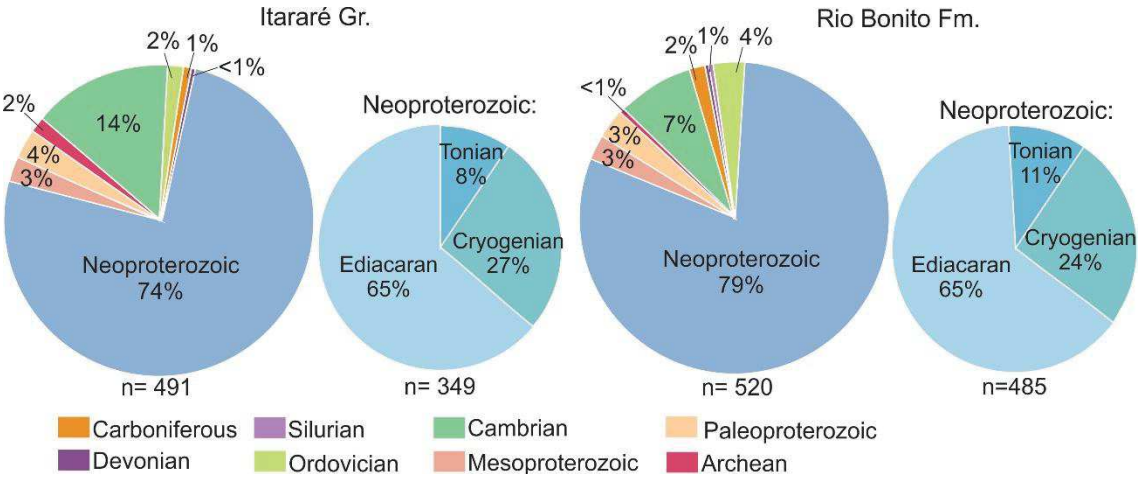

1074

1075 Figure 4

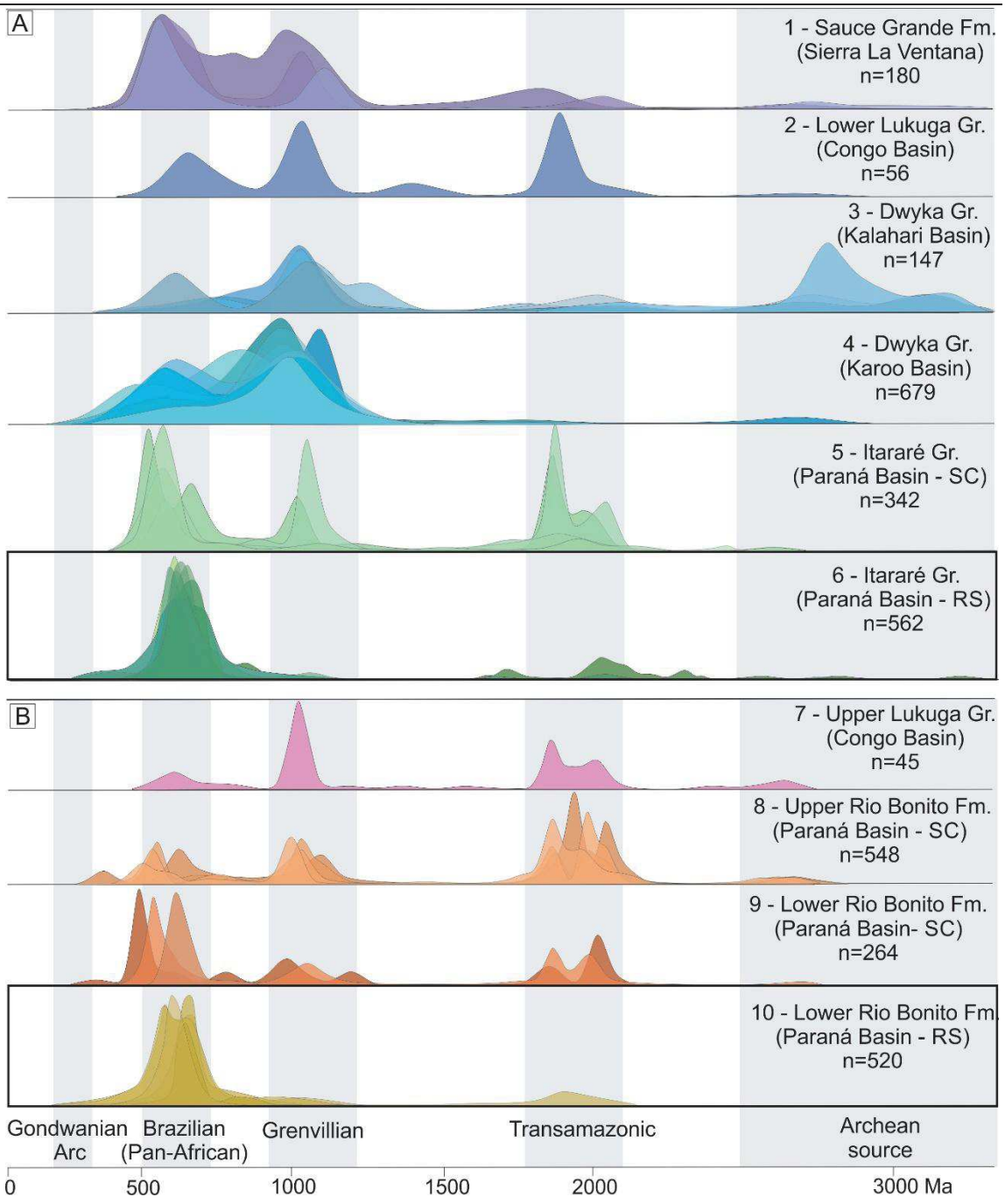
A
1 - Sauce Grande Fm.
(Sierra La Ventana)
n=180
2 - Lower Lukuga Gr.
(Congo Basin)
n=56
3 - Dwyka Gr.
(Kalahari Basin)
n=147
4 - Dwyka Gr.
(Karoo Basin)
n=679
5 - Itararé Gr.
(Paraná Basin - SC)
n=342
6 - Itararé Gr.
(Paraná Basin - RS)
n=562
B
7 - Upper Lukuga Gr.
(Congo Basin)
n=45
8 - Upper Rio Bonito Fm.
(Paraná Basin - SC)
n=548
9 - Lower Rio Bonito Fm.
(Paraná Basin- SC)
n=264
10 - Lower Rio Bonito Fm.
(Paraná Basin - RS)
n=520
Gondwanian Arc
Brazilian (Pan-African)
Grenvillian
Transamazonic
Archean source
0
500
1000
1500
2000
3000 Ma

Figure 5

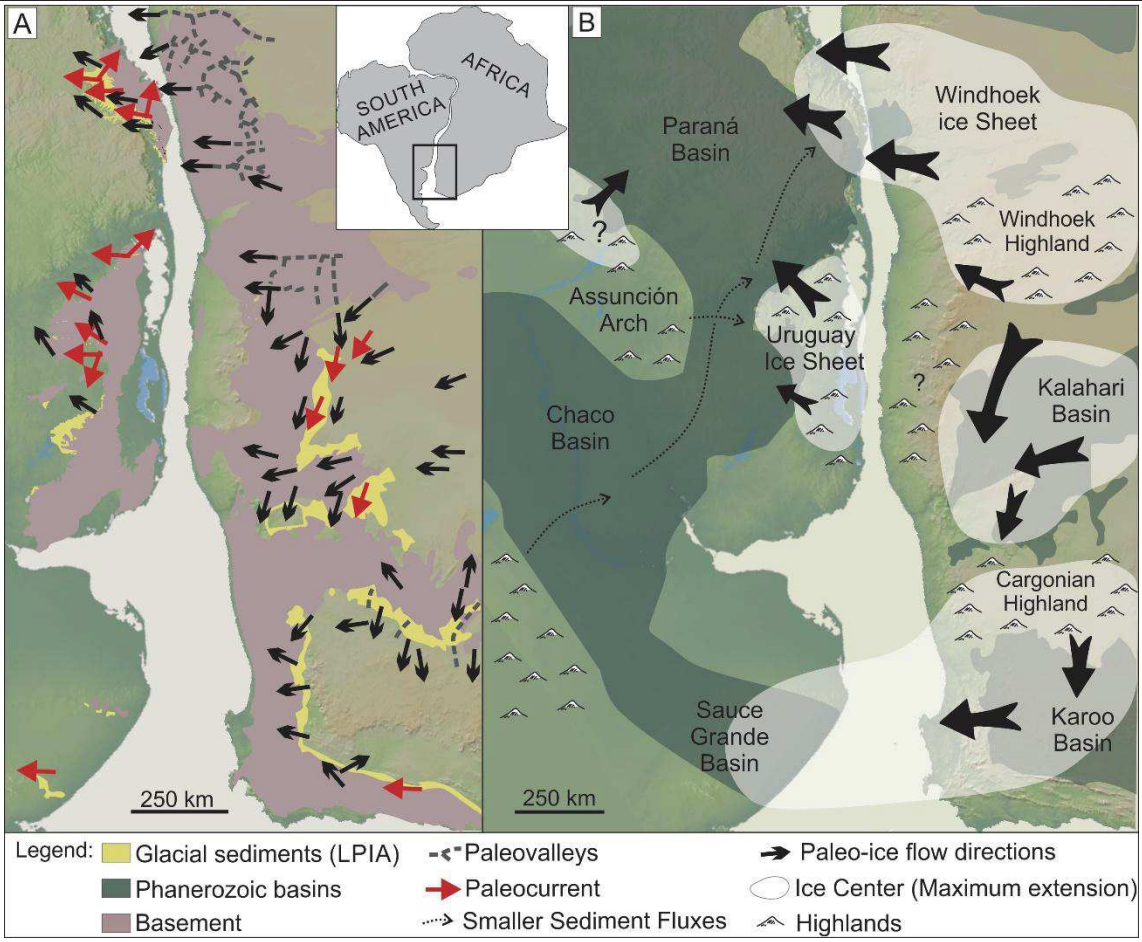

1078

1079 Figure 6

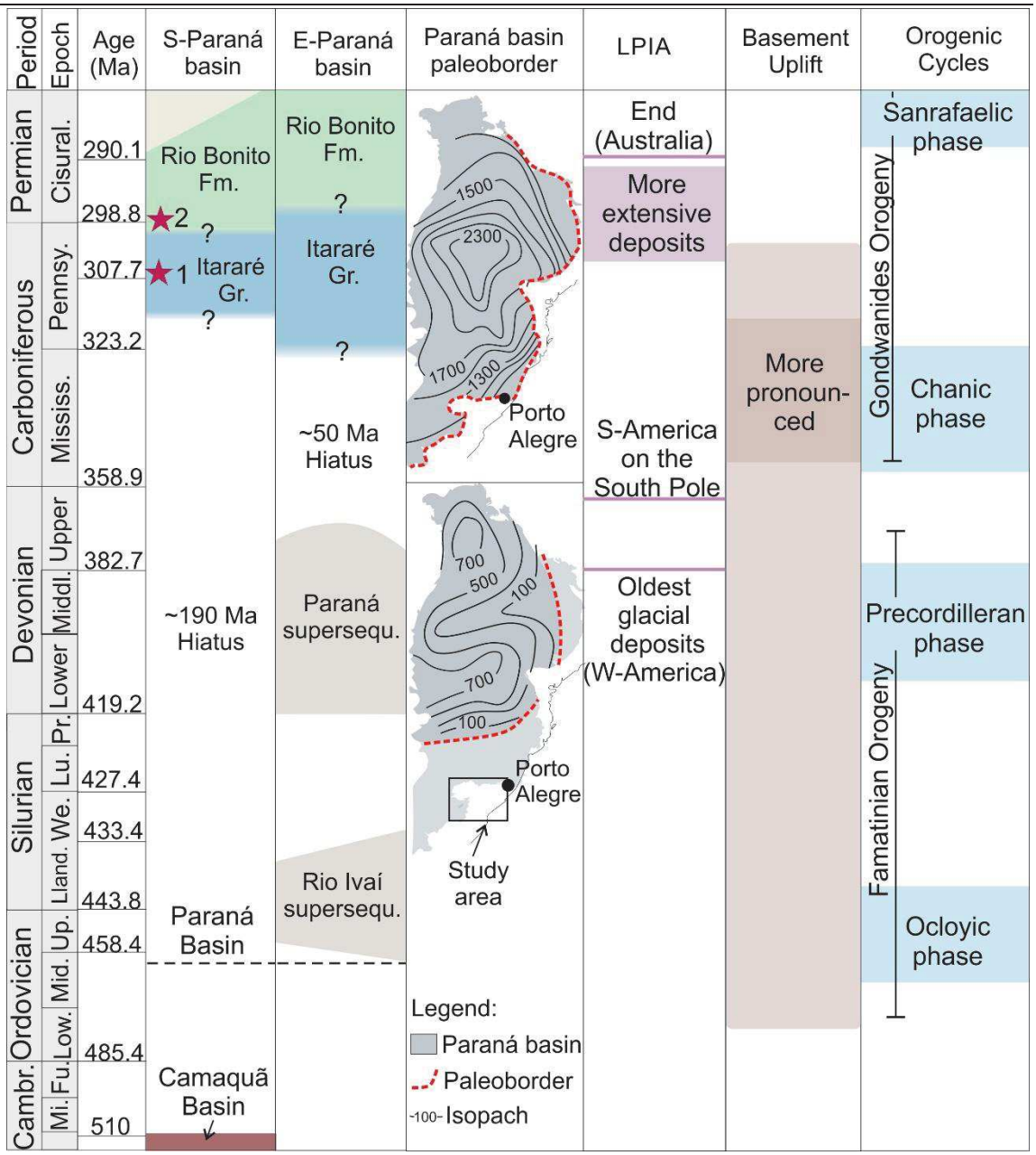
Period
Epoch
Age (Ma)
S-Paraná basin
E-Paraná basin
Paraná basin paleoborder
LPIA
Basement Uplift
Orogenic Cycles
Permian
Carboniferous
Devonian
Silurian
Ordovician
Cambr.
Cisural.
Pennsy.
Mississ.
Upper
Middl.
Lower
Pr.
Lu.
We.
Llland.
Up.
Mid.
Low.
Fu.
Mi.
290.1
298.8
307.7
323.2
358.9
382.7
419.2
427.4
433.4
443.8
458.4
485.4
510
Rio Bonito Fm.
Itararé Gr.
?
Rio Bonito Fm.
Itararé Gr.
~50 Ma Hiatus
~190 Ma Hiatus
Paraná supersequ.
Rio Ivaí supersequ.
Paraná Basin
Camaquã Basin
1500
2300
1700
1300
Porto Alegre
700
500
100
Study area
Legend:
Paraná basin
Paleoborder
-100- Isopach
End (Australia)
More extensive deposits
S-America on the South Pole
Oldest glacial deposits (W-America)
More pronoun-ced
Sanrafaelic phase
Gondwanides Orogeny
Chanic phase
Precordilleran phase
Famatinian Orogeny
Ocloyic phase

Figure 7

5. Comprovante de submissão - Manuscrito II

Revista: Sedimentary Geology

Situação: submetido

Acknowledgement of receipt of your submitted article

SG

Sedimentary Geology <eesserver@eesmail.elsevier.com>
Seg, 10/06/2019 13:20
Você

*** Automated email sent by the system ***

Dear Mrs. Tedesco,

Your submission entitled "Provenance and paleogeography in Southern Paraná Basin: geochemistry and U-Pb zircon geochronology of the Carboniferous-Permian transition" has been received by Sedimentary Geology.

Your paper will be considered as belonging to the category Research Paper. Please contact us if this is not correct.

Please note that submission of an article is understood to imply that the article is original and is not being considered for publication elsewhere. Submission also implies that all authors have approved the paper for release and are in agreement with its content.

You will be able to check on the progress of your paper by logging on to https://ees.elsevier.com/sedgeo/

Elsevier Editorial SystemTM

Full-Function Web-Enabled Manuscript Submission and Tracking System for Peer Review

ees.elsevier.com

6. Síntese Integradora

A fase Chânica da Orogênia Gondwanides é vinculada a elevação da região sul da Bacia do Paraná no Carbonífero inferior. As áreas elevadas facilitaram a nucleação e desenvolvimento das geleiras na região, e no período final da glaciação na região de estudo hospedaram as camadas de gelo em retração.

Durante a Late Paleozoic Ice Age, as geleiras do extremo sul da Bacia do Paraná não extrapolaram os limites da bacia, apresentando domínio de áreas-fontes regionais para o Grupo Itararé e a base da Formação Rio Bonito. Ao contrário do que era inferido em diversos estudos anteriores, as bacias do oeste da África e o extremo sul da Bacia do Paraná não interagiram ao longo da deposição do Grupo Itararé, ou seus depósitos foram totalmente erodidos. Apesar de não ocorrer um pico de idade Grenviliana, há alguns grãos dessa idade, que podem ser ligado a áreas fontes da Argentina.

As fácies rítmicas estudadas mostram que durante sua deposição já não existia extensas massas de gelo na região. Proxies geoquímicos sugerem deposição em um período de retração das geleiras (período interglacial), com aumento do intemperismo químico, da temperatura e da salinidade. Os ritmitos são vinculados ao topo de trato transgressivo, provavelmente em decorrência da subida do nível de base devido ao derretimento das geleiras. A sequência final de deposição do Grupo Itararé na região mostra indícios de clima mais ameno, com ausência de evidências glaciais e a presença de restos vegetais.

Os objetivos da tese foram alcançados, e a hipótese de que os paleofluxos de gelo poderiam vir África ocidental para o sul da Bacia do Paraná foi falseada. Este trabalho aporta novos dados para os depósitos glácio-influenciados do sul da Bacia do Paraná. Auxiliando na compreensão da evolução sedimentar e climática durante a transição

Carbonífero-Permiano, e contribuindo para o entendimento dos padrões de drenagens glaciais atuantes na Late Paleozoic Ice Age.

Para trabalhos futuros, a assinatura isotópica de háfnio (Hf), que não foi realizada em tempo hábil para ser incorporada a tese, é uma técnica complementar que poderia fornecer dados mais precisos ajudando a elucidar a proveniência.

7. Anexos

Anexo 1- (manuscrito 1)

Table S1. Facies description and interpretation of the Itararé Group.

Code	Facies	Description	Interpretation
Cm	Massive Conglome-rate	Matrix of fine- to coarse-grained arkosic sandstone. Clasts (1-20 cm) are polymictic, sub-angular to sub-rounded, with subtle stratification. Laminae of fine-grained sandstone are present, as well as fluidized and deformed siltstone, and agglomeration of granules deposited horizontally. It sometimes has angular and striated clasts.	Subaqueous gravity flow (e.g. Santos et al., 1996; Vesely, 2006; D'avila et al., 2009) where the sediment is remobilized due to the increase in sediment supply or high slope. High-concentration turbidity currents deposits coarse sand and gravel (Lowe, 1982; Pickering et al., 1989).
Sm	Massive sandstone	Medium- to fine-grained quartz sandstone, massive, with rare granules and pebbles with a diameter of up to 3 cm, and carbonate cementation.	Rapid deposition from high-suspended load flows (Reading and Collinson, 1996). Hyperconcentrated flows deposition, such as low-density turbidity currents (Bouma's [1962] sense), similar the deposits of sandy debris flows (Shanmugam et al. 1995).
Src	climbing-ripple cross-laminated sandstone	Fine- to medium-grained sandstone with thin intercalations of laminated siltstones. With climbing ripples cross-lamination, flame structures, load casts, carbonate cementation, and rare pebbles (with diameter lower than 3 cm). The laminae (up to 6 cm) of siltstone are intercalated, locally bioturbated, with subtle erosion at the top. Locally some ripples cross-lamination have mud drapes on the foresets.	High sediment concentration flow with sediment transport combining suspension and traction. These seem typical to Bouma facies B and C of turbidity currents. Represent repeated stacking of turbidite beds (Visser, 1983; Eyles et al., 1993). Influence of tide is recorded by the mud drape.
R	Rhythmites	Intercalation of siltstones with claystone, couplets with millimeter to centimeter thickness. See Items 4.1.1.1, 4.1.1.2 and 4.1.1.3	See items 4.1.3
Sm	Massive siltstone	Massive siltstone, locally granules and pebbles of granitic composition, up to 5 cm in diameter. Thickness can reach 2 m.	Deposition by suspension settling in a low-energy environment, below the fair-weather wave base.

H	Heterolitic facies	Non-rhythmic alternation of thin layers of very fine- to fine-grained sandstone (locally coarse-grained sandstone) with siltstone. With wavy and lenticular bedding, symmetrical ripples laminations, wave cross lamination, plane-parallel lamination, plant debris, syneresis cracks, bioturbation and granules are common. At the base, siltstone predominates, and towards the top dominates the sandstones.	Deposition under alternation of hydrodynamic energy in shallow marine or estuarine environment, lower shoreface environment. The presence of syneresis cracks provides further evidence for periodic fluctuations in salinity. Plant debris indicate proximity to the continent in marginal environments, and the line of granules suggest the presence of seasonal ice or transport by vegetation
S	Shale	Black shale, fissile, locally with interbeds of fine- to medium-grained sandstones. With cone-in-cone structure, carbonaceous material, granules and pebbles of granitic composition, up to 2 cm in diameter. Can reach 60 m of thickness.	Deposition by suspension settling in a low-energy environment, in relatively deep, quiet water, below the fair-weather wave base. Probably connected to offshore environments.
C	Coal	Coal with thin vitrinite laminae and pirite. Can reach 60 cm of thickness.	Accumulation of organic material in redox environment
St	Arcosean sandstones	Thick to fine-grained sandstone, arcosean, com trough cross-lamination. Can reach 4 m of thickness.	Migration of subaquatic dunes. Fluvial deposits.

Anexo 2- (manuscrito 1)

Table S2.

Major element concentration (wt%) in studied lithologies.

Sample	Litho	SiO_2	Al_2O_3	Fe_2O_3	MgO	CaO	Na_2O	K_2O	TiO_2	P_2O_5	MnO	Cr_2O_3	CIA
A-01	Sandstone	80,7	9,95	1,65	0,24	0,2	2,4	3,6	0,16	0,06	0,01	0,003	55,2
A-02	Conglomerate	79,8	10,38	1,26	0,25	0,56	2,43	4	0,23	0,08	0,02	<0,002	64,7
A-03	Siltstone	72,6	12,93	4,07	0,82	0,39	2,64	3,7	0,57	0,15	0,02	0,005	65
A-04	Siltstone	60,7	16,56	6,1	2,23	0,56	1,48	3,3	0,79	0,22	0,12	0,013	80,8
A-05	Siltstone	72	12,89	4,78	0,82	0,35	2,74	3,7	0,54	0,13	0,02	0,005	57
A-06	Rhtythmite	69,1	19,18	2,02	0,23	0,01	0,03	1	1,37	0,09	0,02	0,012	69,1
A-07	Rhtythmite	55,5	18,4	10,55	0,92	0,25	0,25	4,6	1,02	0,25	0,05	0,01	53,2
A-08	Heterolithic fc.	61,2	19,93	4,08	0,61	0,15	0,99	2,5	0,78	0,04	0,02	0,008	81,5
A-09	Heterolithic fc.	62	20,85	3,78	0,53	0,33	1,12	2,4	0,79	0,04	0,08	0,006	80,8
A-10	Conglomerate	59,7	8,89	2,04	0,72	12,4	1,57	2,4	0,35	0,11	0,24	0,005	60,4
A-11	Heterolithic fc.	67,1	15,13	4,24	1,62	0,38	2,04	4,2	0,7	0,15	0,04	0,009	64,7
A-12	Heterolithic fc.	68,5	14,03	4,14	0,62	0,81	0,89	4,4	0,59	0,05	0,09	0,005	65
A-13	Rhtythmite	52,2	18,56	10,43	2,65	0,35	0,59	4,4	0,73	0,22	0,12	0,014	54,3
A-14	Rhtythmite	59,2	21,81	3,77	1,36	0,13	0,56	3,7	1,24	0,1	0,03	0,015	51,6

Table 3.

Trace element concentrations (ppm) in studied lithologies.

Sample	Litho	Ba	Ni	Sc	Be	Co	Cs	Ga	Hf	Nb	Rb	Sn	Sr	Ta	Th	U	V	W	Zr	Y
A-01	Sandstone	412	<20	3	1	1,3	2,1	13,3	3,8	7,8	161	3	63	0,7	5,9	1,1	17	0,8	138	13,6
A-02	Conglomerate	590	30	11	6	12,7	6,3	19,1	6,9	17,4	167	4	146	1,4	16,6	6,1	85	2	236	27,8
A-03	Siltstone	1404	<20	9	1	7,7	5,2	14,1	16,3	17,6	161	3	135	1,6	23,5	5,2	47	1,4	594	34,5
A-04	Siltstone	349	23	14	4	7,9	15,1	26,5	10,2	20,3	144	6	79,2	1,6	24,8	7,4	85	2,9	354	56,7
A-05	Siltstone	478	<20	7	7	6,3	3	16,8	6,6	18	152	4	77	1,3	11,5	2,9	50	1,5	222	24,4
A-06	Rhtythmite	536	<20	3	2	6,8	0,9	6,9	4,2	4,9	80,2	4	68,2	0,5	3,1	5,9	46	0,8	152	8,3

A-07	Rhtythmite	632	<20	2	6	1,6	3,2	11,1	7,6	10,6	169	3	90,3	1,1	10	2,5	<8	0,5	272	17,3
A-08	Heterolithic fc.	2472	<20	5	2	5,2	1,5	9,4	8,6	9,5	81,9	2	278	0,8	8,3	1,7	28	<0,5	319	19,8
A-09	Heterolithic fc.	349	23	14	4	7,9	15,1	26,5	10,2	20,3	144	6	79,2	1,6	24,8	7,4	85	2,9	354	56,7
A-10	Conglomerate	497	<20	1	<1	5,7	2,3	5,9	1,6	6,1	162	6	52,2	0,5	3,2	1,1	11	1,1	48,3	6,2
A-11	Heterolithic fc.	497	<20	1	<1	5,7	2,3	5,9	1,6	6,1	162	6	52,2	0,5	3,2	1,1	11	1,1	48,3	6,2
A-12	Heterolithic fc.	1404	<20	9	1	7,7	5,2	14,1	16,3	17,6	161	3	135	1,6	23,5	5,2	47	1,4	594	34,5
A-13	Rhtythmite	491	25	9	4	7,7	2,4	10,9	7,8	12,2	103	2	128	0,9	11,7	3,5	52	1,5	291	22
A-14	Rhtythmite	472	36	5	4	6,3	1,6	9	7	7	75,4	1	99,6	0,6	5,4	5,7	37	1,1	275	21

Table 4.

Rare earth elements (ppm) and elemental ratios in studied lithologies.

Sample	Litho	La	Ce	Pr	Nd	Sm	Eu	Gd	Tb	Dy	Ho	Er	Tm	Yb	Lu
A-01	Sandstone	16,3	34,2	3,98	15,3	2,98	0,55	2,52	0,39	2,49	0,46	1,47	0,21	1,55	0,23
A-02	Conglomerate	51,5	102	11,2	39,8	7,34	1,22	5,9	0,89	5,29	1,01	2,98	0,43	3,07	0,46
A-03	Siltstone	50,8	101	11,4	41,3	7,82	1,1	6,38	0,97	6,07	1,22	3,41	0,49	3,45	0,54
A-04	Siltstone	72,7	127	17,3	63,4	12,4	1,97	11	1,64	10,3	1,95	6,22	0,83	5,54	0,85
A-05	Siltstone	36,7	74	8,67	31,8	6,55	1,07	5,3	0,81	4,7	0,94	2,83	0,4	2,78	0,43
A-06	Rhtythmite	12,5	23,6	2,87	11	2,1	0,55	1,97	0,28	1,75	0,31	0,89	0,14	0,99	0,14
A-07	Rhtythmite	28,3	56,3	6,31	22,9	4,26	0,78	3,66	0,53	3,05	0,61	1,83	0,28	1,86	0,28
A-08	Heterolithic fc.	72,4	153	17,2	64,8	12,3	1,85	11,7	1,79	10	1,92	5,59	0,77	5	0,79
A-09	Heterolithic fc.	72,7	127	17,3	63,4	12,4	1,97	11	1,64	10,3	1,95	6,22	0,83	5,54	0,85
A-10	Conglomerate	5,1	9,5	1,08	3,6	0,79	0,25	0,81	0,14	0,88	0,19	0,67	0,09	0,7	0,09
A-11	Heterolithic fc.	51,5	102	11,2	39,8	7,34	1,22	5,9	0,89	5,29	1,01	2,98	0,43	3,07	0,46
A-12	Heterolithic fc.	50,8	101	11,4	41,3	7,82	1,1	6,38	0,97	6,07	1,22	3,41	0,49	3,45	0,54
A-13	Rhtythmite	32,5	67,6	7,7	28	5,23	0,92	4,42	0,65	3,84	0,83	2,54	0,34	2,33	0,36
A-14	Rhtythmite	19	34,7	4,49	18,4	3,42	0,74	3,61	0,54	3,49	0,69	2,03	0,3	2,02	0,32

Anexo 3 – (manuscrito 2)

Materials and Methods

Zircon separation was performed using standard techniques. Heavy and light minerals were separated using heavy liquids. Zircon grains were separated manually, mounted in epoxy disks (~ 2.5 cm) and polished so their nucleus were revealed. Images using Scanning Electron Microscopy JOEL 6510 equipped with Centaurus cathodoluminescence (CL) revealed the crystals internal structure, aiding in the selection of sites for dating. U-Pb-Hf analyzes and CL were performed at Isotope Geology Laboratory of Universidade Federal de Ouro Preto (UFOP), Brazil.

Zircon U-Pb analyzes were obtained by ablation microprobe (Photon-machines ArF excimer Laser 193) coupled to Thermo-Fisher Element II (HR-SF-ICP-MS). All analyzes used spot size of 30 μm (diameter) and 5-10 μm (depth), with a repetition rate of 10 Hz, laser output energy of 40% and a fluence of 8.16 J/cm2.

The abled material was carried by a mix of Ar and N2 gas, combined using two Y piece 50% along the sample transport line to the torch. Data are obtained through 20-second background measurement, and signal + background over 20-seconds. Bracketing standard-sample-standard with 20 points, divided into two points in primary standard, four points two-two in two different secondary standards and 14 points in sample grains, be part of the analysis routine. Reference analyzes of Plešovice Zircon (Sláma et al., 2008), GJ-1 (Jackson et al. 2004) e 91500 (Wiedenbeck et al., 1995) were performed to monitor the accuracy and accuracy of the results. Ages obtained were concordant within the experimental errors: 601.47± 0.89 Ma (n = 119) for GJ-1, 1063.8± 1.5 Ma (n = 124) para 91500 e 338.36± 0.96 Ma (n = 48) for Plešovice. On-line software package GLITTER (Van Achterbergh et al., 2001) was used to data reduce. BB-1 pattern (Santos

et al., 2017) was used to correct the raw data (background, elemental fractionation induced by laser and instrumental mass discrimination). Pb correction was based on the measured composition of 204Pb (of sample) (Stacey e Kramers, 1975). Constant decay values are Jaffey et al. (1971). Data uncertainty obtained is in agreement with Horstwood et al. (2016). Zircon best estimated age for detrital studies was the 206Pb/238U for grains younger than 1 Ga and 207Pb/206Pb for grains older than 1 Ga. Ages concordance between 90 - 110% were utilized. Age calculations and detrital zircon plots were done using the software IsoplotR (Vermeesch, 2018).

Reference

Horstwood, M. S. A., Košler, J., Gehrels, G., Jackson, S. E., McLean, N. M., Paton, C., Pearson, N. J., Sircombe, K., Sylvester, P., Vermeesch, P., Bowring, J. F., Condon, D. J., Schoene, B., 2016. Community-Derived Standards for LA-ICP-MS U-(Th-)Pb Geochronology - Uncertainty Propagation, Age Interpretation and Data Reporting. Geostand. Geoanalytical Res. 40, 311-332. doi:10.1111/j.1751-908X.2016.00379.x

Jackson, S. E., Pearson, N. J., Griffin, W.L., Belousova, E. A., 2004. The application of laser ablation-inductively coupled plasma-mass spectrometry to in situ U–Pb zircon geochronology. Chem. Geol. 211, 47-69. doi:10.1016/j.chemgeo.2004.06.017

Jaffey, A. H., Flynn, K. F., Glendenin, L. E., Bentley, W. C., Essling, A. M., 1971. Precision Measurement of Half-Lives and Specific Activities of 235U and 238U. Phys. Rev. C. 4, 1889-1906. doi:10.1103/PhysRevC.4.1889

Santos, M. M., Lana, C., Scholz, R., Buick, I., Schmitz, M. D., Kamo, S. L., Gerdes, A., Corfu, F., Tapster, S., Lancaster, P., Storey, C. D., Basei, M. A. S., Tohver, E., Alkmim, A., Nalini, H., Krambrock, K., Fantini, C., Wiedenbeck, M., 2017. A New Appraisal of Sri Lankan BB Zircon as a Reference Material for LA-ICP-MS U-Pb Geochronology and Lu-Hf Isotope Tracing. Geostand. Geoanalytical Res. 1-24. doi:10.1111/ggr.12167

Slama J., Kosler J., Condon D. J., Crowley J. L., Gerdes A., Hanchar J. M., Horstwood M. S. A., Morris G. A., Nasdala L., Norberg N., Schaltegger U., Schoene B., Tubrett M. N., Whitehouse M. J., 2008. Plesovice zircon - a new natural reference material for U-Pb and Hf isotopic microanalysis. *Chemical Geology* 249, 1-35.

Stacey, J. S., Kramers, J. D., 1975. Approximation of terrestrial lead isotope evolution by a two-stage model. Earth Planet. Sci. Lett. 26, 207-221. doi:10.1016/0012-821X(75)90088-6

Van Achterbergh, E., Ryan, C. G., Jackson, S. E., Griffin, W. L., 2001. Data reduction software for LA-ICP-MS: appendix. In: P. J. Sylvester (Ed.), Laser Ablation-ICP Mass Spectrometry in the Earth Sciences: Principles and Applications 29, 239-243.

Vermeesch, P., 2018. IsoplotR: a free and open toolbox for geochronology. Geoscience Frontiers, 9, 1479-1493. doi: 10.1016/j.gsf.2018.04.001.

Wiedenbeck M., Alle P., Corfu F., Griffin W.L., Meier M., Oberli F., von Quadt A., Roddick J.C., Spiegel W., 1995. Natural zircon standards for U-Th-Pb, Lu-Hf, trace-element and REE analyses. Geostandards Newsletter 19, 1-23.

Anexo 4 – (manuscrito 2)

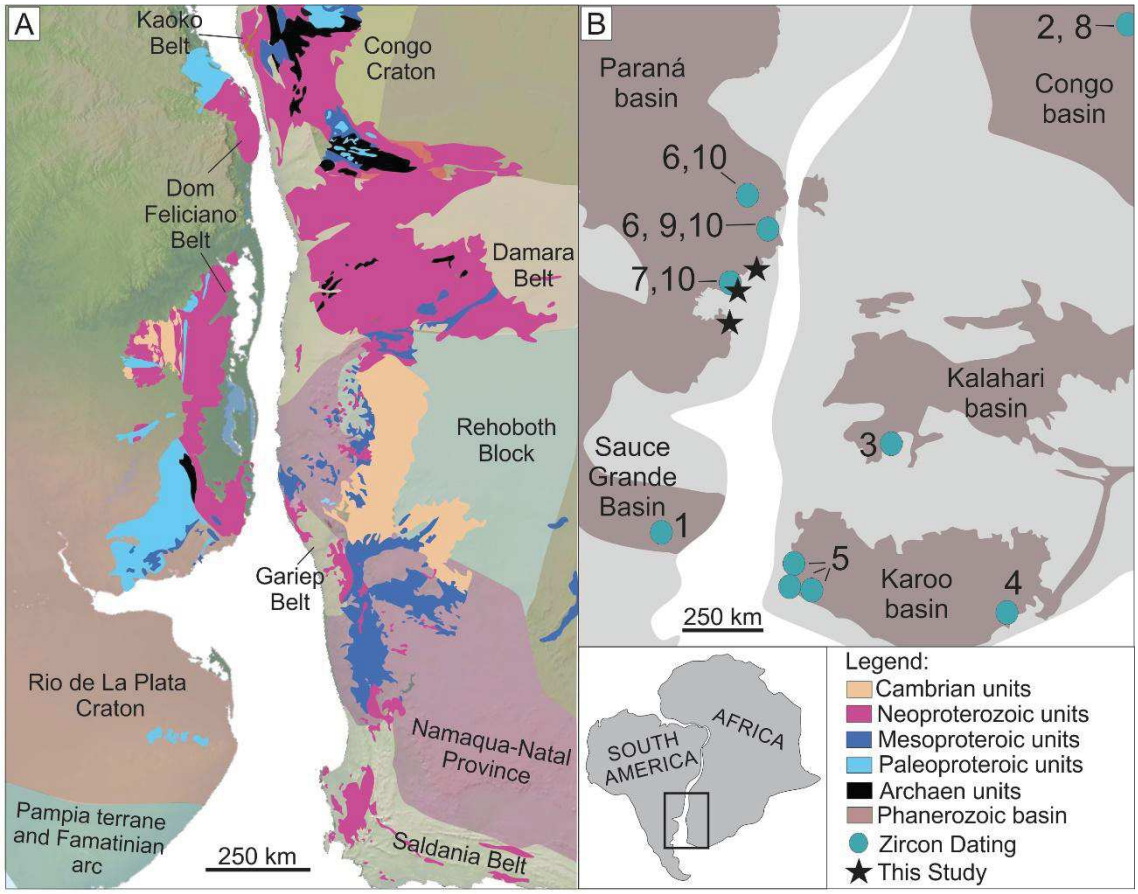

Supplementary File 1. (A) Major tectonic domains, mobile belts and cratons, modified by Luft (2005) and Uriz et al. (2016). **(**B) Location map of dated zircon samples, see figure 6.

Anexo 5 – (manuscrito 2)

Table S1. Selected samples for this study.

Sample	Lithology	Core	Depth (m)	Coordinates		Zircon
				S	W	
Itararé Gr.						
JT-01	Sandstone	CA-53-RS	635	30° 1'51	52°13'28	
JT-02	Siltstone	CA-53-RS	540	30° 1'51	52°13'28	
JT-05	Siltstone	ST-01-RS	206	30°18'53	53° 0'17	
JT-06	Conglomerate	ST-01-RS	186	30°18'53	53° 0'17	
JT-09	Conglomerate	SV-19-RS	68.8	31°26'38	53°38'56	
JT-10	Rthythmite	SV-19-RS	62.4	31°26'38	53°38'56	
JT-13	Conglomerate	IB-93-RS	356	30° 7'21	52° 9'9	
JT-14	Siltstone	IB-93-RS	312	30° 7'21	52° 9'9	sterile
JT-17	Siltstone	Barrocada	-	30°20'39	53°18'20	sterile
JT-18	Rhtythmite	Capané	-	30°26'18	53° 8'40	
JT-19	Rhtythmite	Capané	-	30°26'18	53° 8'40	
JT-20	Rhtythmite	Morro do Papaléo	-	30°18’26	51°38’32	
JT-21	Rhtythmite	Morro do Papaléo	-	30°18’26	51°38’32	
JT-07	Heterolithic fc.	ST-01-RS	140	30°18'53	53° 0'17	sterile
Rio Bonito Fm.						
JT-04	Sandstone	CA-53-RS	415	30° 1'51	52°13'28	
JT-08	Heterolithic fc.	ST-01-RS	130	30°18'53	53° 0'17	
JT-12	Sandstone	SV-19-RS	47	31°26'38	53°38'56	
JT-16	Sandstone	IB-93-RS	257	30° 7'21	52° 9'9	sterile
JT-22	Sandstone	Morro do Papaléo	-	30°18’26	51°38’32	
JT-03	Heterolithic fc.	CA-53-RS	468	30° 1'51	52°13'28	sterile
JT-11	Heterolithic fc.	SV-19-RS	57.7	31°26'38	53°38'56	
JT-15	Heterolithic fc.	IB-93-RS	281	30° 7'21	52° 9'9	

Table S2. Major element concentration (wt%) in studied lithologies.

Sample	Litho	SiO_2	Al_2O_3	Fe_2O_3	MgO	CaO	Na_2O	K_2O	TiO_2	P_2O_5	MnO	Cr_2O_3	CIA
Itararé Gr.													
JT-01	Sandstone	80,7	9,95	1,65	0,24	0,2	2,4	3,6	0,16	0,06	0,01	0,003	55,2
JT-02	Siltstone	72	12,89	4,78	0,82	0,35	2,74	3,7	0,54	0,13	0,02	0,005	57
JT-05	Siltstone	60,7	16,56	6,1	2,23	0,56	1,48	3,3	0,79	0,22	0,12	0,013	80,8
JT-06	Conglomerate	59,7	8,89	2,04	0,72	12,4	1,57	2,4	0,35	0,11	0,24	0,005	60,4
JT-09	Conglomerate	79,8	9,67	1,26	0,47	1,21	1,21	2,7	0,38	0,11	0,03	0,005	71,9
JT-10	Rhtythmite	71,6	11	3,06	0,64	3,02	0,5	3	0,5	0,13	0,03	0,007	24,5
JT-13	Conglomerate	79,8	10,38	1,26	0,25	0,56	2,43	4	0,23	0,08	0,02	<0,002	64,7
JT-14	Siltstone	72,6	12,93	4,07	0,82	0,39	2,64	3,7	0,57	0,15	0,02	0,005	65
JT-17	Siltstone	69	13,39	2,92	1,44	0,63	0,4	1,4	0,45	0,06	0,01	0,004	58,4
JT-18	Rhtythmite	52,2	18,56	10,43	2,65	0,35	0,59	4,4	0,73	0,22	0,12	0,014	54,3
JT-19	Rhtythmite	59,2	21,81	3,77	1,36	0,13	0,56	3,7	1,24	0,1	0,03	0,015	51,6
JT-20	Rhtythmite	69,1	19,18	2,02	0,23	0,01	0,03	1	1,37	0,09	0,02	0,012	69,1
JT-21	Rhtythmite	55,5	18,4	10,55	0,92	0,25	0,25	4,6	1,02	0,25	0,05	0,01	53,2
JT-07	Heterolithic fc.	67,1	15,13	4,24	1,62	0,38	2,04	4,2	0,7	0,15	0,04	0,009	64,7
Rio Bonito Fm.													
JT-04	Sandstone	86,4	7,2	0,51	0,05	0,06	0,13	4,1	0,12	0,03	0,01	0,003	60,4
JT-08	Heterolithic fc.	68,5	14,03	4,14	0,62	0,81	0,89	4,4	0,59	0,05	0,09	0,005	65
JT-12	Sandstone	85,1	7,75	0,63	0,11	0,07	0,27	2,7	0,2	0,02	0,01	0,003	69,1
JT-16	Sandstone	68,6	17,52	3,15	0,56	0,18	1	2	0,56	0,04	0,01	0,005	81,5
JT-22	Sandstone	80,6	12,47	0,15	0,01	<0,01	0,01	0,1	0,27	0,03	0,01	0,002	99,5
JT-03	Heterolithic fc.	62	20,85	3,78	0,53	0,33	1,12	2,4	0,79	0,04	0,08	0,006	80,8
JT-11	Heterolithic fc.	75,8	8,36	2,71	0,25	2,9	0,11	2,4	0,32	0,11	0,06	0,004	51,6
JT-15	Heterolithic fc.	61,2	19,93	4,08	0,61	0,15	0,99	2,5	0,78	0,04	0,02	0,008	81,5

Table 3. Trace element concentrations (ppm) in studied lithologies.

Sample	Litho	Ba	Ni	Sc	Be	Co	Cs	Ga	Hf	Nb	Rb	Sn	Sr	Ta	Th	U	V	W	Zr	Y
Itararé Gr.																				
JT-01	Sandstone	412	<20	3	1	1,3	2,1	13,3	3,8	7,8	161	3	63	0,7	5,9	1,1	17	0,8	138	13,6
JT-02	Siltstone	478	<20	7	7	6,3	3	16,8	6,6	18	152	4	77	1,3	11,5	2,9	50	1,5	222	24,4
JT-05	Siltstone	349	23	14	4	7,9	15,1	26,5	10,2	20,3	144	6	79,2	1,6	24,8	7,4	85	2,9	354	56,7
JT-06	Conglomerate	497	<20	1	<1	5,7	2,3	5,9	1,6	6,1	162	6	52,2	0,5	3,2	1,1	11	1,1	48,3	6,2
JT-09	Conglomerate	711	45	15	5	16,3	7,9	21,1	6,9	17,7	135	3	606	1,1	17,1	7,4	124	1,9	239	40,7
JT-10	Rhythmite	2472	<20	5	2	5,2	1,5	9,4	8,6	9,5	81,9	2	278	0,8	8,3	1,7	28	<0,5	319	19,8
JT-13	Conglomerate	590	30	11	6	12,7	6,3	19,1	6,9	17,4	167	4	146	1,4	16,6	6,1	85	2	236	27,8
JT-14	Siltstone	1404	<20	9	1	7,7	5,2	14,1	16,3	17,6	161	3	135	1,6	23,5	5,2	47	1,4	594	34,5
JT-17	Siltstone	592	<20	4	5	2,7	1,2	9	8,5	10,2	87	<1	128	0,7	6	1,2	24	0,7	318	15,5
JT-18	Rhtythmite	491	25	9	4	7,7	2,4	10,9	7,8	12,2	103	2	128	0,9	11,7	3,5	52	1,5	291	22
JT-19	Rhtythmite	472	36	5	4	6,3	1,6	9	7	7	75,4	1	99,6	0,6	5,4	5,7	37	1,1	275	21
JT-20	Rhtythmite	536	<20	3	2	6,8	0,9	6,9	4,2	4,9	80,2	4	68,2	0,5	3,1	5,9	46	0,8	152	8,3
JT-21	Rhtythmite	632	<20	2	6	1,6	3,2	11,1	7,6	10,6	169	3	90,3	1,1	10	2,5	<8	0,5	272	17,3
JT-07	Heterolithic fc.	497	<20	1	<1	5,7	2,3	5,9	1,6	6,1	162	6	52,2	0,5	3,2	1,1	11	1,1	48,3	6,2
Rio Bonito Fm.																				
JT-04	Sandstone	497	<20	1	<1	5,7	2,3	5,9	1,6	6,1	162	6	52,2	0,5	3,2	1,1	11	1,1	48,3	6,2
JT-08	Heterolithic fc.	1404	<20	9	1	7,7	5,2	14,1	16,3	17,6	161	3	135	1,6	23,5	5,2	47	1,4	594	34,5
JT-12	Sandstone	536	<20	3	2	6,8	0,9	6,9	4,2	4,9	80,2	4	68,2	0,5	3,1	5,9	46	0,8	152	8,3
JT-16	Sandstone	291	<20	12	4	2,5	26,1	27,5	7	23,3	178	10	88,1	2	23,6	8,1	55	3,9	224	70
JT-22	Sandstone	23	<20	3	<1	1,7	0,3	10,3	1,8	11,3	6,5	<1	63,2	1	4,6	1,8	18	0,7	51,4	5,3
JT-03	Heterolithic fc.	349	23	14	4	7,9	15,1	26,5	10,2	20,3	144	6	79,2	1,6	24,8	7,4	85	2,9	354	56,7
JT-11	Heterolithic fc.	711	45	15	5	16	7,9	21,1	6,9	17,7	135	3	606	1,1	17,1	7,4	124	1,9	239	40,7
JT-15	Heterolithic fc.	2472	<20	5	2	5,2	1,5	9,4	8,6	9,5	81,9	2	278	0,8	8,3	1,7	28	<0,5	319	19,8

Table 4. Rare earth elements (ppm) and elemental ratios in studied lithologies.

Sample	Litho	La	Ce	Pr	Nd	Sm	Eu	Gd	Tb	Dy	Ho	Er	Tm	Yb	Lu
Itararé Gr.															
JT-01	Sandstone	16,3	34,2	3,98	15,3	2,98	0,55	2,52	0,39	2,49	0,46	1,47	0,21	1,55	0,23
JT-02	Siltstone	36,7	74	8,67	31,8	6,55	1,07	5,3	0,81	4,7	0,94	2,83	0,4	2,78	0,43
JT-05	Siltstone	72,7	127	17,3	63,4	12,4	1,97	11	1,64	10,3	1,95	6,22	0,83	5,54	0,85
JT-06	Conglomerate	5,1	9,5	1,08	3,6	0,79	0,25	0,81	0,14	0,88	0,19	0,67	0,09	0,7	0,09
JT-09	Conglomerate	83,2	164	17,9	64,3	10,7	1,83	8,47	1,21	7,22	1,46	4,1	0,57	3,78	0,57
JT-10	Rhtythmite	25	48,7	5,68	21,4	4,06	0,64	3,71	0,55	3,41	0,68	2	0,3	2,03	0,34
JT-13	Conglomerate	51,5	102	11,2	39,8	7,34	1,22	5,9	0,89	5,29	1,01	2,98	0,43	3,07	0,46
JT-14	Siltstone	50,8	101	11,4	41,3	7,82	1,1	6,38	0,97	6,07	1,22	3,41	0,49	3,45	0,54
JT-17	Siltstone	23,1	42,2	4,88	17,7	3,33	0,7	3	0,45	2,89	0,58	1,79	0,25	1,71	0,26
JT-18	Rhtythmite	32,5	67,6	7,7	28	5,23	0,92	4,42	0,65	3,84	0,83	2,54	0,34	2,33	0,36
JT-19	Rhtythmite	19	34,7	4,49	18,4	3,42	0,74	3,61	0,54	3,49	0,69	2,03	0,3	2,02	0,32
JT-20	Rhtythmite	12,5	23,6	2,87	11	2,1	0,55	1,97	0,28	1,75	0,31	0,89	0,14	0,99	0,14
JT-21	Rhtythmite	28,3	56,3	6,31	22,9	4,26	0,78	3,66	0,53	3,05	0,61	1,83	0,28	1,86	0,28
JT-07	Heterolithic fc.	51,5	102	11,2	39,8	7,34	1,22	5,9	0,89	5,29	1,01	2,98	0,43	3,07	0,46
Rio Bonito Fm.															
JT-04	Sandstone	5,1	9,5	1,08	3,6	0,79	0,25	0,81	0,14	0,88	0,19	0,67	0,09	0,7	0,09
JT-08	Heterolithic fc.	50,8	101	11,4	41,3	7,82	1,1	6,38	0,97	6,07	1,22	3,41	0,49	3,45	0,54
JT-12	Sandstone	23,1	42,2	4,88	17,7	3,33	0,7	3	0,45	2,89	0,58	1,79	0,25	1,71	0,26
JT-16	Sandstone	98,4	184	22,7	87,8	17	2,08	16,1	2,4	14	2,59	7,22	1,05	6,83	0,99
JT-22	Sandstone	42,1	83,7	9,44	35,6	6,43	1,11	5,87	0,96	6,08	1,29	3,93	0,57	3,79	0,6
JT-03	Heterolithic fc.	72,7	127	17,3	63,4	12,4	1,97	11	1,64	10,3	1,95	6,22	0,83	5,54	0,85
JT-11	Heterolithic fc.	19	34,7	4,49	18,4	3,42	0,74	3,61	0,54	3,49	0,69	2,03	0,3	2,02	0,32
JT-15	Heterolithic fc.	72,4	153	17,2	64,8	12,3	1,85	11,7	1,79	10	1,92	5,59	0,77	5	0,79

Anexo 6 – (manuscrito 2)

Idades dos zircões detriticos

Spot number	Best Estimated Age Age (Ma)	$2s_{sys}$ Abs
JT#8_007	572	15
JT#8_008	583	13
JT#8_009	598	13
JT#8_010	606	13
JT#8_011	601	13
JT#8_012	879	21
JT#8_013	597	13
JT#8_014	907	20
JT#8_016	614	14
JT#8_018	600	13
JT#8_019	583	13
JT#8_020	592	13
JT#8_027	614	18
JT#8_029	598	13
JT#8_030	611	14
JT#8_031	694	15
JT#8_032	574	13
JT#8_033	639	15
JT#8_034	534	12
JT#8_035	616	14
JT#8_036	744	17
JT#8_037	304	7
JT#8_038	2114	37
JT#8_039	629	14
JT#8_040	656	15
JT#8_047	664	28
JT#8_049	637	14
JT#8_050	607	14
JT#8_051	602	14
JT#8_052	670	37
JT#8_053	665	15
JT#8_054	619	14
JT#8_055	736	17
JT#8_056	575	13
JT#8_057	707	16
JT#8_058	744	16
JT#8_059	632	15
JT#8_060	645	15
JT#8_067	647	15
JT#8_068	460	11
JT#8_069	847	22
JT#8_070	641	18
JT#8_071	610	14
JT#8_072	564	14
JT#8_073	370	10
JT#8_074	622	14
JT#8_075	691	15
JT#8_076	640	14
JT#8_078	749	17
JT#8_079	643	14
JT#8_080	493	11
JT#8_087	448	13
JT#8_088	705	16
JT#8_090	617	18
JT#8_091	652	15
JT#8_093	940	21
JT#8_094	578	13
JT#8_095	468	11
JT#8_096	665	15
JT#8_097	659	15
JT#8_098	534	12
JT#8_099	874	22
JT#8_100	589	13
JT#8_107	621	19
JT#8_108	675	15
JT#8_109	796	18
JT#8_110	615	14
JT#8_112	658	15
JT#8_113	782	17
JT#8_114	557	13
JT#8_115	584	13
JT#8_116	633	14
JT#8_117	609	14
JT#8_118	898	20
JT#8_119	575	13
JT#8_120	573	20
JT#8_127	378	9
JT#8_128	538	13
JT#8_129	1034	100

JT#8_130	625	14
JT#8_131	523	12
JT#8_132	534	13
JT#8_133	566	13
JT#8_134	727	17
JT#8_135	617	14
JT#8_136	633	14
JT#8_137	640	15
JT#8_139	655	18
JT#8_140	631	15
JT#8_147	2207	38
JT#8_148	645	15
JT#8_149	734	17
JT#8_150	800	18
JT#8_151	1015	126
JT#8_152	804	34
JT#8_153	780	18
JT#8_154	640	14
JT#8_156	630	14
JT#8_157	817	18
JT#8_158	684	16
JT#8_167	655	15
JT#8_168	662	15
JT#8_169	431	16
JT#8_170	616	16
JT#8_172	633	14
JT#8_173	608	14
JT#8_174	598	18
JT#8_175	617	15
JT#8_176	509	12
JT#8_177	524	12
JT#8_178	622	14
JT#8_179	1485	44
JT#8_180	856	19
JT#8_187	641	19
JT#8_188	2121	39
JT#8_189	643	15
JT#8_190	816	18
JT#8_191	601	14
JT#8_193	666	16
JT#8_194	636	15
JT#8_195	1937	38
JT#8_196	613	14
JT#8_198	1959	43
JT#8_199	633	15
JT#8_200	628	15

Spot number	Best Estimated Age Age (Ma)	$2s_{sys}$ Abs
J#9_051	561	13
J#9_007	560	13
J#9_008	568	14
J#9_009	617	14
J#9_011	2703	41
J#9_012	602	15
J#9_013	604	14
J#9_014	650	15
J#9_015	1506	43
J#9_016	2200	44
J#9_017	2099	39
J#9_018	573	13
J#9_019	1487	60
J#9_020	2931	36
J#9_027	2704	37
J#9_028	598	14
J#9_029	719	16
J#9_030	640	14
J#9_031	555	13
J#9_032	588	13
J#9_033	696	16
J#9_034	628	18
J#9_037	647	19
J#9_038	577	18
J#9_039	647	14
J#9_040	2088	39
J#9_047	616	14
J#9_048	1107	69
J#9_049	641	14
J#9_053	470	16
J#9_054	597	14
J#9_055	829	22
J#9_056	1122	47
J#9_057	711	31

J#9_058	587	24
J#9_059	656	16
J#9_060	641	18
J#9_067	2086	47
J#9_068	685	16
J#9_069	604	18
J#9_070	571	16
J#9_071	590	13
J#9_073	654	18
J#9_074	2215	38
J#9_075	693	15
J#9_076	690	15
J#9_077	650	15
J#9_079	648	15
J#9_080	625	38
J#9_087	709	16
J#9_088	671	19
J#9_089	2095	39
J#9_090	1794	40
J#9_091	550	17
J#9_092	555	15
J#9_093	551	13
J#9_094	646	14
J#9_095	688	15
J#9_096	624	14
J#9_097	671	15
J#9_098	1579	42
J#9_099	1028	49
J#9_100	512	12
J#9_107	674	16
J#9_108	483	12
J#9_109	586	13
J#9_110	561	13
J#9_111	551	13
J#9_112	576	13
J#9_113	638	15
J#9_114	560	13
J#9_115	2051	39
J#9_116	412	15
J#9_117	588	13
J#9_118	560	13
J#9_119	575	13
J#9_120	673	15
J#9_127	627	32
J#9_128	629	18
J#9_129	544	12
J#9_130	1240	48
J#9_131	632	14
J#9_132	626	14
J#9_134	658	15
J#9_135	637	14
J#9_136	657	15
J#9_137	567	13
J#9_138	636	14
J#9_139	1879	39
J#9_140	596	14
J#9_147	2901	41
J#9_148	637	14
J#9_149	2080	40
J#9_150	665	15
J#9_151	896	19
J#9_152	1664	45
J#9_153	447	10
J#9_154	606	14
J#9_155	631	15
J#9_156	598	14
J#9_157	597	13
J#9_158	453	10
J#9_159	562	13
J#9_160	507	11
J#9_167	591	13
J#9_168	513	17
J#9_169	2851	37
J#9_170	632	14
J#9_171	669	15
J#9_172	601	18
J#9_174	642	14
J#9_176	659	15
J#9_177	537	16
J#9_178	642	14
J#9_180	2837	35
J#9_187	634	16
J#9_188	464	16
J#9_189	775	17
J#9_190	614	14
J#9_191	619	14
J#9_192	889	19
J#9_193	602	13
J#9_194	686	15
J#9_195	633	14
J#9_196	658	15
J#9_197	563	36

J#9_198	640	63
J#9_200	537	18

Spot number	Best Estimated Age Age (Ma)	$2s_{sys}$ Abs
JT#10_031	494	16
JT#10_010	751	20
JT#10_011	517	15
JT#10_012	582	15
JT#10_013	740	20
JT#10_014	300	7
JT#10_015	542	12
JT#10_016	600	18
JT#10_017	874	42
JT#10_018	1566	30
JT#10_019	648	18
JT#10_020	562	17
JT#10_027	582	20
JT#10_028	513	17
JT#10_029	474	11
JT#10_030	607	13
JT#10_032	1090	63
JT#10_033	352	10
JT#10_034	551	12
JT#10_035	558	17
JT#10_037	522	12
JT#10_038	521	12
JT#10_039	625	15
JT#10_040	516	18
JT#10_048	619	43
JT#10_049	631	18
JT#10_050	449	16
JT#10_051	639	62
JT#10_052	828	21
JT#10_053	450	10
JT#10_054	638	14
JT#10_055	410	13
JT#10_056	686	19
JT#10_058	496	11
JT#10_059	656	15
JT#10_060	560	17
JT#10_067	3654	294
JT#10_069	597	49
JT#10_070	546	17
JT#10_071	706	19
JT#10_072	932	20
JT#10_073	633	14
JT#10_074	583	17
JT#10_075	678	15
JT#10_076	553	22
JT#10_078	488	16
JT#10_079	441	10
JT#10_080	311	27

Spot number	Best Estimated Age Age (Ma)	$2s_{sys}$ Abs
J#11_007	525	15
J#11_008	641	15
J#11_009	616	14
J#11_010	547	12
J#11_011	560	28
J#11_013	968	21
J#11_014	608	14
J#11_015	482	11
J#11_016	585	13
J#11_017	2630	38
J#11_018	568	13
J#11_019	457	10
J#11_020	547	12
J#11_027	787	21
J#11_028	570	19
J#11_029	613	14
J#11_030	528	17
J#11_031	666	28
J#11_032	557	13
J#11_033	646	15
J#11_034	673	15
J#11_035	546	13
J#11_036	666	15
J#11_037	617	14
J#11_038	538	12
J#11_039	1065	53
J#11_040	622	14
J#11_047	715	16
J#11_048	576	16

J#11_049	582	13
J#11_050	408	9
J#11_051	592	13
J#11_052	2093	39
J#11_053	535	12
J#11_055	311	9
J#11_056	705	16
J#11_057	615	14
J#11_058	651	15
J#11_059	470	16
J#11_060	552	12
J#11_067	543	12
J#11_068	648	16
J#11_069	569	16
J#11_070	961	46
J#11_071	454	14
J#11_072	528	12
J#11_073	649	19
J#11_074	541	12
J#11_075	622	14
J#11_076	643	14
J#11_077	668	15
J#11_078	628	14
J#11_080	532	12
J#11_087	557	17
J#11_088	642	14
J#11_089	711	16
J#11_090	584	14
J#11_091	451	10
J#11_092	507	11
J#11_093	685	15
J#11_094	680	16
J#11_095	608	14
J#11_096	569	13
J#11_097	605	14
J#11_098	659	19
J#11_099	886	23
J#11_100	660	16
J#11_107	550	16
J#11_108	563	13
J#11_109	703	20
J#11_110	579	13
J#11_111	663	15
J#11_112	647	18
J#11_113	1020	46
J#11_114	784	17
J#11_116	666	15
J#11_117	736	16
J#11_119	307	7
J#11_120	583	13
J#11_128	720	16
J#11_129	570	13
J#11_130	527	12
J#11_131	617	17
J#11_132	697	16
J#11_133	1392	95
J#11_134	621	14
J#11_135	314	7
J#11_137	801	18
J#11_139	648	29
J#11_140	643	16
J#11_147	451	10
J#11_148	1096	49
J#11_149	1102	47
J#11_150	902	23
J#11_151	427	10
J#11_152	537	12
J#11_153	718	16
J#11_156	573	13
J#11_160	602	13
J#11_167	528	12
J#11_168	785	17
J#11_169	622	14
J#11_170	571	13
J#11_171	518	12
J#11_172	572	13
J#11_173	653	15
J#11_174	609	14
J#11_175	640	14
J#11_176	464	11
J#11_177	501	11
J#11_178	695	15
J#11_179	1062	48
J#11_180	574	41
J#11_187	651	20
J#11_188	641	15
J#11_189	585	13
J#11_190	429	11
J#11_191	647	14
J#11_192	574	13
J#11_193	561	13
J#11_194	411	9

J#11_195	685	15
J#11_196	530	12
J#11_197	692	23
J#11_198	322	18

Spot number	Best Estimated Age Age (Ma)	$2s_{sys}$ Abs
J#12_133	1673	57
J#12_047	469	9
J#12_007	569	15
J#12_007	584	10
J#12_008	665	16
J#12_008	658	14
J#12_009	625	11
J#12_009	1065	47
J#12_010	723	15
J#12_010	786	13
J#12_011	607	15
J#12_011	651	10
J#12_012	404	7
J#12_013	579	15
J#12_014	682	11
J#12_014	934	14
J#12_015	581	9
J#12_015	613	10
J#12_016	484	8
J#12_016	565	9
J#12_017	597	15
J#12_017	647	10
J#12_018	750	12
J#12_018	1085	45
J#12_019	607	10
J#12_019	993	15
J#12_020	658	11
J#12_020	596	10
J#12_027	684	16
J#12_027	716	16
J#12_028	351	16
J#12_028	396	6
J#12_029	548	15
J#12_030	661	16
J#12_030	536	9
J#12_031	657	11
J#12_031	674	11
J#12_032	755	12
J#12_033	558	11
J#12_033	947	15
J#12_034	569	9
J#12_034	655	10
J#12_035	490	14
J#12_035	681	16
J#12_036	639	15
J#12_036	660	16
J#12_037	550	15
J#12_037	649	10
J#12_038	566	10
J#12_039	618	10
J#12_039	924	14
J#12_040	440	14
J#12_040	662	16
J#12_048	606	15
J#12_048	805	13
J#12_049	431	14
J#12_049	633	12
J#12_050	591	12
J#12_050	1196	46
J#12_051	605	15
J#12_051	785	17
J#12_052	560	9
J#12_052	739	12
J#12_053	573	10
J#12_054	627	11
J#12_054	550	9
J#12_055	563	9
J#12_055	697	11
J#12_056	660	16
J#12_056	598	12
J#12_057	655	10
J#12_058	549	15
J#12_058	835	13
J#12_059	636	10
J#12_059	857	14
J#12_060	590	15
J#12_060	1073	44
J#12_067	582	9
J#12_068	547	15
J#12_069	581	15
J#12_070	484	8

J#12_071	1999	101
J#12_072	661	14
J#12_073	442	14
J#12_075	612	10
J#12_076	494	14
J#12_077	639	11
J#12_078	459	9
J#12_079	570	13
J#12_080	664	13
J#12_088	550	9
J#12_089	545	15
J#12_090	589	15
J#12_091	762	12
J#12_092	725	16
J#12_093	507	8
J#12_094	581	15
J#12_095	685	11
J#12_097	552	14
J#12_099	657	16
J#12_100	592	10
J#12_108	527	9
J#12_109	618	15
J#12_110	563	9
J#12_111	629	16
J#12_112	507	15
J#12_113	547	15
J#12_114	648	11
J#12_115	308	5
J#12_117	864	15
J#12_118	548	9
J#12_119	918	22
J#12_120	562	15
J#12_127	567	15
J#12_128	695	13
J#12_129	503	15
J#12_130	990	16
J#12_131	669	11
J#12_132	686	16
J#12_134	997	16
J#12_135	2217	47
J#12_136	633	10
J#12_137	3350	38
J#12_139	505	8
J#12_140	537	9

	Best Estimated Age	
Spot **number**	Age (Ma)	$2s_{sys}$ Abs
JT#13_007	572	13
JT#13_008	754	18
JT#13_009	571	13
JT#13_010	1589	45
JT#13_011	2013	50
JT#13_013	543	17
JT#13_014	594	13
JT#13_015	631	14
JT#13_016	658	16
JT#13_017	2060	38
JT#13_018	631	14
JT#13_019	628	18
JT#13_020	619	14
JT#13_027	598	18
JT#13_028	545	12
JT#13_029	599	14
JT#13_030	598	15
JT#13_031	614	14
JT#13_032	651	14
JT#13_033	582	13
JT#13_034	609	13
JT#13_035	553	17
JT#13_036	594	13
JT#13_037	592	13
JT#13_038	652	14
JT#13_039	1809	40
JT#13_040	607	18
JT#13_047	701	15
JT#13_048	549	12
JT#13_049	605	13
JT#13_050	764	18
JT#13_051	627	14
JT#13_052	589	14
JT#13_054	1950	43
JT#13_055	630	15
JT#13_057	598	13
JT#13_058	539	12
JT#13_059	617	14
JT#13_060	582	17
JT#13_067	581	13
JT#13_068	732	16
JT#13_070	606	13

JT#13_071	619	14
JT#13_072	593	13
JT#13_073	550	12
JT#13_074	622	14
JT#13_075	756	18
JT#13_076	582	13
JT#13_078	596	13
JT#13_080	598	13
JT#13_087	601	13
JT#13_088	357	8
JT#13_089	578	13
JT#13_090	591	13
JT#13_091	473	10
JT#13_092	2993	38
JT#13_094	600	13
JT#13_096	628	14
JT#13_097	792	17
JT#13_098	592	13
JT#13_099	600	13
JT#13_100	664	14
JT#13_107	616	13
JT#13_108	648	18
JT#13_109	583	13
JT#13_110	674	15
JT#13_111	591	13
JT#13_112	442	10
JT#13_114	647	18
JT#13_115	680	15
JT#13_116	1103	44
JT#13_117	624	14
JT#13_118	540	13
JT#13_119	596	13
JT#13_120	712	15
JT#13_127	639	14
JT#13_129	1927	42
JT#13_130	613	13
JT#13_131	643	18
JT#13_133	554	12
JT#13_134	586	13
JT#13_135	542	12
JT#13_136	604	13
JT#13_137	633	14
JT#13_138	776	17
JT#13_139	769	17
JT#13_140	658	15
JT#13_147	549	12
JT#13_148	768	17
JT#13_149	711	16
JT#13_150	610	13
JT#13_151	535	12
JT#13_152	670	15
JT#13_153	590	23
JT#13_154	1466	43
JT#13_155	691	15
JT#13_157	786	17
JT#13_158	541	12
JT#13_160	563	12
JT#13_167	611	13
JT#13_168	621	18
JT#13_170	582	13
JT#13_171	590	13
JT#13_172	573	19
JT#13_173	609	13
JT#13_174	968	21
JT#13_175	555	12
JT#13_176	550	12
JT#13_177	548	13
JT#13_178	573	13
JT#13_179	589	13
JT#13_187	2049	40
JT#13_188	611	13
JT#13_189	606	18
JT#13_190	1888	39
JT#13_191	586	13
JT#13_192	590	13
JT#13_193	592	13
JT#13_194	579	17
JT#13_195	586	13
JT#13_196	572	17
JT#13_197	605	16
JT#13_198	598	15
JT#13_199	2962	33
JT#13_200	623	15

	Best Estimated Age	
Spot **number**	Age (Ma)	$2s_{sys}$ Abs
JT#15_036	1955	37
JT#15_007	1860	37
JT#15_009	627	12
JT#15_010	619	17

JT#15_012	1803	39
JT#15_013	1731	37
JT#15_015	1891	36
JT#15_017	642	14
JT#15_018	1913	47
JT#15_019	647	12
JT#15_020	611	16
JT#15_027	566	11
JT#15_028	2010	48
JT#15_029	563	11
JT#15_030	1886	37
JT#15_031	603	13
JT#15_032	600	12
JT#15_033	1560	38
JT#15_034	780	15
JT#15_037	2019	38
JT#15_038	606	12
JT#15_039	793	15
JT#15_047	602	12
JT#15_048	574	16
JT#15_049	615	17
JT#15_050	606	17
JT#15_051	590	13
JT#15_052	774	19
JT#15_053	619	12
JT#15_054	619	21
JT#15_055	568	12
JT#15_056	577	16
JT#15_059	506	10
JT#15_060	590	17

	Best Estimated Age	
Spot number	Age (Ma)	$2s_{sys}$ Abs
J#20_011	558	16
J#20_012	637	14
J#20_013	479	12
J#20_015	707	15
J#20_016	823	17
J#20_018	575	12
J#20_027	741	20
J#20_029	554	14
J#20_030	573	17
J#20_031	667	14
J#20_032	766	16
J#20_034	618	13
J#20_035	639	14
J#20_036	594	12
J#20_039	504	17
J#20_040	594	12
J#20_047	710	15
J#20_049	595	17
J#20_050	743	17
J#20_052	618	13
J#20_054	645	13
J#20_056	538	12
J#20_058	681	18
J#20_059	587	15
J#20_060	574	12
J#20_069	611	15
J#20_071	580	12
J#20_072	602	13
J#20_073	640	14
J#20_074	565	12
J#20_075	569	12
J#20_076	341	14
J#20_077	339	8
J#20_078	1055	50
J#20_079	1047	93

	Best Estimated Age	
Spot number	Age (Ma)	$2s_{sys}$ Abs
JT#21_129	557	18
JT#21_007	593	22
JT#21_008	592	19
JT#21_010	614	26
JT#21_011	659	24
JT#21_012	647	24
JT#21_013	598	19
JT#21_014	580	19
JT#21_016	626	25
JT#21_017	588	20
JT#21_018	642	24
JT#21_019	616	20
JT#21_020	557	22

JT#21_029	558	17
JT#21_030	638	21
JT#21_031	565	19
JT#21_033	586	18
JT#21_034	633	20
JT#21_035	543	30
JT#21_036	616	19
JT#21_037	591	18
JT#21_038	533	25
JT#21_039	563	18
JT#21_040	632	21
JT#21_047	629	23
JT#21_048	798	27
JT#21_049	549	19
JT#21_050	624	19
JT#21_051	576	21
JT#21_052	600	19
JT#21_053	665	22
JT#21_054	647	20
JT#21_056	543	20
JT#21_057	556	24
JT#21_058	622	22
JT#21_059	618	20
JT#21_060	660	22
JT#21_067	609	19
JT#21_069	581	19
JT#21_070	566	24
JT#21_071	600	21
JT#21_072	549	26
JT#21_074	582	18
JT#21_075	644	21
JT#21_077	652	20
JT#21_078	639	23
JT#21_079	509	23
JT#21_080	594	21
JT#21_087	654	21
JT#21_088	578	21
JT#21_089	627	21
JT#21_090	665	21
JT#21_091	578	18
JT#21_092	615	20
JT#21_094	626	20
JT#21_096	674	31
JT#21_098	663	23
JT#21_099	605	23
JT#21_100	592	23
JT#21_107	626	33
JT#21_108	613	20
JT#21_109	588	19
JT#21_110	589	19
JT#21_111	593	19
JT#21_112	588	20
JT#21_113	625	20
JT#21_114	568	22
JT#21_115	563	20
JT#21_116	605	31
JT#21_117	643	27
JT#21_118	586	22
JT#21_119	604	22
JT#21_120	632	22
JT#21_127	542	22
JT#21_128	629	20
JT#21_130	561	24
JT#21_131	595	20
JT#21_133	579	24
JT#21_134	668	22
JT#21_135	604	21
JT#21_136	540	18
JT#21_138	679	25
JT#21_139	605	21
JT#21_140	601	23
JT#21_148	641	22
JT#21_151	574	24
JT#21_153	607	20
JT#21_154	545	24
JT#21_155	651	23
JT#21_156	573	20
JT#21_157	589	20
JT#21_158	514	21
JT#21_159	788	27
JT#21_160	677	39
JT#21_167	607	19
JT#21_168	609	21
JT#21_169	608	19
JT#21_170	571	25
JT#21_173	634	29
JT#21_174	585	19
JT#21_175	807	26
JT#21_176	579	19
JT#21_177	671	22
JT#21_178	590	21
JT#21_179	561	23

JT#21_180	594	24
JT#21_187	629	22
JT#21_189	741	39
JT#21_190	704	22
JT#21_191	574	21
JT#21_192	841	26
JT#21_193	564	20
JT#21_194	649	24
JT#21_195	542	20
JT#21_196	626	22
JT#21_197	666	32
JT#21_198	674	21
JT#21_199	620	20

	Best Estimated Age	
Spot number	Age (Ma)	$2s_{sys}$ Abs
JT#22_007	586	11
JT#22_008	596	15
JT#22_009	516	13
JT#22_010	579	9
JT#22_011	475	8
JT#22_013	506	8
JT#22_014	589	13
JT#22_015	622	15
JT#22_017	580	9
JT#22_018	647	16
JT#22_019	593	12
JT#22_020	623	10
JT#22_027	576	15
JT#22_028	635	11
JT#22_029	590	9
JT#22_030	586	15
JT#22_031	638	16
JT#22_032	578	15
JT#22_033	519	11
JT#22_035	623	11
JT#22_036	579	9
JT#22_037	603	15
JT#22_039	559	16
JT#22_040	576	15
JT#22_131	563	12
JT#22_007	568	17
JT#22_008	534	11
JT#22_009	616	13
JT#22_010	624	17
JT#22_012	584	12
JT#22_014	574	12
JT#22_015	571	12
JT#22_016	622	13
JT#22_018	609	13
JT#22_019	614	16
JT#22_020	652	18
JT#22_027	633	16
JT#22_031	599	12
JT#22_032	590	25
JT#22_033	641	13
JT#22_034	581	12
JT#22_035	566	12
JT#22_036	482	12
JT#22_037	506	11
JT#22_038	564	12
JT#22_039	646	13
JT#22_047	659	15
JT#22_049	578	17
JT#22_050	562	12
JT#22_051	600	13
JT#22_052	621	13
JT#22_053	663	18
JT#22_055	562	12
JT#22_056	358	8
JT#22_057	637	13
JT#22_058	606	13
JT#22_059	596	13
JT#22_060	603	13
JT#22_067	616	14
JT#22_068	549	11
JT#22_069	580	14
JT#22_070	534	16
JT#22_071	615	13
JT#22_072	688	15
JT#22_073	735	15
JT#22_074	679	14
JT#22_075	644	13
JT#22_076	610	17
JT#22_077	578	14
JT#22_078	655	14
JT#22_079	608	13
JT#22_087	647	14
JT#22_088	610	13
JT#22_090	576	12

JT#22_092	656	35
JT#22_093	657	14
JT#22_094	584	12
JT#22_096	615	13
JT#22_097	437	9
JT#22_098	624	16
JT#22_099	593	13
JT#22_100	631	13
JT#22_107	537	29
JT#22_108	742	19
JT#22_109	602	13
JT#22_110	621	13
JT#22_111	680	14
JT#22_112	581	12
JT#22_113	547	12
JT#22_114	712	15
JT#22_115	592	38
JT#22_116	660	14
JT#22_117	632	14
JT#22_118	659	14
JT#22_119	636	14
JT#22_120	606	15
JT#22_129	600	12
JT#22_130	555	12
JT#22_132	618	13
JT#22_133	613	13
JT#22_134	551	12
JT#22_135	575	15
JT#22_137	590	12
JT#22_138	609	13
JT#22_139	614	17
JT#22_140	586	14
JT#22_150	584	17
JT#22_152	586	12
JT#22_154	555	12
JT#22_158	571	12
JT#22_159	608	13